Tampere University

Emilia Löfman

ENTRAPMENT OF PHOTON UPCONVERSION MICELLES IN ANIONIC NANOFIBRILLAR CELLULOSE HYDROGEL

Study on System Stability, Upconversion Efficiency and Optimization

Master's thesis
Faculty of Engineering and Natural Sciences
Elina Vuorimaa-Laukkanen
Timo Laaksonen
May 2022

ABSTRACT

Emilia Löfman: Entrapment of Photon Upconversion Micelles in Anionic Nanofibrillar Cellulose Hydrogel
Master's Thesis
Tampere University
Environmental, Energy and Biotechnology
05/2022

Triplet fusion upconversion, TF-UC, is a photochemical process where the properties of two molecule types, sensitizer, and annihilator, are combined to produce high energy emission upon low energy excitation. The phenomenon is especially interesting in the field of targeted drug delivery, where the constraints of tissue absorption can be broken, and high energy blue light can be generated inside the tissue and used as a photocatalyst for different chemical reactions.

In this work we aimed to introduce photon upconversion via TF-UC inside anionic nanofibrillar cellulose hydrogel, non-toxic and biocompatible gel which has been studied as a drug reservoir. However, to guarantee efficient upconversion, the three different sensitizers, PdTPTBP, PtTPTBP and PtOEP paired with the annihilator TTBPer, were first loaded into micelles composed of two different surfactants, CrEL and T80 to solubilize the dyes and these micelles were then entrapped in the hydrogel. Since it was hypothesized that Coulombic interactions between the micelles and anionic nanocellulose fibres could improve the retention of the micelles inside the hydrogel, we modified the micelles using two different cationic co-surfactants, STA and DOTAP. The micelles were characterized by measuring their size, size distribution and ζ-potential, and their upconversion properties were studied by determining the power density threshold and upconversion quantum yield. The leaking of the micelles from hydrogel and the signal stability of TTBPer in the released micelles was studied up to two weeks. Finally, upconversion spectrum of entrapped micelles inside hydrogel was recorded with different excitation power densities.

It was established that the surface charge modification of micelles did not improve their retention in the hydrogel, but on the contrary made the system overall more unstable in terms of both the release rate of the micelles and TTBPer signal stability in the released micelles. CrEL based micelles performed better to T80 based micelles, and it was shown that the higher loading of micelles in hydrogel causes them to be released slower and the TTBPer signal to stay more stable. Out of the three sensitizers tested, PdTPTBP and PtOEP showed the best promise in terms of upconversion efficiency in physiological conditions. PdTPTBP loaded STA modified CrEL micelles showed upconversion quantum yield of 0.6 % in line with the previous records. The upconverted emission spectrum of PdTPTBP loaded CrEL micelles (unmodified) entrapped in hydrogel was successfully recorded although high excitation power densities had to used suggesting that the oxygen sensitivity of the studied system might be too high. PtOEP loaded micelles entrapped in hydrogel were not yet studied but they showed decent upconversion emission in oxic water solution making them an interesting system for further studies..

Keywords: micelle, hydrogel, triplet fusion, nanocellulose, surfactant

TIIVISTELMÄ

Emilia Löfman: Ylöskonversiomisellien integraatio anioniseen nanokuituselluloosasta valmistettuun hydrogeeliin
Diplomityö
Tampereen yliopisto
Ympäristö-, energia- ja biotekniikka
05/2022

Triplettifuusioon perustuva valon ylöskonversio, TF-UC on valokemiallilnen prosessi, jonka avulla voidaan tuottaa korkeaenergistä valon emissiota käyttäen viritykseen matalaenergistä valoa. Tämä tehdään yhdistämällä kahden molekyylityypin, herkistin- ja annihilaatioaineen ominaisuudet. Tämä ilmiö on erityisen kiinnostava kohdistetussa lääkeaineen vapautuksessa. Valon ylöskonversion avulla voidaan tuottaa korkeaenergistä valoa kudosten sisälle, jonne sitä ei ulkoisella korkeaenergisellä eksitaatiolla voida saada kudosten vahvan absorption vuoksi. Korkeaenergistä valoa voitaisiin näin edelleen käyttää valokatalyyttinä erilaisille kemiallisille reaktiolle luoden muun muassa lääkeaineiden vapautusmekanismeja.

Tässä työssä tarkasteltiin mahdollisuutta tuottaa valon ylöskonversio anionisesta nanokuituselluloosasta valmistetussa hydrogeelissä. Nanokuituselluloosa on myrkytön ja bioyhteensopiva materiaali, ja siitä valmistetun hydrogeelin käytettävyyttä lääkeainevarantona on tutkittu. Tehokkaan ylöskonversion aikaansaamiseksi kolme herkistinainetta, PdTPTBP, PtTPTBP ja PtOEP yhdessä TTBPer-annihilaatioaineen kanssa liuotettiin ensin veteen käyttäen kahdesta surfaktantista, CrEL ja T80, valmistetuja misellejä. Vasta tämän jälkeen väriaineet sekoitettiin hydrogeeliin. Työssä haluttiin erityisesti tutkia, voisiko misellien vapautumista hydrogeelistä hidastaa käyttäen hyväksi elektrostaattisia voimia selluloosananokuitujen ja misellien välillä. Tätä varten misellien pintavarausta muokkaamista testattiin kahdella kosurfaktantilla, STA ja DOTAP. Valmistettujen misellien koko, PDI ja ζ-potentiaali mitattiin, ja niiden ylöskonversio-ominaisuuksia tarkasteltiin määrittämällä ylöskonversion tehotiheyskynnys ja kvanttisaanto. Misellien vapautumista hydrogeelistä ja annihilaatioaineen intensiteetin stabiilisuutta vapautuneissa miselleissä seurattiin kuudesta päivästä kahteen viikkoon. Lopulta hydrogeelissä olevien misellien ylöskonversiospektri mitattiin eri viritysvalon voimakkuuksilla.

Työssä osoitettiin, vastoin aluperäistä oletusta, että misellien pintavarauksen muokkaaminen ei parantanut misellien retentiota vaan päinvastoin. Muokatut misellit vapautuivat hydrogeelistä muokaamattomia nopeammin ja annihilaatioaineen intensiteetin stabiilius oli muokatuissa vapautuneissa miselleissä heikompi. CrEL-surfaktantista muodostetut misellit vapautuivat keskimäärin hitaammin kuin T80-surfaktanteista muodostetut misellit. Hydrogeeliin sekoitettujen misellien määrällä huomattiin myös olevan vaikutusta sekä misellien vapautumisnopeuteen että annihilaatioaineen intensiteetin stabiiliuteen. Sekä misellien vapautuminen että intensiteetin lasku oli hitaampaa hydrogeeleissä, joiden misellikonsentraatio oli suurempi. Testatuista herkistinaineista PdTPTBP ja PtOEP vaikuttivat potentiaalisimmilta vaihtoehdoilta fysiologisissa sovelluksissa käytettäväksi. PdTPTBP-TTBPer-parin ylöskonversiosaanto STA-muokatuissa CrEL-miselleissä oli 0.587 % vastaten aiemmin raportoituja arvoja. Lisäksi PdTPTBP-TTBPer-parin ylöskonversiospektri muokkaamattomissa CrEL-miselleissä sekoitettuna hydogeeliin saatiin mitattua, mutta käytetyt eksitaatiotehotiheydet olivat melko korkeita ja täten mahdollisesti soveltumattomia käytettäväksi kudosten ulkoiseen eksitaatioon. PtOEP-TTBPer-parin vapautumisnopeutta ja ylöskonversiota hydrogeelissä ei tässä työssä testattu, mutta kyseisellä parilla saatiin aikaan melko tehokas valon ylöskonversio muokkaamattomissa CrEL-miselleissä vedessä hapen läsnäollessa. Tämä ylöskonversiopari CrEL-miselleissä voisikin olla mielenkiintoinen systeemi, jonka käyttäytymistä voisi tutkia myös hydrogeelissä tulevaisuudessa.

Avainsanat: miselli, hydrogeeli, tripletti fuusio, nanoselluloosa, surfaktantti

PREFACE

This thesis was done in the Supramolecular Chemistry of Bio- and Nanomaterials team in Tampere University during the autumn of 2021 and spring of 2022. I was given this extraordinary chance to work, learn and grow as a scientist by professor Timo Laaksonen and I am forever grateful for this opportunity. Thank you for your gentle guidance and understanding. And thank you my lab mentors, Doctoral Researcher Jussi Isokuortti and especially Dr. Nikita Durandin. Throughout the year you tirelessly guided me through a field of science I previously knew nothing about and that is far from an easy thing to do. I applaud you for your seemingly endless knowledge on the topic that you both clearly care about deeply.

I want to thank both Dr. Elina Vuorimaa Laukkanen and Dr. Alexander Efimov who over these years have helped me to grow into the person I am, both academically and personally. Your encouraging words have helped me to keep going no matter what and thanks to you I am a little bit less scared and a little bit more ready to continue my journey. And to my colleagues in the Festia office, Ramsha, Joko, Iida, Kaisa, Annika and especially you Olga, you managed to lift my spirits up every day with the numerous chats and laughs we shared together. You showed me what a true warm and welcoming work community means, and I will miss each and every one of you.

And to my dear friends. Gille, thank you for offering me both your humor, wisdom and support whenever I needed them. Ella, thank you for keeping my feet on the ground and head in the clouds. And finally Antti, my spouse and best friend, without you I would have never gotten as far as I did, and I am forever thankful for that.

Tampere, 16.5.2022

Emilia Löfman

CONTENTS

LIST OF SYMBOLS AND ABBREVIATIONS

CrEL	Cremophor EL
DCM	dichloromethane
DLS	differential light scattering
DPBS	Dulbecco's Phosphate Buffered Saline
DOTAP	dioleoyl-3-trimethylammonium propane
EO	ethyl oleate
FL	fluorescence
ISC	inter system crossing
NFC	nanofibrillar cellulose
OEP	octaethylporphyrin
PDI	polydispersity index
STA	stearyl amine
T80	Tween 80
TEMPO	2,2,6,6-tetramethylpiperidine-1-oxyl radical
TET	triplet energy transfer
TF	triplet fusion
TF-UC	triplet fusion upconversion
TIPS-An	9,10-((triisopropylsilyl)ethynyl) anthracene
TPA	two photon absorption
TPTBP	tetraphenyl-tetrabenzoporfine
TTBPer	tetra-tertbutyl perylene
SHG	second harmonic generation

$\boldsymbol{A}$	annihilator
$\boldsymbol{a}$	fraction of the reabsorbed emission
α	absorption coefficient
CMC	critical micelle concentration
D	diffusion constant
ΔE_{UC}	Stokes shift, eV
E	energy, eV
$\boldsymbol{f}$	spin statistical factor
f	fraction
I	power density, mW/cm2 or intensity, a.u.
λ	wavelength, nm
m_s	spin quantum number
n	refractive index
η	normalized efficiency
$\boldsymbol{S}$	sensitizer
S	singlet state or spin
T	triplet state
T_K	Kraft temperature, K
τ	lifetime, s
OD	optical density
P	power, W
PD	power density, mW/cm2
r	radius, cm

1. INTRODUCTION

Photon upconversion is a phenomenon where low energy photons are converted into high energy ones, and blue shifted light, as opposed to the excitation wavelength used, is emitted [1–6]. The phenomenon has been adapted to different biological applications such as bioimaging and phototherapy due to the possibility to use long excitation wavelengths falling to the red and near infrared part of the electromagnetic spectrum. Low energy excitation light in this region is not absorbed by biological tissues thus making it able to penetrate deep (up to 1 cm) into them without causing substantial damage. [1,3–6] Then, blue-shifted light can be created inside the tissue and used e.g., as a catalyst for different photo-cleavable reactions utilized in e.g., externally activatable systems for controlled release of drugs [3,5]. There are different methods to produce upconverted light, such as two-photon absorption (TPA), second-harmonic generation (SHG) and lanthanoid ion based upconversion. However, these methods have proven to be challenging for bio-applications due their demand of high excitation intensities or power densities over $1\ \mathrm{W/cm^2}$, or even in the range of $\mathrm{MW/cm^2}$ or $\mathrm{GW/cm^2}$ in the case of TPA and SHG, which can cause damage to the tissues especially over prolonged periods of time. [1,2,4–6]

Triplet-fusion upconversion, TF-UC, has risen as a solution to this problem. Photon upconversion can be induced via TF-UC using lower excitation power densities of about $0.1\ \mathrm{W/cm^2}$ [5] or even less than $10\ \mathrm{mW/cm^2}$, a similar power density as is caused by the sunlight outside [7]. In addition to this, TF-UC is also versatile, since the excitation and upconverted emission wavelength can be tuned depending on the choice of the TF-UC dyes [8,9]. TF-UC has been applied to e.g., photocatalysis and phototherapy [4].

TF-UC is an upconversion process that combines the properties of two different dye molecules in a series of photochemical reactions to emit blue-shifted light. However, even TF-UC is not completely free of challenges, and there are two main obstacles hindering its use in bio-applications. First problem arises from the hydrophobicity of the dye molecules. Solubilization of the dyes is essential to ensure sufficient diffusion of the molecules and thus efficient upconversion of photons. However, hydrophobicity of the dyes delimits their use to often harmful organic solvents instead of bioavailable aqueous environment. Second, the process of TF-UC is extremely sensitive to oxygen. Molecular oxygen quenches effectively the emission of blue-shifted light making it difficult to induce upconversion in physiological conditions. [4,5]

Several systems have been created to solve these problems, with different nanoparticles becoming one of the most popular solutions. **Micelles** are one type of nanoparticle used

for TF-UC. Micelles solubilize the TF-UC dyes in an aqueous environment by storing them in the hydrophobic core of the micelle while allowing them enough mobility and high local concentration to enable efficient upconversion of the incident light. For example, Kohane et. al [10] were able to use the upconverted light produced by green-to-blue upconverting polymeric micelles at low excitation power density ($200\,\mathrm{mW/cm^2}$) to activate photocleavable reaction to release tumour targeting moieties in vivo. For different bio-applications however, simple solution-based systems are often not useful. **Nanofibrillar cellulose hydrogel**, a wood derived biocompatible gel with a high water content, could be one possible material to work as a secondary matrix and reservoir. In addition to this, hydrogel could also work as an additional protection barrier from oxygen. [11]

Auvinen et. al. (unpublished work) studied several different nanoparticles, including micelles, liposomes, and DNA origami, entrapped into anionic nanofibrillar cellulose. They assessed the release rates of these nanoparticles from the cellulose matrix and were able to observe an interesting difference between the nanoparticles. According to their results, generally the smaller the nanoparticle, the faster it got released from the hydrogel matrix. However, liposomes labeled with fluorescent Cy5 dye, exhibited a behaviour deviating from the rest: even though the particles were small (50 nm in diameter), they seemed to be retained in the cellulose matrix. In contrast, similarly sized liposomes labeled with fluorescent NBD dye showed over 20 % release after just one day and roughly 60 % release after 8 days. The difference between these nanoparticles was their surface charge, which for Cy5 labeled liposomes was assumed to be cationic thanks to the structure of the dye. Thus, it was hypothesized that cationic surface charge could interact with the anionic charge of the nanofibrils and prevent them from leaking out of the gel.

With this hypothesis in mind, there are two objectives for this research. First objective is to formulate positively charged micelles containing dye molecules able to produce TF-UC. Second objective is to incorporate these micelles are into anionic nanocellulose hydrogel and study the stability, i.e., release of the micelles from the hydrogel, and upconversion properties of this system.

This work is divided into two parts. First, the theoretical overview on TF-UC, and its use in micelles and nanocellulose hydrogel is introduced. In the second experimental part the different micellar formulations with varying TF-UC properties are studied for their upconversion properties and stability in both water and nanocellulose hydrogel. Results are analysed to assess the best working micelle formulation out of the ones studied and suggestions are given for the future work to improve the retention and upconversion properties of micelles in hydrogel.

2. TRIPLET FUSION UPCONVERSION

2.1. Basic Concepts to Understand TF-UC

Before diving into the detailed explanation of triplet fusion upconversion, let us first go through some of the fundamental terms of photochemistry to aid a more in-depth understanding of the phenomenon at hand.

An electronic state is the quantized energy level of an atom or a molecule corresponding to a certain distribution of the electrons present in the system. For atoms, the electronic state or energy level is different for different electron configurations whereas for molecules the distribution of electrons is determined by the formation of molecular orbitals forming a molecular electron configuration. [12]

Spin multiplicity states the type of electronic state of the atom or molecule. It is determined as

$$Spin\ multiplicity = 2S + 1 \tag{1}$$

Here, S is the total spin of the atom or molecule at hand and is determined as a sum of its electrons' spin quantum numbers

$$S = \sum m_s \tag{2}$$

where m_s is the spin quantum number of the electron, having either the value $+\frac{1}{2}$ or $-\frac{1}{2}$ (spin up (↑) or spin down (↓)). If $spin\ multiplicity$ has the value of 1 ($S = 0$) the overall electronic state is called **a singlet state,** and if $spin\ multiplicity$ has the value of 3 ($S = 1$) the overall electronic state is called **a triplet state**. [12] The effect of the electron spin on the electronic state are demonstrated in the Figure 1 below.

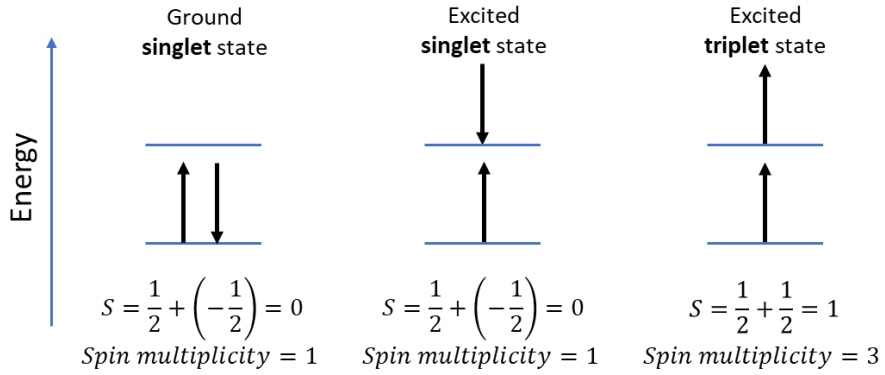

Figure 1. *Electronic states of two electron system: ground singlet state, excited singlet state, and excited triplet state.*

Different electronic states are denoted as S_0 for the ground singlet state, $S_i, i > 0$ for the excited singlet states (1st, 2nd, and so on) and T_0 and $T_i, i > 0$ similarly for triplet states. [12]

The Jablonski diagram (in Figure 2) illustrates different transitions between the electronic states of a molecule when it absorbs and emits light. The diagram shows the energetic relations between the different electronic states (bolded horizontal lines, S_i for singlet states and T_i for triplet states) as well as some of the vibrational energy states, v of each electronic state (thin horizontal lines) that arise from the movement of the molecule's atoms relative to one another. It is also worth mentioning that the energy of a triplet state (purple) is often lower than that of the singlet state (black) it corresponds to (e.g., T_1 has lower energy than S_1) [12]. [13]

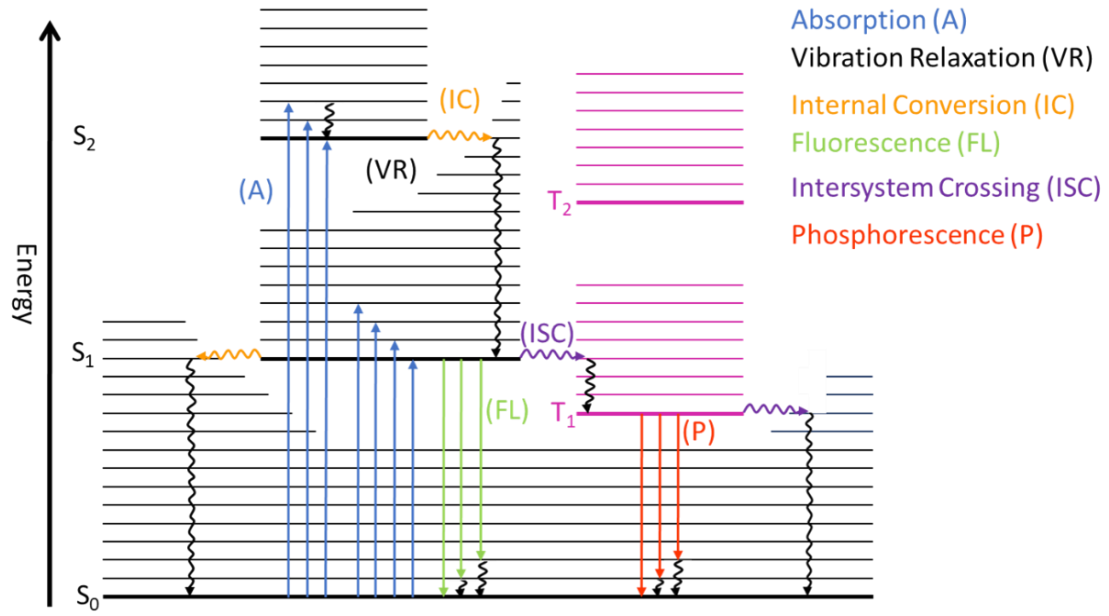

Figure 2. *Different photochemical processes illustrated by the Jablonski diagram. Bolded horizontal lines represent the different electronic states (S_i or T_i) and thin horizontal lines the vibrational energy states (v) of each electronic state arising from the movement of the molecule's atoms relative to one another.*

A molecule forms an excited state upon absorption of a photon. This causes the promotion of an electron from the ground singlet state S_0 to an excited singlet state. The newly formed excited state can then decay back towards its lowest energy ground state via various radiative and non-radiative processes that are depicted in Figure 2. [13]

The non-radiative processes relax or transfer the energy of the system without the emission of photons. Upon **vibrational relaxation,** the excited molecule with an excess of vibrational energy (e.g., $S_1(v = 2)$) collides with another molecule, e.g., a solvent molecule and relaxes to the lowest vibrational state of the electronic state it is at (e.g.,

$S_1(v = 0)$). This relaxation generally happens right after absorption and before any other type of relaxation/transition since these generally start from the lowest vibrational state of an electronic state (see Figure 2). **Internal conversion** is a transition between two isoenergetic vibronic states of the same $spin\ multiplicity$ and the same total energy, i.e., the transition from the lowest vibrational state of some excited singlet state to some vibrational state of the singlet state energetically below it (e.g., $S_2(v = 0) \rightarrow S_1(v = 2)$). **Intersystem crossing** on the other hand is the transition between two isoenergetic vibronic states with different $spin\ multiplicities$, and it is generally the transition from the lowest vibrational state of the first excited singlet state to some vibrational state of the excited triplet state (e.g., $S_1(v = 0) \rightarrow T_1(v = 2)$). [13]

Generally, there are two types of radiative decay processes. **Fluorescence** is the spin allowed transition between electronic states with the same $spin\ multiplicity$, which is generally the transition from the lowest vibrational state of the first excited singlet state to some vibrational state of the ground singlet state (e.g., $S_1(v = 0) \rightarrow S_0(v = 2)$). **Phosphorescence** on the other hand is the spin forbidden transition between electronic states with different $spin\ multiplicities$, i.e., from the lowest vibrational state of the first excited triplet state to some vibrational state of the ground singlet state (e.g., $T_1(v = 0) \rightarrow S_0(v = 2)$). Fluorescence is a fast decay process with the **lifetime** i.e., the time it takes for the concentration of excited molecules to decrease to $1/e$ ($\approx 36.8\,\%$) of the initial concentration, ranging from $10^{-12}\,s$ to $10^{-6}\,s$. Phosphorescence lifetimes are notably longer ($10^{-3} - 10^{2}\,s$) since it requires the extremely improbable spin-flip from triplet state to singlet state to happen. [13]

2.2. Theory and Mechanism of TF-UC

Both radiative processes mentioned in chapter 2.1 feature the **Stokes shift** i.e., the shift to the lower energy (redshift) between the absorbed and emitted light [6]. This means that the peak of the absorption (or excitation) spectrum has a lower wavelength (i.e., higher energy) than the peak of the emission spectrum (higher wavelength i.e., lower energy). This happens due to relaxation of the system via different non-radiative vibrational processes alongside the radiative processes. Due to these non-radiative processes and the requirement of energy conservation, the absorbed light has higher energy than the emitted light.

Thus, it would seem improbable to be able to have a system that can do the exact opposite: to emit light at a shorter wavelength (higher energy) than what it was excited with. However, this energy shift, called **anti-Stokes shift,** ΔE_{UC} [4] is possible, and it can

be created by processes that combine the energy of different excitation sources like heat or additional photons. There are different processes able to do this: two photon absorption (TPA) (absorption of two photons simultaneously via virtual non-stationary energy state), second-harmonic generation (SHG) (frequency doubling of photons without absorption), lanthanoid ion based upconversion (subsequent absorption of photons via long-living intermediate energy state), hot-band absorption (combination of thermal energy and light absorption) and **triplet fusion upconversion (TF-UC)**, also known as triplet-triplet annihilation upconversion, TTA-UC, a second-order reaction, where higher energy photons are created via real excited intermediate state. [1,5,6]

Triplet fusion upconversion (TF-UC) was first described by Parker and Hatchard in the early 1960s when they were able to observe anti-Stokes delayed fluorescence in a molecular system consisting of phenanthrene or proflavin hydrochloride as so-called **sensitizers** and naphthalene and anthracene as **annihilators or emitters** [14]. These systems corresponded to anti-stokes shifts of $\Delta E_{UC} = 0.21 - 0.43\ \mathrm{eV}$ (i.e., the shift from 341 or 362 nm (UV) to 322 nm (UV)) for phenanthrene/naphthalene system and $\Delta E_{UC} = 0.22\ \mathrm{eV}$ (i.e., 436 nm (visible) to 402 nm (visible)) for proflavine hydrochloride/anthracene system [4].

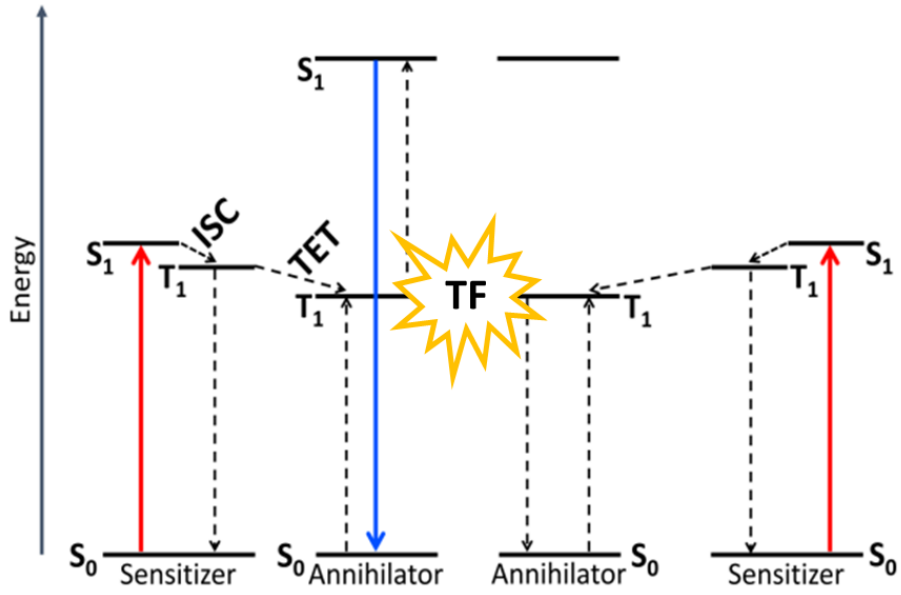

Figure 3. *Radiative and non-radiative transitions of triplet fusion upconversion. Electronic states are denoted as S_0 for the ground singlet state, S_1 for excited singlet state and T_1 for the excited triplet state, and the transitions between electronic states are denoted as ISC for inter-system crossing and TET for triplet energy transfer. Finally, TF stands for triplet fusion of two annihilator triplets. Modified with permission from [15].*

TF-UC process combines the properties of the sensitizer and annihilator molecules in a series of radiative and non-radiative processes forming a molecular system able to convert low energy photons into higher energy ones. The schematic presentation of the exact

mechanism is provided in Figure 3. The TF-UC process proceeds as follows: first, the sensitizer molecule $\boldsymbol{S}$ absorbs the excitation light ($\boldsymbol{S}(S_0) \rightarrow \boldsymbol{S}(S_1)$), and after this it undergoes non-radiative **intersystem crossing (ISC)** from excited singlet state to the excited triplet state ($\boldsymbol{S}(S_1) \rightarrow \boldsymbol{S}(T_1)$). Then, via **triplet-triplet energy transfer (TET),** the energy of excited triplet state of the sensitizer is transferred to the ground state of an annihilator $\boldsymbol{A}$ generating an excited triplet state via Dexter energy transfer mechanism [16] ($\boldsymbol{S}(T_1) \rightarrow \boldsymbol{A}(S_0) \rightarrow \boldsymbol{A}(T_1)$). Now, when two triplet state annihilators collide, **triplet fusion** (also known as **triplet-triplet annihilation**) occurs and, via employing the energies of the two annihilator triplet states, one annihilator is promoted to its excited singlet state annihilator while the other returns to its ground singlet state ($\boldsymbol{A}(T_1) + \boldsymbol{A}(T_1) \rightarrow \boldsymbol{A}(S_1) + \boldsymbol{A}(S_0)$). When the excited annihilator relaxes the system emits via fluorescence ($\boldsymbol{A}(S_1) \rightarrow \boldsymbol{A}(S_0)$) at a shorter wavelength than what was initially absorbed by the sensitizer [4,6,17,18].

Naturally, not every pair of molecules will be able to work as a TF-UC system. To obtain efficient upconversion of the incident light, both the sensitizer and annihilator must meet certain requirements. The **sensitizer** must be able to absorb the incident light efficiently (i.e., have a high molar extinction coefficient at the desired excitation wavelength), have an intersystem crossing quantum yield of near unity ($\Phi_{\mathrm{ISC}} \sim 1$) to efficiently start the series of energy transfer processes and exhibit a long triplet state lifetime ($> 10\ \mu\mathrm{s}$) to ensure the efficiency of the diffusion (i.e., collision) based triplet-triplet energy transfer from sensitizer triplet state to the annihilator ground state. The **annihilator** must likewise have a long triplet state lifetime ($> 100\ \mu\mathrm{s}$) to further enable efficient triplet fusion (TF) of two annihilator triplet states, and high fluorescence quantum yield ($\Phi_{\mathrm{FL}} \sim 1$) to efficiently observe the upconversion of the incident light. [17,18] Additionally, the probability of generating an excited singlet state upon the fusion of the two annihilators, **described by spin statistical factor, $\boldsymbol{f}$**, should be near unity [4,19].

The sensitizer and annihilator must meet some energetic requirements as well. These are shown also in Figure 3. Firstly, the sensitizer excited singlet state must naturally have lower energy than that of the annihilator (i.e., $E(\boldsymbol{S}(S_1)) < E(\boldsymbol{A}(S_1))$) [18]. This ensures that the emitted light has a shorter wavelength than the light the system initially absorbed (i.e., the anti-Stokes shift). Secondly, the energy gap between the sensitizer singlet and triplet states should be small (i.e., $E(\boldsymbol{S}(S_1)) \sim E(\boldsymbol{S}(T_1))$) so that the energy loss during the inter-system crossing is minimized [17]. Thirdly, the sensitizer triplet state should have higher energy than that of the annihilator (i.e., $E(\boldsymbol{S}(T_1)) > E(\boldsymbol{A}(T_1))$), and the energy difference should be high enough to make the process of triplet-triplet energy transfer diffusion controlled and thus more favourable [18]. Finally, to make triplet fusion of annihilator

energetically favourable, the energy of the annihilator singlet excited state should be slightly lower or equal to the sum of the energies of the two fusing annihilator triplet states (i.e., $E(\boldsymbol{A}(S_1)) \leq 2E(\boldsymbol{A}(T_1))$) [6,7]. So, to have an efficient TF-UC system, the energetic order of the sensitizer and annihilator singlet and triplet states should be as such:

$$E(\boldsymbol{A}(T_1)) < E(\boldsymbol{S}(T_1)) \sim E(\boldsymbol{S}(S_1)) < E(\boldsymbol{A}(S_1)) \leq 2E(\boldsymbol{A}(T_1))$$

In addition to this, the combined energy of two **sensitizer** triplet states should be lower than the second excited triplet state of the **sensitizer** (i.e., $2E(\boldsymbol{S}(T_1)) < E(\boldsymbol{S}(T_2))$), since this could work as a competing relaxation channel [17].

2.3. Molecules for TF-UC

Several molecules can be utilized in TF-UC. For sensitizers, the most commonly used molecules include Ru(II) polypyridyls, Pt(II), and Pd(II) porphyrin and phthalocyanine complexes and cyclometallated Pt(II) complexes as well as supramolecular chromophores with high molar extinction coefficients to ensure strong absorption at the excitation wavelength [5]. For annihilators, especially rubrene, perylenes, anthracenes and borodipyrroles are commonly used. [20]

In our research, we used three different porphyrine complexes, palladium (II) and platinum (II) tetraphenyl-tetrabenzoporfine (PdTPTBP and PtTPTBP) and platinum (II) octaethylporphyrin (PtOEP) as sensitizers and a perylene compound, tetra-tertbutyl perylene (TTBPer), as an annihilator. The photochemical properties of each sensitizer-annihilator pair are presented in the Table 1 below, and the chemical structures of the molecules are presented in the Figure 4.

Table 1. *Photochemical properties of each sensitizer-annihilator pair: λ_{abs} is the wavelength of the absorption maximum of the sensitizer, λ_{em} the emission wavelength of the annihilator, E_{abs} and E_{em} are the energies corresponding to λ_{exc} and λ_{em} and ΔE_{UC} is the anti-stokes shift of the system. Values for sensitizers (λ_{abs} and E_{abs}) from* [18] *and for annihilator (λ_{em}) from* [21].

TF-UC pair	λ_{abs}, [nm]	E_{abs}, [eV]	λ_{em}, [nm]	E_{em}, [eV]	ΔE_{UC}, [eV]	Upconversion
PdTPTBP- TTBPer	633	1,96	460	2,70	0,74	red to blue
PtTPTBP- TTBPer	635	1,95	460	2,70	0,75	red to blue
PtOEP- TTBPer	533	2,33	460	2,70	0,37	green to blue

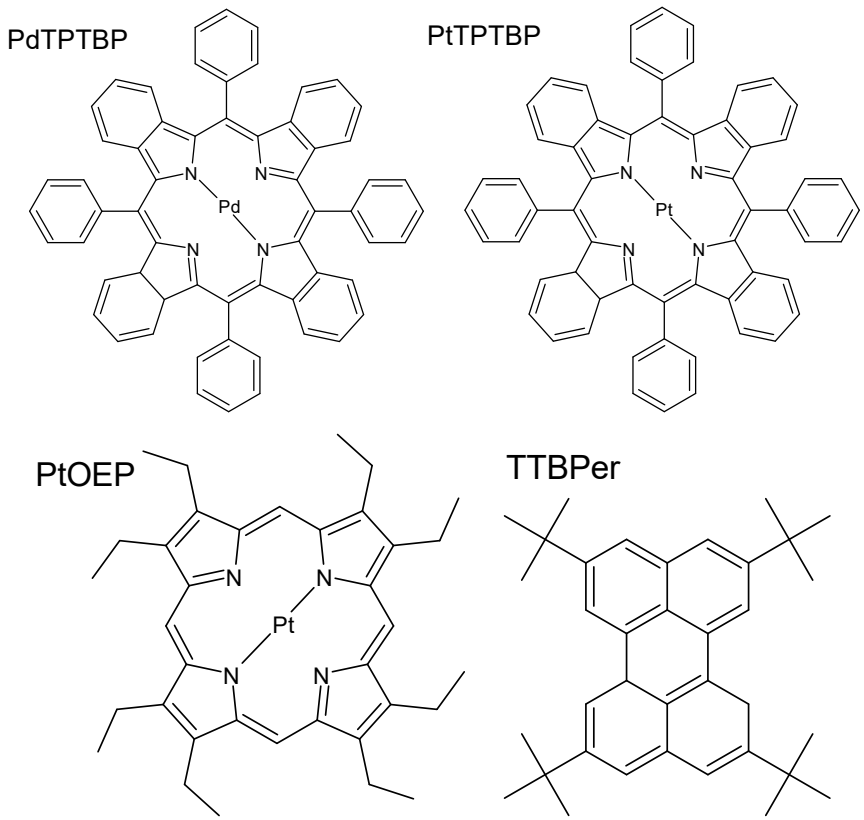

Figure 4. *Molecules used in this study: Sensitizers palladium (II) meso-tetraphenyl-tetrabenzoporphyrin (PdTPTBP), platinum(II)tetraphenyl-tetrabenzoporphyrin (PtTPTBP) and platinum (II) octaethylporphyrin (PtOEP), as well as annihilator 2,5,8,11-tetra-tert-butylperylene (TTBPer).*

Heavy metal coordinated complexes like the porphyrine compounds presented above not only have long triplet lifetimes at room temperature [4] but they are also able to absorb and emit close to the red and near infrared region of the spectrum thanks to their π-conjugated aromatic rings [9,18]. Usually the heavy metals used in the complexes are precious metals like Pt(II), Pd(II), Ir(III), Ru(II) or Re(I) because of their heavy atom effect enabling efficient ISC of the complex, but also a non-precious metal complex with Zn(II) has been successfully used in TF-UC [8]. The emitter molecule TTBPer is also an aromatic hydrocarbon [7], and it was chosen due to its unity efficiency in regards of singlet excited state generation via triplet fusion [19].

2.4. Efficiency of TF-UC

To demonstrate the efficiency of TF-UC, in addition to the anti-stokes shift ΔE_{UC}, there are two crucial parameters to consider: upconversion quantum yield, Φ_{UC} and power density threshold, I_{th} [22]. In this section, we will go through the definitions of these two parameters, their relation to each other and their contribution to describe the efficiency and applicability of a sensitizer-annihilator pair for different applications.

Quantum yield, Φ is defined in general photochemistry by IUPAC as the "number of defined events occurring per photon absorbed by the system" [23]:

$$\Phi = \frac{number\ of\ events}{number\ of\ photons\ absorbed} \tag{3}$$

However, since TF-UC consists of a series of different processes, they all affect the overall quantum yield of the upconversion. The **upconversion quantum yield**, Φ_{UC} is defined by the equation 4

$$\Phi_{UC} = \frac{1}{2}\boldsymbol{f}\Phi_{ISC}\Phi_{TET}\Phi_{TF}\Phi_{FL} \tag{4}$$

where the $\boldsymbol{f}$ is the spin statistical factor, i.e., the probability of two fusing annihilators generating an excited singlet, and Φ is the quantum yield of each process of TF-UC (Φ_{ISC} of the intersystem crossing of the sensitizer, Φ_{TET} of the triplet-triplet energy transfer from sensitizer to annihilator, Φ_{TF} of the fusion of two annihilator triplets and Φ_{FL} of the fluorescence of the formed annihilator singlet). The multiplier $\frac{1}{2}$ is needed because for every emitted upconverted photon 2 photons of the incident light must be absorbed (the term $\boldsymbol{f}\Phi_{ISC}\Phi_{TET}\Phi_{TF}\Phi_{FL}$ alone represents just one sensitizer-annihilator molecule pair). This causes the maximum TF-UC quantum yield to be only 50%. [4] In contrast, for a traditional photochemical process, e.g., fluorescence, the maximum quantum yield is 100% because for every photon absorbed a new photon is emitted.

Castellano, Hanson, and Schmidt have proposed **normalized upconversion efficiency,** η_{UC} to be used instead of upconversion quantum yield, and it is defined as [24]

$$\eta_{UC} = 2 \times \Phi_{UC} \tag{5}$$

This was suggested mainly to clear the confusion between reported quantum yield values as well as to report the values in a more self-explanatory manner [24]. Later however, an overview from ACS Energy Letters [25] has been published where this normalization practice is discouraged due to inconsistent reporting practices in the field. In this work we report the efficiency of TF-UC using the traditional upconversion quantum yield Φ_{UC} as presented in equations 3 and 4 since we believe this to be the most truthful representation of the phenomenon.

Experimentally, upconversion quantum yield can be determined by using a standard for which the quantum yield is known. The upconversion quantum yield can be then calculated as

$$\Phi_{UC} = \Phi_{std}\left(\frac{OD_{std}}{OD_{unk}}\right)\left(\frac{I_{unk}}{I_{std}}\right)\left(\frac{n_{std}}{n_{unk}}\right)^2 \tag{6}$$

where OD is optical density or absorbance at the excitation wavelength, I is the integrated fluorescence intensity and n is the refractive index of the solvents used for sample and standard. Subscript std refers to the standard and unk refers to the upconverting sample. [18]

Next, let us look at **power density threshold**, I_{th}, the other parameter used to describe TF-UC. Power density threshold is the excitation power density PD_{exc} that allows half of the annihilator triplets to fuse and relax as upconverted light. Alternatively, it can also be defined as the excitation power density needed to reach half of the maximum possible quantum yield. [26]

If the excitation power density is very low in respect to the threshold value, the number of annihilator triplets generated is too small for them to collide and fuse within their lifetime and thus efficiently emit upconverted light. As the excitation power density is increased gradually closer to the threshold value, more annihilator triplets are generated, and their fusions become more probable. This is observed as a quadratic dependence between excitation power density and upconversion emission intensity (in this study referred to as **weak annihilation regime**). On the other hand, at high excitation power densities exceeding the threshold, the number of annihilator triplets grows large enough for most of these triplets to collide and fuse making the probability of annihilator triplet fusion mediated relaxation near unity ($\Phi_{TF} \approx 1$). This can be observed as a linear dependence between the excitation power density and upconversion emission intensity (**strong annihilation regime**). [27]

The value of I_{th} depends on the absorption coefficient α of the sensitizer, the efficiency of the triplet-triplet energy transfer Φ_{TET} from sensitizer to annihilator, diffusion constant of annihilator triplets D_T, the distance a_0 between annihilator triplets as well as their lifetime τ_T as described in the equation 7

$$I_{th} = \frac{1}{\alpha \Phi_{TET} 8\pi D_T a_0 (\tau_T)^2} \tag{7}$$

From this, it can be deduced that to achieve the low values of I_{th} required for biological applications, the upconversion system must have a high triplet-triplet energy transfer efficiency between the sensitizer and annihilator triplets as well as notable diffusion and long lifetimes of annihilator triplets. [4]

I_{th} is commonly determined by measuring upconversion emission intensity using different excitation power densities and plotting them in a double logarithmic scale (**cross-section method**). Then, two slopes are fitted to the data: slope of 2 that corresponds to the weak annihilation and slope of 1 that corresponds to the strong annihilation regime. The value

of I_{th} is then found at the cross-section of these two slopes. [4,26,27] However, this method is not reliable if the upconversion system does not fully reach the annihilation regimes [27]. In this case it might be possible to use the **formal definition** of I_{th}: at $PD_{exc} = I_{th}$ the upconversion system reaches half of its maximum possible upconversion quantum yield. This is done by plotting the excitation power density against the fraction of maximum possible quantum yield, f_Φ, which can be calculated as [22]

$$f_\Phi = \frac{I_{em}}{I_{em,max}} \times \frac{PD_{exc,max}}{PD_{exc}} \times 100\% \quad (8)$$

where I_{em} is the upconversion emission intensity at the varied excitation power density PD_{exc}, and $I_{em,max}$ is the upconversion emission intensity at the maximum excitation power density $PD_{exc,max}$. To use this relation, the strong annihilation regime and thus maximum possible upconversion quantum yield must be achieved with the maximum excitation power density $PD_{exc,max}$. So, if $I_{em} = I_{em,max}$ at $PD_{exc} = PD_{exc,max}$, then $f_\Phi = 100\%$. In the plotted data, the weak annihilation regime is seen as the increase in f_Φ as PD_{exc} is increased and as a plateau ($f_\Phi = 100\%$) at high PDs near $PD_{exc,max}$ where the overall upconversion quantum yield is constant at its maximum [27].

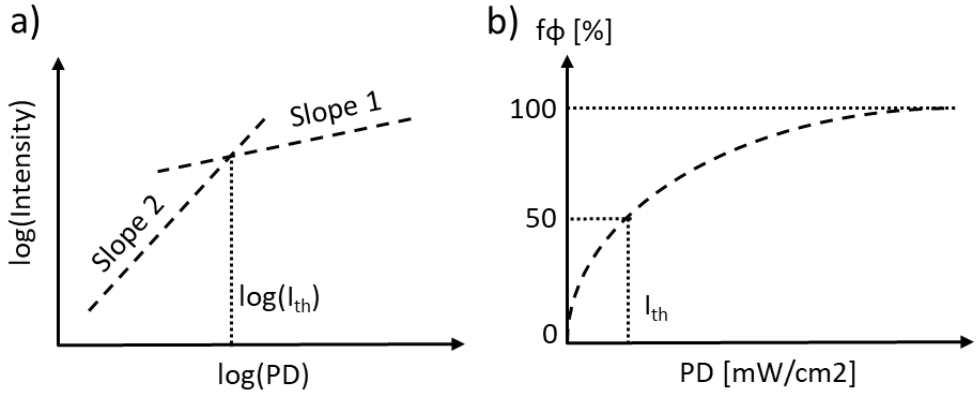

Figure 5. *Demonstration of a) cross-section method and b) formal definition method of determining power density threshold, I_{th} [mW/cm2]. PD is the excitation power density, f_Φ is the fraction of maximum possible quantum yield of the system and intensity is the upconversion emission intensity.*

In this study we have mainly used the abovementioned formal definition, because the weak annihilation regime was not reached in all experiments before the PD_{exc} became too small to induce upconversion emission high enough to observe. However, we have made sure that the slope of 1 in a double logarithmic plot of PD_{exc} vs I_{em} (strong annihilation regime) was reached.

2.5. Quenching of TF-UC by Oxygen

The efficiency of TF-UC can be challenged by many variables, including the choice of molecules, their relative concentrations, and even thermal conditions. However, the effect of molecular oxygen present in the atmosphere at around 21% might be one of the biggest obstacles for TF-UC applications. Just a small amount, even as low as $2 - 10\ ppm$ of molecular oxygen [7], already affects upconversion significantly. This is because the ground state of molecular oxygen is a triplet state, and it can thus react with the triplet states of either a sensitizer or an annihilator quenching the upconversion process. The formed singlet oxygen is also highly reactive, and it can further damage the system by photobleaching the chromophores. [5,7]

The effect of molecular oxygen can be decreased by few different methods. One way is to choose sensitizer and annihilator so that the rates of both TET and TF are higher that the competing reactions with molecular oxygen [5]. However, since this is not always possible, other ways must be considered for the upconversion system to work. Traditional approach to this is to degas the upconversion system but over the past few years other systems have been designed to make TF-UC achievable in the presence of oxygen [28].

There are two main approaches to protect the upconversion system. First approach is so-called **passive protection** where the sensitive molecules are placed behind a physical barrier (e.g., polymer matrix or nanocarriers) that protects them from atmospheric oxygen. The barrier can lower the solubility or permeability of oxygen and prevent its diffusion to the upconverting dyes. The second method is to use **active protection** by incorporating oxygen scavenging species to the upconversion solution. These scavengers react with the oxygen (triplet or singlet) and thus remove it from the system. [5,7] There are different types of scavengers that work on different principles. Sodium sulfite, a common oxygen scavenger in solution reacts with ground state molecular oxygen producing sodium sulfate. Hydrophobic substances like oleic and linoleic acid as well as hyperbranched unsaturated polyphosphates on the other hand rely on their unsaturated double bonds that react with singlet molecular oxygen creating peroxide derivatives. [5,7]

Passive and active protection strategies can be also combined into a **dual-protection system** for the UC process. Main example of this is the incorporation of oxygen scavengers into nanoparticles holding the TF-UC molecules, thus creating upconverting oil-core nanoparticles. [5] Oil inside a nanoparticle works as a scavenger of oxygen but it also creates a hydrophobic environment to aid the diffusion of dyes thus increasing the efficiency of TF-UC while the shell of the nanoparticle either prevents or hinders the diffusion of oxygen to the upconversion dyes. For example, edible soybean oil (which

contains both oleic and linoleic acid [5]) has been used as an oxygen scavenging solvent inside soft nanocapsules formed with bovine serum albumin (also considered as oxygen scavenger [5]) and dextran [29,30]. Oleic acid has been similarly used in nanocapsules made from silica [31].

In the next chapter we will look more closely to one dual-protection system that can allow TF-UC to happen in biorelevant conditions in the presence of oxygen and water.

3. TF-UC IN MICELLES AND NANOCELLULOSE HYDROGEL

Different approaches can be used to make the process of TF-UC more practical for biological systems. As we saw in the last chapter, the TF-UC process has great advantages over other light up-conversion processes, mainly due to its ability to work efficiently at low irradiation intensities and its potential to produce a large anti-stokes shift. However, the main disadvantages of the TF-UC process are also those that can hinder its usability for bio-applications the most. Main disadvantages of TF-UC are the hydrophobicity of the TF-UC dyes, i.e., their inability to dissolve in water, and sensitivity of the system to molecular oxygen.

As discussed in the previous chapter, different approaches can be taken when combatting these issues. While the hydrophobicity of the dyes could be solved with chemical modification, this is often not practical or even possible [32]. In our research we resorted to using **micelles**, colloidal nanostructures formed by amphiphilic surfactants [33] as our dye solubilization and potential oxygen protection vehicle. Micelles have a hydrophilic shell making them soluble in an aqueous environment, while storing the hydrophobic TF-UC dyes in their lipophilic core. Additionally, by incorporating oxygen scavenger of choice into the core of a micelle alongside with the dyes, the TF-UC pair could also potentially be protected from molecular oxygen both actively and passively.

To expand the number of possible applications of TF-UC, upconverting nanoparticles could be used further as dopants for secondary matrixes like polymer films. The secondary matrix, in addition to providing a different platform for TF-UC needed in a variety of applications, could also work as an additional protection barrier from oxygen [11]. In this work TF-UC is introduced in **nanofibrillar cellulose hydrogel** using micelles as dye compartments to ensure the solubilization and high enough local concentration of dyes to induce TF-UC. The first part of this chapter is dedicated to micelles: their structure, properties and use in TF-UC as solubilization vehicles and protectors from atmospheric oxygen. The second half describes the properties nanocellulose hydrogel making it an excellent material for different bio-applications and describes an example of introducing TF-UC in a hydrogel network.

3.1. Micelles as Efficient Upconversion Nanounits

Micelles are conventionally formed via self-assembly of **surfactants** (surface active agents); amphiphilic compounds having an ionic or non-ionic hydrophilic group (head) and

hydrophobic (i.e., lipophilic) group (tail). This class of molecules can lower surface or interfacial tension between mediums (gas-liquid, e.g., air-water or liquid-liquid, e.g., oil-water), and it includes a variety of molecules: soaps, polar molecules like alcohols or amines with long hydro-carbon chains as well as lipids to name a few. The molecules self-assemble into usually spherical shapes to minimize energetically non-optimal interactions between the solutes and the solvent. Depending on the solvent, the surfactants can form in two ways. **Regular micelles** are formed in the aqueous environment where the hydrophilic heads face towards the solvent forming the shell of the micelle while the hydrophobic tails face each other forming the core of the micelle. **Reverse micelles** on the other hand are formed in lipophilic solvent where the lipophilic tails face towards the solvent while the hydrophilic heads form the micelle's core. [33]

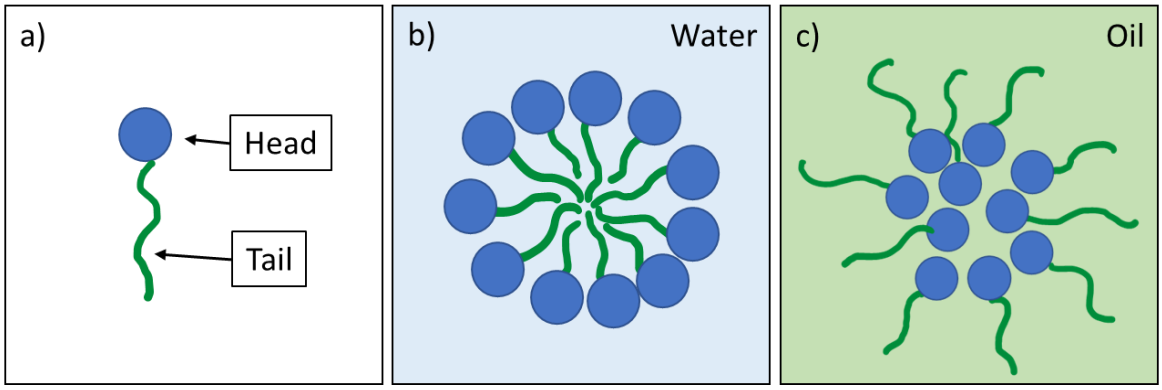

Figure 6. *General structures of (a) surfactant with a hydrophilic head (blue) and hydrophobic tail (green), (b) regular micelle in hydrophilic solvent and (c) reverse micelle in hydrophobic solvent.*

Surfactants form micelles in a solution only after certain criteria are met, and there are two main factors at play in the micellization process. Firstly, the concentration of surfactants must exceed a certain threshold, **critical micelle concentration (CMC)**, for the micelles to form. After this concentration is exceeded in the solution, any new surfactants added will aggregate into micelles instead of adsorbing to the interface of the solvent and air. This is demonstrated in the Figure 7. For a surfactant, CMC can be determined using a variety of methods, e.g., tensiometry, fluorometry or conductometry. Formation of the micelles is detected by measuring the physical variable of choice as a function of surfactant concentration, and CMC is considered as the disruption point where the trend of the plot changes. However, it is important to notice that CMC values obtained by different methods vary slightly. [33,34]

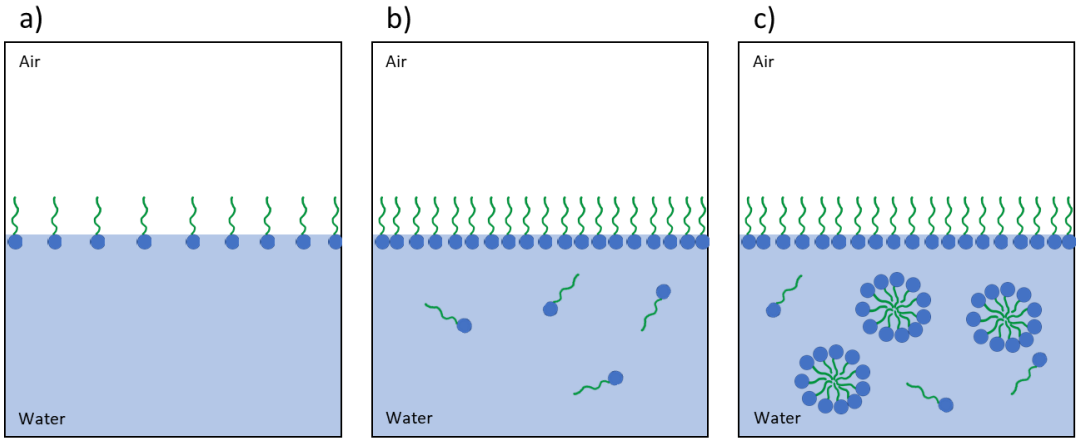

Figure 7. *Progress of the formation of regular micelles in hydrophilic solvent (water). Micelles appear only after a certain threshold concentration, i.e., Critical Micelle Concentration (CMC) is exceeded. Surfactants will first crowd the interface (a) after which singular surfactants start to appear in solution (b). Once there are enough free monomeric surfactants in the solution, surfactants aggregate into micelles (c).*

Secondly, the system must reach a certain temperature before micellization can start. This is the temperature at which the solubility of the surfactant equals the CMC, namely the **Kraft temperature**, T_K. Below this temperature micellization cannot occur, since the overall solubility of the surfactant cannot reach CMC, meaning its total amount in the solvent is too small for the aggregates to form. [35] However, if the temperature reaches high enough value, phase separation occurs upon desolvation of the polar heads of non-ionic surfactants causing the solution to become turbid. This temperature is referred to as **cloud point**. The phase transitions of the micellar system can be demonstrated with a phase transition map (Figure 8) showing the relation between the temperature and surfactant concentration of a micellar solution. [33]

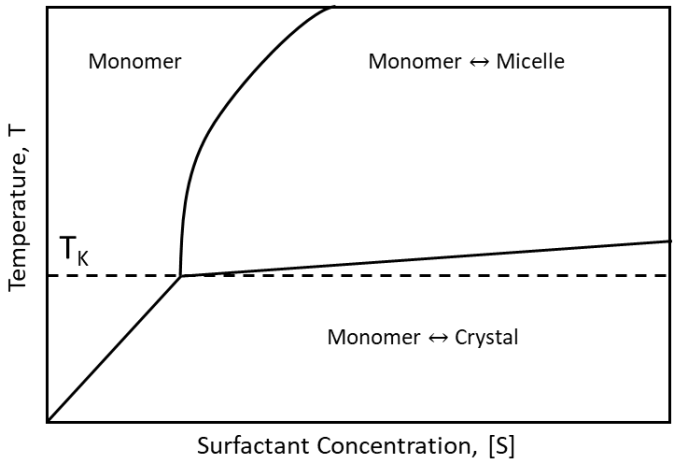

Figure 8. *General representation of a phase transition map of a micellar system, based on [33].*

Alongside with the temperature and surfactant concentration dependence, electrolytic additives like salt can also affect the micellization process. Addition of electrolytes can make the micellization process more thermodynamically favourable by lowering the repulsion of headgroups in ionic surfactant micelles and thus lowering the CMC of these micelles. Electrolytes are shown to lower the surface tension of anionic surfactant solutions and cause the formation of generally larger micelles and swelling of micelles formed by sodium dodecyl sulphate. [36]

Surfactants are generally used to help solubilization of hydrophobic compounds in hydrophilic environment and vice versa. This **micellar solubilization** happens when the insoluble components are entrapped inside the micelle core while the micelle shell makes the entire aggregate soluble producing a type of **microemulsion**. Generally, there are three different classes of microemulsions: oil-in-water (O/W) microemulsion, water-in-oil (W/O) microemulsion and bi-continuous microemulsion. These consist of swollen regular micelles in hydrophilic solvent (O/W), swollen reverse micelles in hydrophobic solvent (W/O) or almost equal parts of both hydrophobic and hydrophilic compounds homogenized into a droplet mixture with the help of surfactants. [37] (Chapter 2)

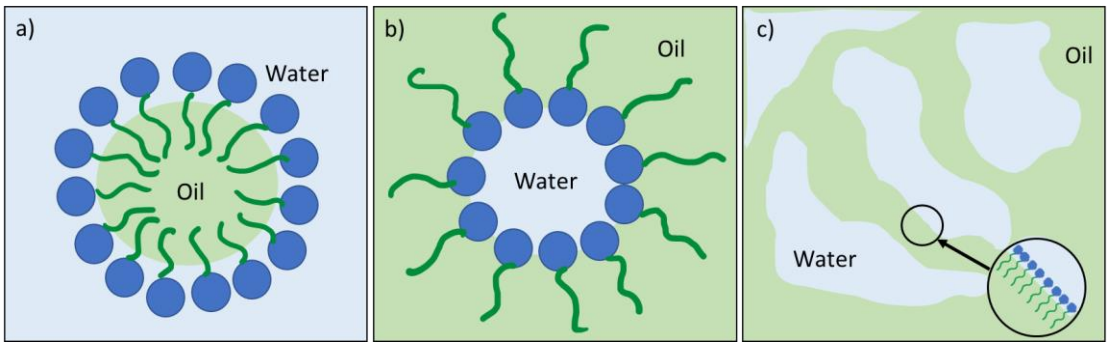

Figure 9. *Micellar solubilization: a) swollen regular micelle (oil-in-water microemulsion), b) swollen reverse micelle (water-in-oil) and c) bi-continuous microemulsion with almost equal parts of water and oil stabilized with surfactants. Based on [37] (Chapter 2).*

Occasionally the conventional micelles formed by just one surfactant lack properties desired in either research or industry. **Mixed micelles**, formed by two or more different surfactants, are usually prepared to improve the micellization process as well as the overall properties of the micelle. The choice of surfactants affects the main variables of micelle formation: CMC, Kraft point and cloud point usually by making the micellization process more favourable. Two-component mixed micelles can be divided into different groups based on the choice of the surfactant pair. Both surfactants can be similar, either non-ionic or ionic, or one surfactant can be ionic and one non-ionic. In the case of non-ionic/ionic micelles, the CMC is usually lower due to smaller electric or steric repulsion between the head groups. [37] (Chapter 3)

Different micellar nanocarriers have been used before for TF-UCs [10,30,32,38–40]. Polymeric micelles hosting PdOEP–DPA (PdOEP = octaethylporphyrin palladium complex and DPA = 9,10-diphenylanthracene) [39] and PtTPTBP – BODIPY (BODIPY = boron-dipyrromethene) [30] sensitizer- annihilator pairs have been prepared from non-ionic copolymer Pluronic F127 with alternating hydrophilic and hydrophobic blocks and coated with silica. Both micellar systems showed upconverted emission in aqueous environment with the PdOEP – DPA pair having higher quantum yield probably due to the oxygen scavenging ability of DPA [5]. Pluronic F127 micelles have also been formulated with trichlorobenzene as the oily core which provides more mobility and reduces aggregation of the dyes [40]. Another block copolymer, polyoxyethanyl α-tocopheryl sebacate (PTS) has also been used as a surfactant and solubilizing agent in water for PdTPTBP – perylene pair [32].

Also more conventional surfactants have been used for upconverting micelles in the presence of ambient oxygen. Tween 20, polyoxyethylene (20) sorbitan monolaurate, has been used to prepare oil-in-water (toluene-water) microemulsion for Pd(II)tetratolylporphyrin - 9,10-dinaphthylanthracene sensitizer-annihilator pairs [28]. In this study two non-ionic surfactants were used as the main micelle building blocks in water: **Cremophor EL (CrEL)** (aka. Kolliphor EL, polyoxyl-35 castor oil [41]) and **Tween 80 (T80)** (polyoxyethylene (20) sorbitan monooleate) both of which are approved by U.S. Food & Drug Administration (FDA) [42] and presented in the Figure 10. Additionally, we used ethyl oleate (ethyl ester of oleic acid, EO) as the oil core for the micelles. Traditional oil-core micelles made with these two surfactants and ethyl oleate oil have been used to mediate upconversion with PtOEP as a sensitizer and 9,10-diphenylanthracene (DPA) as the annihilator [43].

We also used two different cationic co-surfactants to modify the surface charge of the micelles. In this work **stearyl amine (STA)** was used as a co-surfactant mixed with CrEL and **DOTAP (1,2-dioleoyl-3-trimethylammoniopropane)** with T80, both presented in the Figure 10. STA is a primary amine that works as a cationic surfactant. Its electrostatic interactions have been used for example to compact DNA in nanoemulsions consisting of oil-core droplets formed in water with STA and T80 [44]. The micelle forming capability of CrEL when mixed with cationic surfactants has also been studied, and it was found that both the tail lengths of surfactants and steric repulsion of the head groups affect the stability of the formed micelles [45]. DOTAP is a cationic lipid able to form bilayers that are stable and fluid, and it is often used with a neutral co-lipid to improve the structural stability of liposomes, nanoparticles made from lipid bilayer instead of surfactant monolayers like micelles [46].

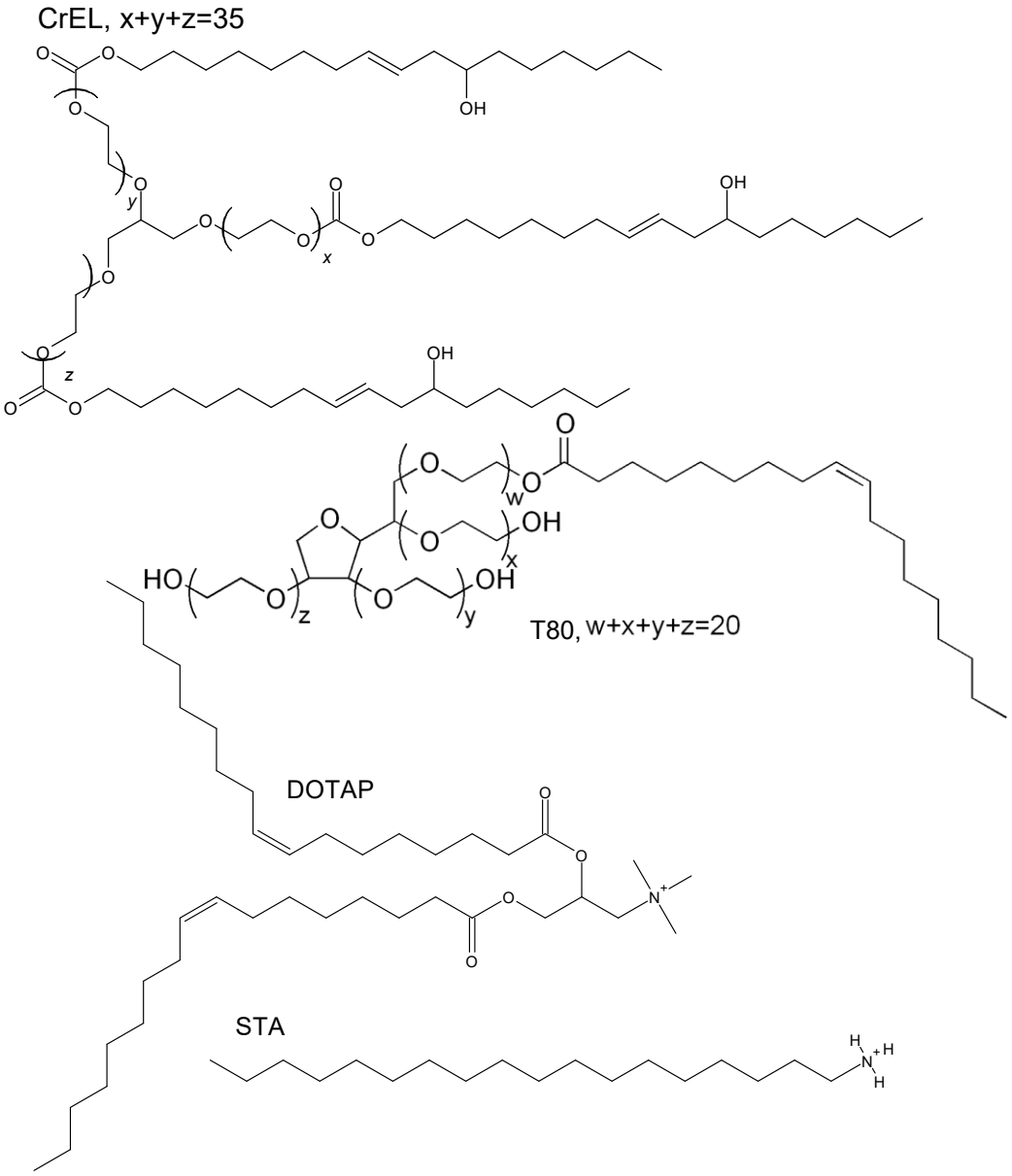

Figure 10. *Chemical structures of the main surfactants Cremophor EL (CrEL) and Tween 80 (T80) and co-surfactants (i.e., charge modifiers) dioleoyl-3-trimethylammonium propane (DOTAP) and stearyl amine (STA).*

Few different methods have been used to characterize micelles and nanoemulsions, like transmission electron microscopy [38,39] and differential light scattering, DLS [39,44]. In this work we used DLS, which is based on Brownian motion of the particles, to characterize the prepared micelles by measuring their hydrodynamic size, polydispersity index (PDI) and surface ζ -potential. The size characterization is done by detecting the light scattered from the particles, and ζ-potential is measured based on electrophoresis, i.e., the movement of the particles in electric field [47].

3.2. Nanocellulose Hydrogel as Upconversion Reservoir

Nano(fibrillar)cellulose hydrogel is a gel with extremely high water content (95 to 99.9 m-%) formed with nanocellulose fibres derived from wood pulp. This type of hydrogel is not only biodegradable and renewable, but also biocompatible and non-toxic, making it a suitable material for a variety of different applications in biomedicine. In this field nanocellulose hydrogel can be used to simulate the conditions of the human body (physical and biochemical) or as a platform for targeted drug delivery. [48,49]

Cellulose is a natural polymer formed by D-glucan units and it makes up 40 – 45 % of wood mass. [49] It is very a versatile material to use in bio-applications thanks to hydrophilicity and different modification possibilities of the cellulose chain. Nanocellulose, first reported by Bengt Rånby (1951) [50], is defined as cellulosic material with the size on the nanometre scale in at least one dimension [51]. Generally, three types of nanocelluloses are recognized: nanocrystalline cellulose, bacterial nanocellulose and nanofibrillar cellulose. Nanocrystalline cellulose consists of rod-shaped cellulose crystals produced by acid hydrolysis from cellulose fibres, and bacterial nanocellulose is produced bottom up by aerobic bacteria (e.g. *Gluconacetobacter*) [51]. **Nanofibrillar cellulose,** the nanocellulose component of the hydrogel used in this study, consists of cellulose fibres that are less than 100 nm in diameter and up to several micrometres in length. [48,49,51]

Nanofibrillar cellulose, NFC is generally manufactured from wood pulp by TEMPO-mediated oxidation [52], where 2,2,6,6-tetramethylpiperidine-1-oxyl radical (TEMPO) is used as the oxidizer of cellulose pulp which is then treated mechanically to produce cellulose fibres with a 5 – 60 nm diameter and length up to several micrometres. This process causes the nanocellulose fibres to have an **anionic charge** caused by newly formed carboxylic acid groups. Nanofibrillar celluloses can be studied by various methods including atomic force microscopy, field emission scanning-electron microscopy, and transmission electron microscopy. [48,51]

Nanofibrillar cellulose itself is not soluble in water due to the strong hydrogen bonding between cellulose chains making the fibres very stable [49]. So, when mixed with water, NFC forms a colloidal suspension, a **hydrogel**, even with extremely low concentrations of NFC [51]. The gel is formed as an entangled network of nanocellulose fibres that is stabilized by electrostatic interactions. The stability of the gel can be further increased via chemical cross-linking of the fibres with e.g., metal ions, citric acid, or succinic anhydride to name a few. This can be also used to modify the porosity of the hydrogel since it is dependent on the cross-linking density of the fibres. The pore size further dictates the

diffusion rate of different moieties entrapped in the nanocellulose fibre network used in several biomedical applications. [48]

Meir et. al have previously introduced TF-UC in a hydrogel formed with fibrin (a protein participating in the blood clotting) [53]. In their study, Meir et. al first incorporated PdTPTBP sensitizer and TIPS-An (9,10-((triisopropylsilyl)ethynyl) anthracene) annihilator into Pluronic F127 micelles with a reductive soybean oil core and then entrapped these emulsion droplets in the hydrogel alongside with Cry2olig expressing HeLa-cells to study their optogenetic response on the generated blue light upon a red-light excitation. By using confocal microscopy, they were able to study and characterize the cell-laden TF-UC hydrogel. In the paper they concluded that the size of the TF-UC emulsion droplets (almost 2 μm) was necessary to achieve to prevent the leaking of droplet from the hydrogel. The hydrogel used in the study was also cross-linked using the Thrombin enzyme to form a stiff gel.

4. EXPERIMENTAL

Sensitizer-annihilator pair PdTPTBP – TTBPer was loaded into unmodified (CrEL:EO micelles) and STA-modified CrEL micelles (CrEL:EO:STA -micelles) as well as in DOTAP-modified T80-micelles (T80:EO:DOTAP -micelles). In addition, PtTPTBP and PtOEP were also tested as sensitizer alternatives to PdTPTBP paired with TTBPer. For these pairs unmodified CrEL micelles (CrEL:EO micelles) were used. The different micelle formulations used in the study are presented in the Table 2 below.

Table 2. *Upconversion micelles used in the study. Three different sensitizers were paired with TTBPer and loaded into different micelles formulated with either Cremophor EL (CrEL) or Tween 80 (T80) as the main surfactant, stearyl amine (STA) or 1,2-dioleoyl-3-trimethylammoniopropane (DOTAP) as a co-surfactant to modify the surface charge of the micelle and ethyl oleate (EO).*

Sensitizer	**PdTPTBP**			**PtTPTBP**	**PtOEP**
Annihilator	TTBPer			TTBPer	TTBPer
Surfactant	CrEL	CrEL	T80	CrEL	CrEL
Oil	EO	EO	EO	EO	EO
Modifier	STA	-	DOTAP	-	-

Dye-loaded micelles were characterized by recording their sizes, size distributions and surface charges (surface ζ-potential). Release rates of micelles from anionic 1 m-% nanocellulose hydrogel were studied by recoding their release from hydrogel for up to two weeks. Upconversion properties of micelles in water were studied by determining the power density threshold and quantum yield, but due to limited time these could not be measured for all micelle types. Finally, upconversion spectrum of micelles entrapped in hydrogel at different excitation power densities was recorded as well.

4.1. Preparation and Characterization of Upconversion Micelles

The micelles were prepared as follows: first, the surfactant (CrEL or T80) and ethyl oleate (EO) were weighed to a vial and dichloromethane (DCM) solutions of the surface charge modifier (STA or DOTAP) and dyes were added. Then more DCM was added (total final volume 4 – 5 ml) and everything was solubilized. The DCM solvent was then evaporated under 5 mbar pressure for 2 hours at 20 – 30 ˚C temperature. After this, 3 ml of pure water purified by a Milli-Q system (Millipore, resistivity >18.0 MΩ cm), later referred to as “Milli-Q water”, was added, and the formed film was hydrated for 1.5 hours at room temperature while gently mixing and a water suspension of upconversion oil-core micelles (later referred to as *Micelle suspensions*) was produced. The *Micelle suspensions* were stored at room temperature protected from light. Compositions of micelles and concentrations of dyes in *Micelle suspensions* are presented in Table 3.

Table 3. *Compositions of sensitizer – annihilator loaded upconversion micelles: mass ratios of surfactant, oil, and charge modifier in each micelle type, as well as the concentrations, c, of sensitizer and annihilator in the final Micelle suspension.*

Sensitizer	Annihilator	Micelle	Mass Ratios of Components	c(sensitizer) [μM]	c(annihilator) [mM]
PdTPTBP	TTBPer	CrEL:EO:STA	84.5:15:0.5	150	2.55
		CrEL:EO	84.9:15.1	150	2.55* /1.50**
		T80:EO:DOTAP	88.9:10:1.1	150	1.50
PtTPTBP	TTBPer	CrEL:EO	84.9:15.1	150	1.50
PtOEP	TTBPer	CrEL:EO	84.9:15.1	50	1.0

* Micelles used in release studies (chapter 4.2)
** Micelles used in upconversion studies (power density threshold, chapter 4.3)

Micelles were characterized by measuring their hydrodynamic sizes (ζ -average sizes), size distributions and surface charges (surface ζ -potential) with Zetasizer Nano (Malvern Instruments Ltd., UK) using differential light scattering (DLS). For these measurements *Micelle suspensions* were diluted 10 times (300 μl of *Micelle suspension* and 2.7 ml Milli-Q water) to decrease multiple scattering, i.e., scattering of the light multiple times in a concentrated sample [47].

4.2. Release of Upconversion Micelles from Nanocellulose Hydrogel

Release rates of PdTPTBP – TTBPer loaded micelles (CrEL:EO:STA, CrEL:EO and T80:EO:DOATP) from hydrogel were studied. Entrapment of micelles in hydrogel was done by simply mixing certain amounts of prepared *Micelle suspension* and nanocellulose hydrogel stock (2.69 m-% of nanocellulose in water) to obtain micelle-doped hydrogel in the desired strength (1 m-%).

Two different micelle-doped hydrogels were prepared with each micelle type: *High-loading gel* which was prepared by mixing *Micelle suspension* with hydrogel stock (2.69 m-%) and *Low-loading gel*, which was prepared with diluted *Micelle suspension* (diluted 10 times with Milli-Q water) instead. The final amounts of *Micelle suspension* in each gel type were approximately:

High-loading gel: 630 μl / g gel

Low-loading gel: 63 μl / g gel

The release rate of each micelle type from both *High-loading* and *Low-loading gel* was studied in triplicates. The *Release Samples* were prepared as follows: to the bottom of a 1.5 ml Eppendorf 100 μl of *High-loading* or *Low-loading gel* was added, and the mass of

added gel was measured and recorded. On top of this 1.4 ml of Dulbecco's phosphate-buffered saline (DPBS, 1x) buffer was added. A weight made of copper wire was also added to keep the gel submerged in buffer. The Eppendorf was sealed tightly to prevent any evaporation and/or leaking of the buffer during the experiment. The samples were incubated in a thermoshaker (250 rpm, 37 ˚C, darkness) for up to two weeks, and they were removed only to measure the release of micelles from the gel.

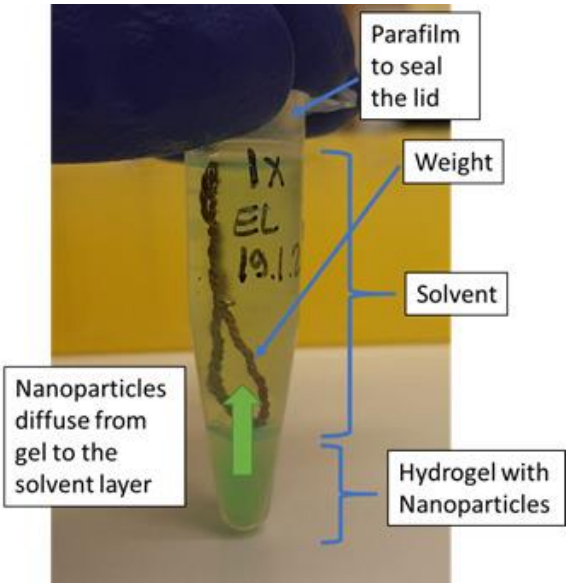

Figure 11. *The set-up for studying the release rate of micelles form hydrogel.*

The relative release $(Release - \%)$ of the micelles from the gel was determined by measuring the fluorescence spectra of TTBPer in the *Release Sample's* buffer layer on FLS1000 Photoluminescence Spectrometer (Edinburgh Instruments). The intensities of the *Release Sample's* buffer layer were compared to that of a *Control Sample*. The *Control Sample* was prepared by adding same amount of *Micelle suspension* than was in the gel layer of the *Release Sample* to 1.4 ml of DPBS to mimic total release of micelles from hydrogel layer to buffer layer. The *Control Sample* was prepared the day after starting the release experiments, and this same solution was used throughout the entire release experiment (up to two weeks). Then, $Release - \%$ for each day was calculated as:

$$Release - \% = \frac{I(Release\ sample)}{I(Control\ sample)} * 100\% \qquad (9)$$

where I is the fluorescence intensity at 458 nm after excitation at 400 nm (450 W xenon arc lamp).

The fluorescence intensity of *Control Sample* was measured every time the *Release Sample* fluorescence intensity was measured to minimize the possible differences between measurements on different days. For fluorescence measurements 100 µl of the

Control Sample or the buffer layer of the *Release Sample* was diluted with 1.4 ml of DPBS-buffer. (To reconstitute the lost volume in *Release Samples*, 100 µl of DPBS buffer was added back to the Eppendorf.)

4.3. Power Density Threshold

The power density thresholds were measured for the following micelles:

- CrEL:EO:STA (PdTPTBP – TTBPer), anoxia
- CrEL:EO (PdTPTBP – TTBPer), anoxia
- CrEL:EO (PtTPTBP – TTBPer), anoxia
- CrEL:EO (PtOEP – TTBPer), anoxia and oxia

Measurements to determine power density threshold were done for all above mentioned micelles in water suspension (referred to as *Free micelles*) mainly in oxygen free environment (anoxia). However, CrEL:EO (PtOEP – TTBPer) micelles were also measured in the presence of oxygen (oxia) to see how the system behaved. PdTPTBP – TTBPer loaded CrEL:EO micelles entrapped in hydrogel (referred to as *Entrapped micelles*) were also measured. It is worth mentioning that these micelles had less TTBPer (1.5 mM instead of 2.55 mM in *Micelle suspension*) than those used in the release experiments (chapter 4.2) due to crystallization problems that occurred after these experiments.

Free micelles for the power density threshold measurements were prepared as follows: to 3 ml of Milli-Q in a SOG9 flash cuvette about 30 µl of *Micelle suspension* was added so that the absorbance at the excitation wavelength (632.8 nm for PdTPTBP) was roughly 0,10 – 0.15. Experiments were done in anoxia, which was achieved by scavenging oxygen from the sample with 30 µl of saturated sodium sulfite, Na_2SO_3, solution.

Entrapped micelles for the measurements were prepared as a *Medium-loading gel: Micelle suspension* was diluted 3.77 times and mixed with hydrogel stock (2.69 m-%) to get total of 10 ml of micelle loaded gel (167 µl of *Micelle suspension* per g gel). The gel was circulated through a flow cuvette with an inlet and outlet using peristaltic hose pump (Orion Diagnostica) to prevent bleaching of the gel and to keep the fluorescence intensity stable.

To determine power density threshold, the upconversion spectrum of micelles was recorded at different excitation power densities. The instrument setup used for the determination of the power density thresholds for *Free micelles* and *Entrapped micelles* is

shown in Figure 12. The excitation source is the helium-neon (HeNe) laser (6HNL210LB, 21 mW, polarized, Thorlabs) for sensitizers PdTPTBP and PtTPTBP (excitation wavelength 632.8 nm) or NdYAG-laser (VerdiV6 second harmonic Nd:YAG laser, Coherent Inc.) for PtOEP (excitation wavelength 532 nm). The excitation source was combined with the beam aligning optics, the wavelength selecting monochromators, and the photomultiplier tube of the Edinburgh Instruments FLS1000 Photoluminescence Spectrometer that detects the signal.

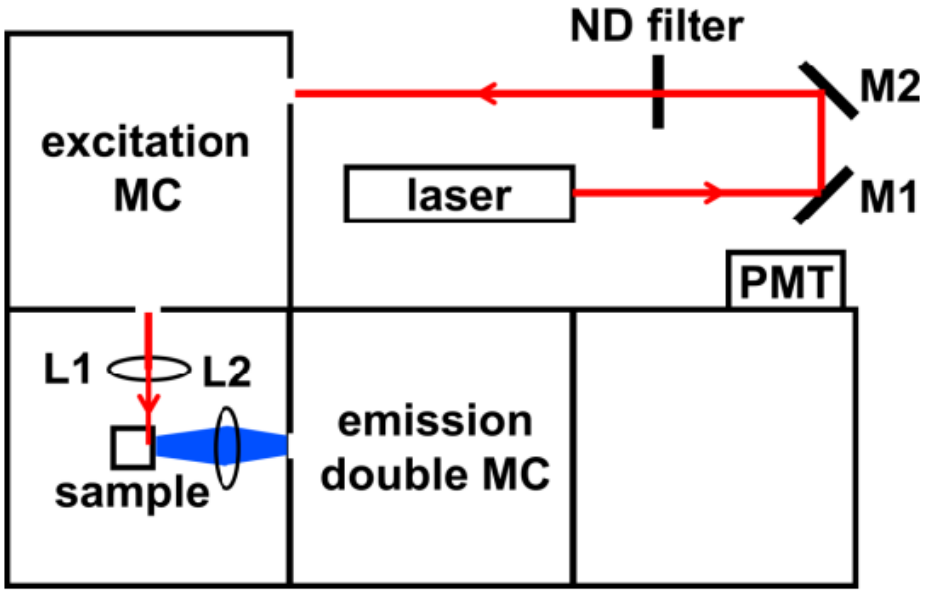

Figure 12. *The experimental setup for measuring the upconversion intensity and spectrum needed for the determination of the power density. The beam from excitation source (laser) is guided with mirrors (M1 and M2) through neutral density filters (ND filters) that are used to vary the excitation power density. The beam passes through the excitation monochromator (MC) to the sample compartment where convex lenses L1 and L2 guide the beam to the sample and collect the upconverted light which is them guided to the emission double monochromator and photomultiplier tube (PMT). Reprinted with permission from [15]*

To calculate the excitation power densities both maximum excitation power and size of the laser beam had to be measured. The power density is defined in equation 10

$$PD = \frac{P}{\pi r_x r_y} \tag{10}$$

where r_x and r_y are the radiuses of the ellipsoidal beam in cm and P is the laser power in mW. Excitation power density was varied by attenuating the maximum excitation power with neutral density filters (Edmund Optics).

The maximum excitation power of the HeNe-laser was measured with PM100D Digital Optical Power and Energy Meter (Thorlabs) that was combined to a S120VC Si photodiode power sensor (Thorlabs). The profile and the dimensions of the laser beam

were measured and analysed with a LBP2-HR-VIS2 Laser Beam Profiler (Newport) and LBP2 Software (Newport) using $D4\sigma^{ISO}$ computation. The beam size was measured using the full power of the laser attenuated with neutral density filters to reach the optimal beam profile for the dimension measurements and to prevent damaging of the profiler.

Table 4. *Radiuses of the ellipsoidal beam (r_x and r_y) in cm, maximum power of the excitation laser used, P, in mW and calculated maximum excitation power density PD in mW/cm^2.*

Upconversion Micelles Studied	r_x [cm]	r_y [cm]	P [mW]	PD [mW/cm2]
CrEL:EO:STA (PdTPTBP-TTBPer)	≈ 0.02	≈ 0.02	5.67	4514
CrEL:EO (PdTPTBP-TTBPer)	0.02145	0.0219	9.76	6617
CrEL:EO (PtTPTBP-TTBPer)	≈ 0.02145	≈ 0.0219	9.76	6617
CrEL:EO (PtOEP-TTBPer)	0.028	0.0305	34.6	12903

The measured laser power, and thus calculated maximum excitation power density, for PtOEP loaded micelles is notably higher because NdYAG laser was used instead of the HeNe laser.

4.4. Quantum yield

Quantum yield was determined only for PdTPTBP – TTBPer loaded CrEL:EO:STA micelles in water suspension using methylene blue (MetBlue, $\Phi_{fluo} = 0.04 \text{ or } 4\%$ [54]) as a standard. To determine the quantum yield, absorption spectra of micelles and standard were measured, as well as their fluorescence spectra at different excitation power densities.

Micelles were prepared for the measurements by adding 30 µl *Micellar suspension* and 30 µl saturated Na_2SO_3 to 3 ml of Milli-Q water and the MetBlue standard by adding 7.5 µl of 1.03 mM dye stock to 3 ml of Milli-Q. These dilutions were used to have samples with optical densities of about 0.15 or less at the used excitation wavelength (HeNe laser: 632.8 nm) to avoid **primary inner filter effect** i.e., the strong attenuation of the excitation beam as it progresses through the sample [55]. Absorption spectra of both samples were recorded using Shimadzu UV-3600 UV-Vis-NIR Spectrophotometer.

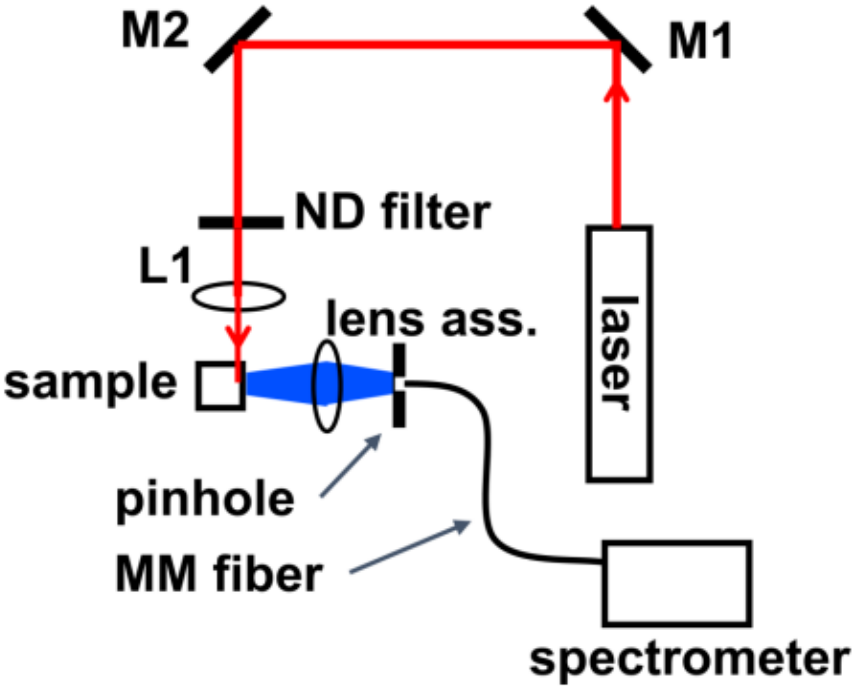

Figure 13. *The setup used for measuring the fluorescence spectra for upconversion quantum yield. Mirrors M1 and M2 guide the laser beam through neutral density filters (ND) that are used to vary the excitation power density. The beam passes through the first lens L1 to the sample, and the emitted light is collected guided with two more convex lenses (lens assembly) through a pinhole and all the way to the spectrophotometer (AvaSpec-ULS2048L (Avantes) fiber-optic spectrometer). Reprinted with permission from [15].*

Fluorescence spectra of both micelles and standard were recorded using the experimental setup presented in the Figure 13. Different excitation power densities from the strong annihilation regime well above the measured I_{th} of the micelles were used to record the spectra to obtain a relation between the integrated fluorescence intensities of the fluorescence and power density. The measured spectra are presented in Appendix C. The **secondary inner filter** effect, i.e., the reabsorption of the upconverted photons by the sample due to the overlap of excitation and emission spectra [55], was decreased by guiding the excitation beam right next to the cuvette wall (see Figure 13) to minimize the pathlength of upconverted photons in the sample.

5. RESULTS AND DISCUSSION

5.1. Characterization of Upconversion Micelles

The results on the characterization measurements of micelles are presented in the Table 5 below. Size, PDI and ζ-potential of CrEL:EO:STA and T80:EO:DOTAP micelles were calculated as averages of multiple separate batches that were prepared and measured. The data of each of these separate batches is presented in the Appendix A.

Table 5. *Sensitizer – annihilator loaded upconversion micelles: ζ -average sizes (Size), polydispersity indexes (PDI), and ζ-potentials.*

Sensitizer	Annihilator	Micelle	Size [nm]	PDI	ζ-potential [mV]
PdTPTBP	TTBPer	CrEL:EO:STA	27.50 ± 6.22	0.215 ± 0.050	0.34 ± 4.09
		CrEL:EO	30.49* / 17.52**	0.215* / 0.070**	n.d.
		T80:EO:DOTAP	11.28 ± 0.37	0.244 ± 0.037	-2.71 ± 0.80
PtTPTBP	TTBPer	CrEL:EO	17.36	0.033	n.d.
PtOEP	TTBPer	CrEL:EO	17.87	0.068	n.d.

* Micelles used in release studies
** Micelles used in upconversion studies (power density threshold)

Micelles used in this study were generally smaller (10-30 nm) than the liposomes in the work by Auvinen et. al (50 nm) as was discussed in the Introduction. The monodispersity of the *Micelle suspensions* were determined by their PDI and because all the values were below 0.3 the *Micelle suspensions* were be considered as monodisperse. The measured surface ζ-potentials were close to 0 mV suggesting that the surface charges of the modified micelles were generally neutral instead of clearly positive. However, the initial ζ-potential of unmodified micelles were considerably negative. CrEL:EO micelles not loaded with dyes had ζ-potential of -20 mV and dye-loaded T80:EO micelles -12.4 mV. This means that the charge modification, the dye loading or both together successfully improved the cationic surface charge of the micelles. To confirm this, it would be suggested to measure the ζ-potential of the dye-loaded CrEL:EO micelles and T80:EO micelles not loaded with dyes.

5.2. Release of Upconversion Micelles from Hydrogel

During the release studies of micelles entrapped in hydrogel **a decrease in the monitored TTBPer fluorescence intensity** was observed. This decrease can be seen as an intensity drop in the fluorescence spectra towards the end of the experiment in *Control samples* (see Appendix B). In the *Release samples* this is seen as stagnation of intensity increase.

This happens because as micelles get released from the gel the intensity increases at a similar rate as the fluorescence is quenching, thus making the intensity seem constant throughout the experiment. This might be e.g. due to decomposition of micelles and aggregation of released dyes, but this would have to be confirmed by monitoring the size and PDI of the released micelles throughout the release experiments.

Due to this decrease in intensity, the release-% had to be corrected. To take the effect of intensity decrease of TTBPer into account the **fractions of the remaining fluorescence intensity**, f_d, had to be calculated for each day:

$$f_d = \frac{I_t}{I_0} \tag{11}$$

where I_0 is the intensity of the measured *Control sample* on the first day the release was measured (the day after the release experiment was started) when no decreasing of TTBPer intensity had not yet taken place and I_t the intensity measured on the following days. Thus, for day 1, $f_d = 1$ (i.e., 100 %) where it is assumed that no decrease in TTBPer intensity has yet happened. The values for f_d were calculated for all micelles that were studied for their release from *High-loading* and *Low-loading gel* and plotted against time to determine the rates of intensity decrease of TTBPer in each system. These rates are presented in Figure 14.

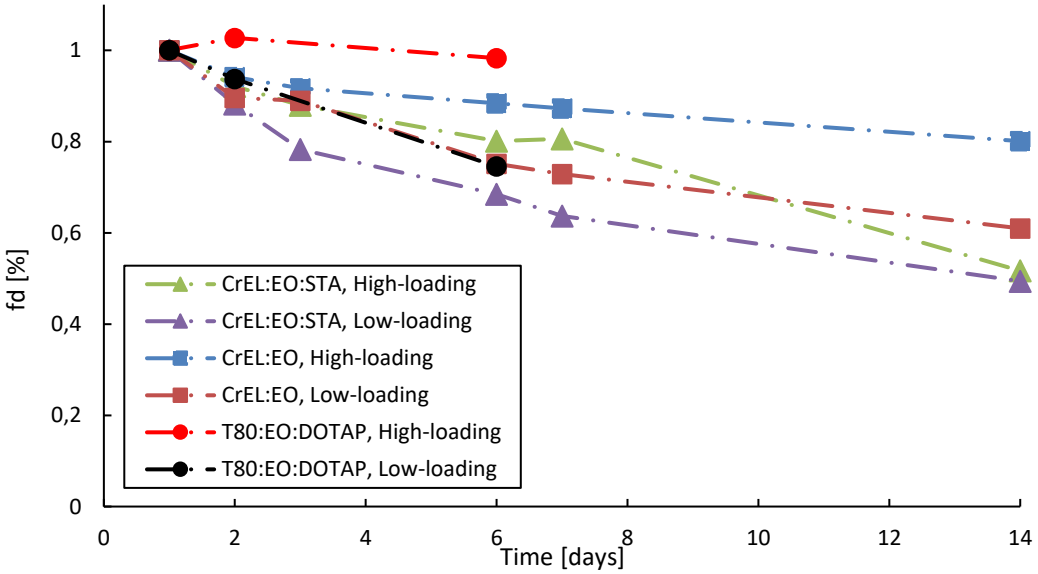

Figure 14. *Fractions of the remaining fluorescence intensity, f_d, of modified and unmodified CrEL micelles and modified T80-micelles entrapped in High-loading and Low-loading gel as a function of time (i.e., duration of the release studies).*

An intensity decrease of about 50 % was observed in STA-modified CrEL micelles during the two-week release experiment regardless of the initial amount of *Micelle suspension* in the sample. Between the unmodified CrEL micelles however, there is a clear difference

between the rate of the intensity decrease for micelles released form *High-loading* and *Low-loading gel.* The intensity decrease rate of unmodified CrEL micelles in *High-loading gel* is much slower than in *Low-loading gel*, which is just slightly slower than that of the modified CrEL micelles. An intensity decrease of about 40 % was observed in unmodified CrEL micelles in *Low-loading gel* during the experiment whereas for *High-loading gel* this decrease was only about 20 %.

For DOTAP-modified T80-micelles released from *High-loading gel* the intensity of TTBPer remained much more stable throughout the release experiments. However, since it was monitored only for 6 days this cannot be said for certain. Micelles released from *Low-loading gel* showed faster intensity decrease rate very similar to that of CrEL:EO micelles released from *Low-loading gel*.

The $Release - \%$ values were then calculated and corrected for the TTBPer intensity decrease as presented in the equation 12

$$Release - \% = \frac{I(Release)}{I(Control)} \cdot \frac{1}{f_d} \cdot 100\% \qquad (12)$$

where both $I(Release)$ and $I(Control)$ are the intensities of *Release* and *Control samples* measured on the same day, and f_d is the decomposition factor calculated for that day. These corrected release rates ($Release - \%$ as a function of time) of modified and unmodified CrEL micelles and modified T80-micelles from both *High-loading* and *Low-loading gel* are presented in the Figure 15. Additionally, graphs showing the difference between the corrected and uncorrected release-% values are presented in Appendix B.

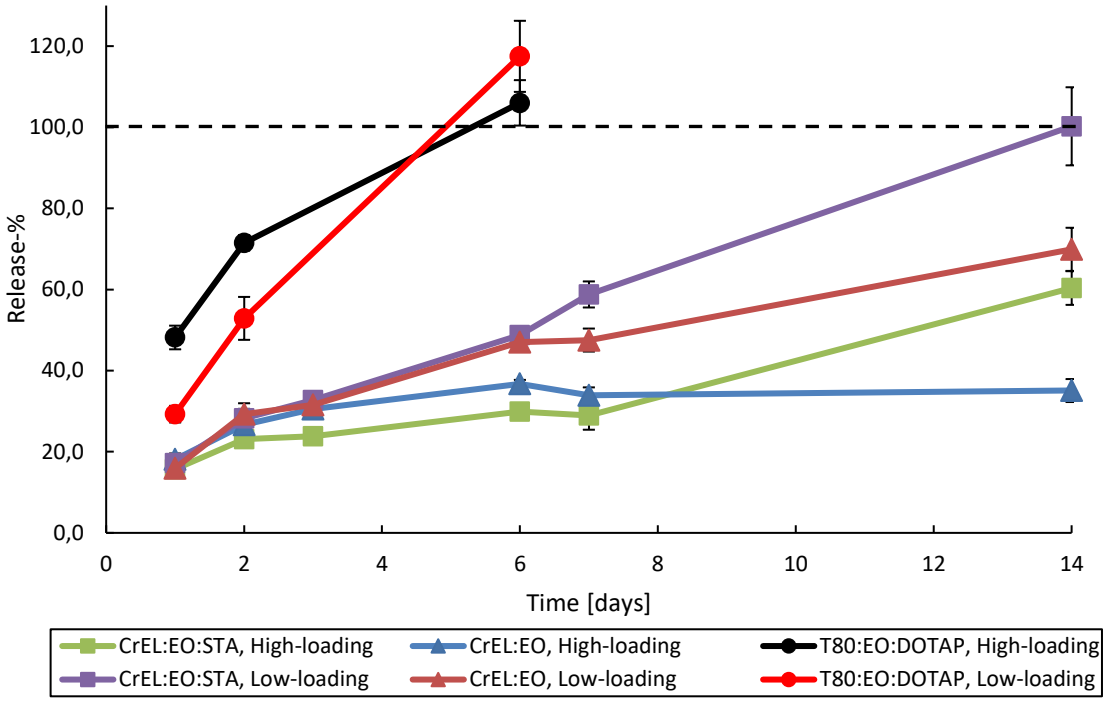

Figure 15. *Release-% as a function of time of the studied CrEL and T80 micelles entrapped in High-loading and Low-loading gel.*

DOTAP modified T80-micelles were released completely in less than a week regardless of the initial micelle loading and are thus unsuitable for our future applications even though the intensity of TTBPer was stable in these samples. In the case of CrEL micelles, the STA modification seems to increase the leaking of micelles from both *High-loading and Low-loading gel* as opposed to the preliminary hypothesis. It appears that the small size of the micelles causes them to be released regardless of any possible Coulombic interactions between the micelles and nanocellulose fibres. It might also be that the STA modification makes the micelle more unstable overall as is suggested by the rapid decrease in TTBPer intensity in these micelles. In contrast, the unmodified CrEL micelles generally seem to have better retention in hydrogel than their modified counterparts. Additionally, it seems that the leaching of micelles from *High-loading gel* is generally slower than from *Low-loading gel* suggesting that higher loading of micelles improves their retention.

Out of all the studied systems, CrEL:EO micelles entrapped in *High-loading gel* seemed to work best overall. Only 35 % of the entrapped micelles were released over the course of two weeks and the stability of TTBPer fluorescence intensity was found to be better in *High-loading gel* making a high loading of unmodified CrEL:EO micelles in hydrogel the most suitable system out of those studied for future applications.

5.3. Upconversion of Micelles in Water

Let us first look at the results regarding **power density threshold**. As discussed before, the power density thresholds were determined for the following micelles in water suspension:

- CrEL:EO:STA (PdTPTBP – TTBPer), anoxia
- CrEL:EO (PdTPTBP – TTBPer), anoxia
- CrEL:EO (PtTPTBP – TTBPer), anoxia
- CrEL:EO (PtOEP – TTBPer), anoxia and oxia

To calculate the values of I_{th}, mainly the formal definition of power density threshold was used, and the relation of I_{em} vs PD_{exc} on a double logarithmic scale was only used to confirm that the strong annihilation regime had been reached (slope of 1). However, in those cases where also the weak annihilation regime was reliably reached, I_{th} was also calculated using the cross-section method and for these I_{th} are presented as an average of the values obtained by both methods.

For the **formal definition -method**, f_Φ (equation 8) were calculated from intensities at 460 nm and plotted against the used PD_{exc}, and a natural logarithmic trend was fitted to the data (Logarithmic Trendline by Excel). The obtained relation $y = a * ln(x) + b$, was then used to calculate I_{th} as follows, assuming $f_\Phi = 0.5$ (since I_{th} is the excitation power density needed to reach half of the maximum possible quantum yield):

$$I_{th} = \exp\frac{0.5 - b}{a} \tag{13}$$

For the **cross-section method**, I_{em} at 460 nm was plotted against the used PD_{exc} on a double logarithmic scale (log10), and two linear trends $y = ax + b$ (Linear Trendline by Excel) were fitted to the data: one to the higher values of I_{em} and PD_{exc} so that it had the slope of 1 and another to the lowest values to see if the slope of 2 was reached or not. If both annihilation regimes were reached, I_{th} was calculated from the cross-section of the two slopes as follows:

$$\log_{10} \mathrm{I_{th}} = \frac{b_1 - b_2}{a_2 - a_1} \tag{14}$$

$$I_{th} = 10^{\log_{10} I_{th}} \tag{15}$$

The plotted data and fitted trendlines for each micelle formulation measured in anoxia are presented in the figure below.

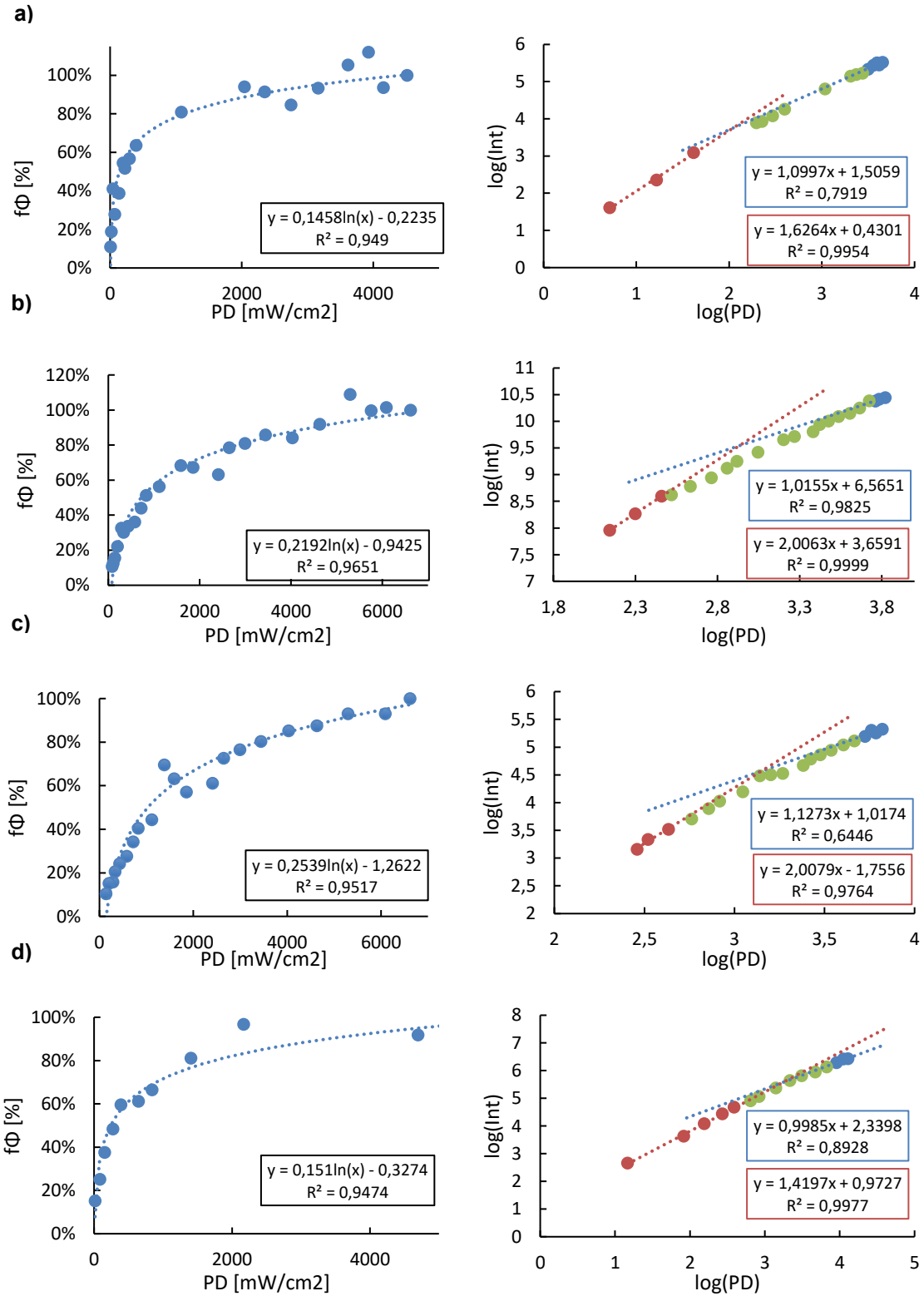

Figure 16. *Determination of power density threshold of micelles* ***in anoxia*** *by formal definition (left) and cross-section method (right): a) CrEL:EO:STA (PdTPTBP – TTBPer), b) CrEL:EO (PdTPTBP – TTBPer), c) CrEL:EO (PtTPTBP – TTBPer) and d) CrEL:EO (PtOEP – TTBPer)*

Additionally, power density threshold was determined in the presence of oxygen for CrEL:EO (PtOEP – TTBPer) micelles. These plotted data and fitted trendlines are presented in the Figure 17.

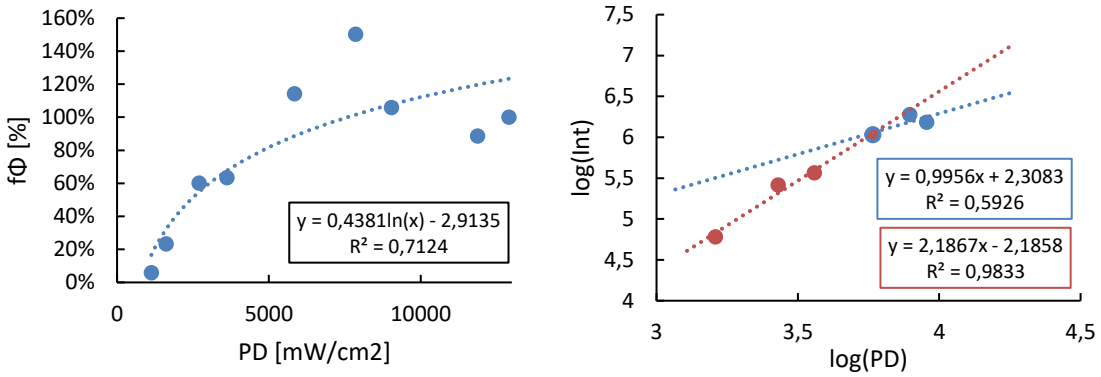

Figure 17. *Determination of power density threshold of CrEL:EO (PtOEP – TTBPer) micelles in oxia by formal definition (left) and cross-section method (right).*

The calculated I_{th} values are presented in the Table 6 below.

Table 6. *Power density thresholds, I_{th} of the studied upconversion micelles in water.*

Sensitizer	**PdTPTBP**		**PtTPTBP**	**PtOEP**
Annihilator	TTBPer		TTBPer	TTBPer
Surfactant	CrEL	CrEL	CrEL	CrEL
Oil	EO	EO	EO	EO
Modifier	STA	-	-	-
I_{th}, anoxia [mW/cm^2]	143	789*	1221*	240
I_{th}, oxia [mW/cm^2]	n.d.	n.d.	n.d.	2424

* I_{th} calculated as an average from values obtained by both formal definition and cross-section method.

Both PdTPTBP – TTBPer loaded CrEL:EO:STA micelles and PtOEP – TTBPer loaded CrEL:EO micelles had power density threshold considered suitable for biological applications in anoxic conditions (143 mW/cm^2 and 240 mW/cm^2), and PtOEP showed some upconversion capabilities even in the presence of oxygen, although after excitation with roughly 10 times higher power density (2424 mW/cm^2). Additionally, even though the power density threshold of PdTPTBP – TTBPer loaded CrEL:EO micelles was higher than its STA-modified counterpart, this could also be low enough to induce sufficient upconversion with low enough excitation power densities. It also recommended that the power density threshold of these micelles would be determined in the presence of oxygen as well.

Let us then look at the results regarding the **quantum yield** determination. As discussed previously, quantum yield was determined only for PdTPTBP – TTBPer loaded

CrEL:EO:STA micelles in water suspension. First, so-called **observed quantum yield,** a quantum yield based solely on the observed emission that is not corrected for (secondary) inner filter effect, was calculated using a modification of the equation 6. Since both micelles (unk) and methylene blue (std) had the same solvent, the refractive indexes had no effect on Φ_{UC}. Furthermore, to decrease the error of the fluorescence measurements, several fluorescence spectra were measured with different excitation power densities in the strong annihilation regime. By plotting the integrated fluorescence intensities from these spectra against the excitation power densities used, the slopes for both micelles and standard were acquired and used in the place of the term $\left(\frac{I_{unk}}{I_{std}}\right)$. Thus, the new equation for calculating the observable quantum yield is

$$\Phi_{UC,obs} = \Phi_{std}\left(\frac{OD_{std}}{OD_{unk}}\right)\left(\frac{Slope_{unk}}{Slope_{std}}\right) \tag{16}$$

The absorption spectra of micelle and standard samples are presented in the Figure 18. The integrated fluorescence intensities of the recorded fluorescence spectra of both micelles and standard plotted against the excitation power are presented in Figure 19.

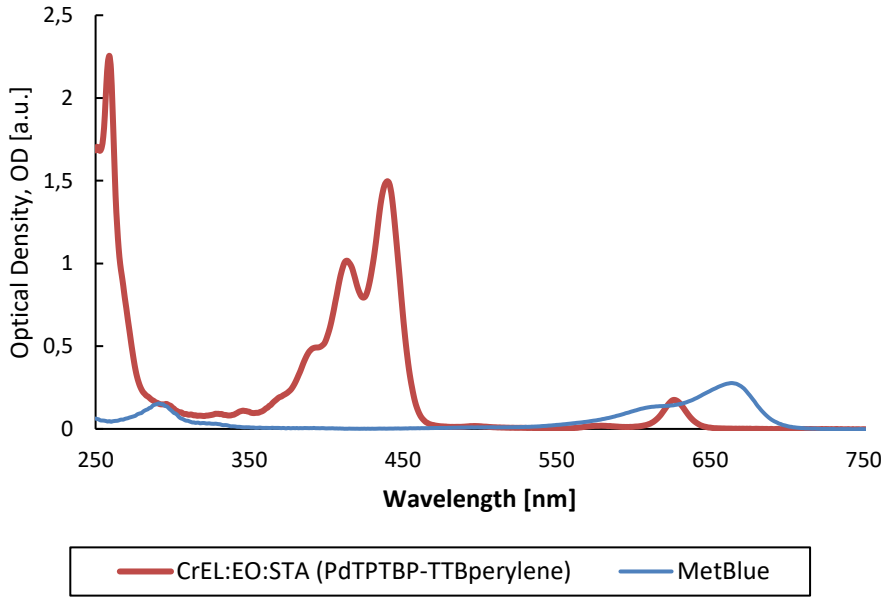

Figure 18. *Absorption spectra of PdTPTBP – TTBPer loaded CrEL:EO:STA micelles and Methylene Blue standard. The optical densities at the excitation wavelength 633 nm were 0.122627 for micelles and 0.156495 for methylene blue standard.*

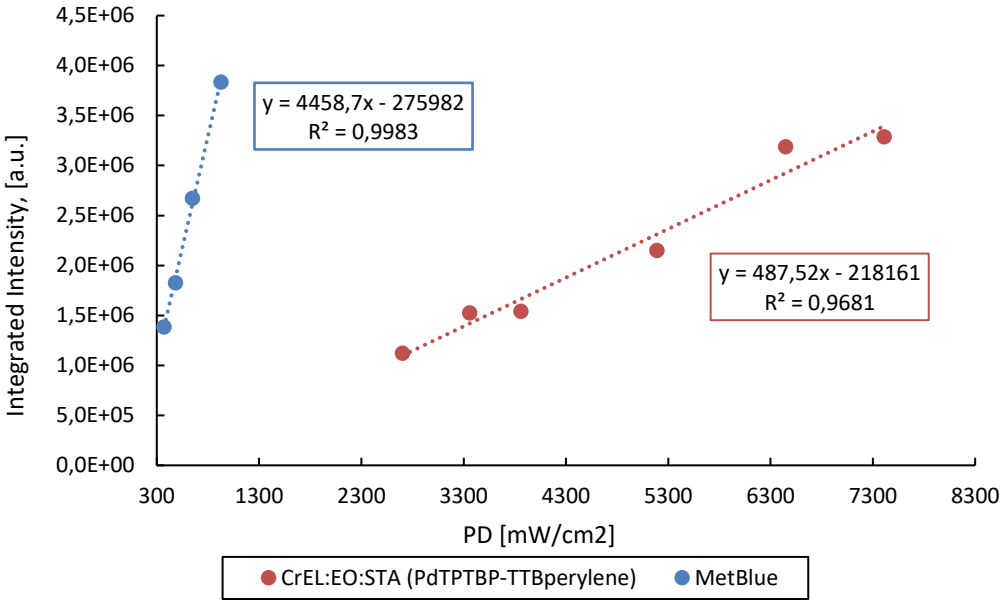

Figure 19. *Integrated fluorescence intensities of the recorded fluorescence spectra measured with different power densities (PD) and the linear trends fitted to the data.*

From this, the observable quantum yield was calculated to be

$$\Phi_{UC,obs} = 4\,\% \times \left(\frac{0.156495}{0.122627}\right) \times \left(\frac{487.52}{4458.75}\right) = \mathbf{0.558}\,\% \qquad (\ \ )$$

This calculated observable quantum yield was then corrected for the (secondary) inner filter effect using the tail fitting procedure described in the Reference Guide for FLS980 by Edinburgh Instruments [56] to obtain a value for the **true quantum yield**. Even though the equipment setup was adjusted to diminish the effect of secondary inner filter effect it was corrected for the measured sample. First, the spectrum of TTBPer in micelle was corrected by rescaling it to match the shape of emission spectrum of TTBPer alone in an organic solvent with low optical density, i.e., true emission spectrum of the annihilator. This was done by matching the fluorescence intensities of TTBPer in micelles and free TTBPer in an emission range where no inner filter effect took place and recalculating the intensities of TTBPer in micelles using the relative intensities of free TTBPer (tail-fitting). The corrected emission spectrum of TTBPer in micelles and the measured emission spectrum are presented in Figure 20.

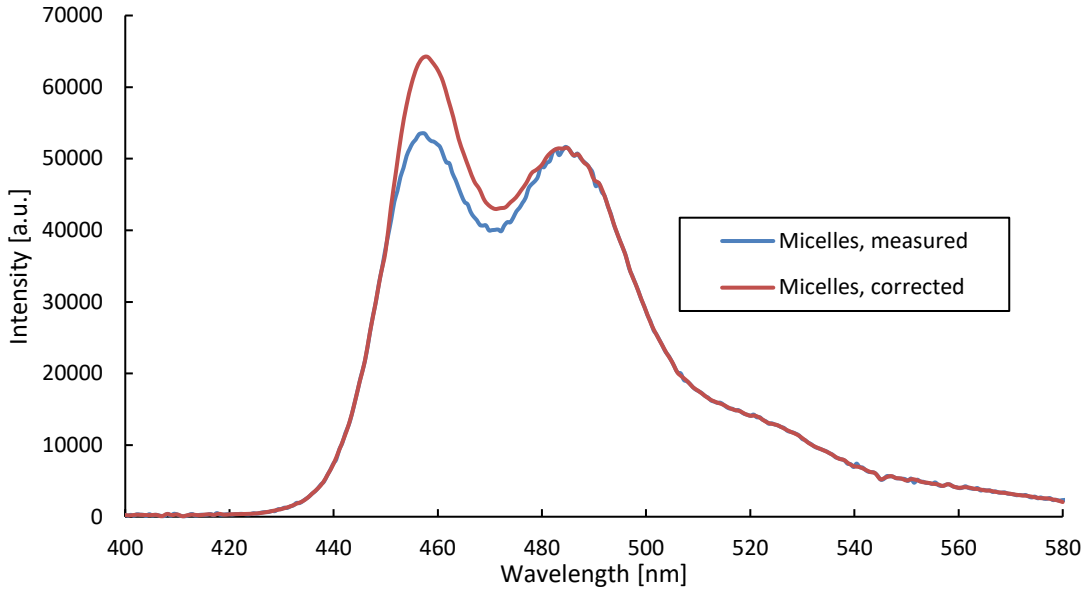

Figure 20. *The measured emission spectrum of TTBPer in micelles and emission spectrum corrected using the tail-fitting method.*

Then, the **fraction of the reabsorbed emission**, $\boldsymbol{a}$, was calculated from the integrated intensities of the corrected emission of micelles, I_{true}, and measured emission of micelles, I_{obs}:

$$\boldsymbol{a} = \frac{I_{true} - I_{obs}}{I_{true}} \tag{17}$$

where $I = \sum_{400\ \mathrm{nm}}^{580\ \mathrm{nm}} I_\lambda$ and I_λ is the fluorescence intensity at the emission wavelength λ. The fraction $\boldsymbol{a}$ was calculated to be:

$$\boldsymbol{a} = \frac{3431689.042 - 3267804.804}{3431689.042} = 0.047756 \approx 0.05 \tag{18}$$

Finally, the fraction a was used as a correction factor to calculate the true upconversion quantum yield [56]

$$\Phi_{UC} = \frac{\Phi_{UC,obs}}{1 - \boldsymbol{a} + \frac{\boldsymbol{a}\Phi_{UC,obs}}{100}} \tag{19}$$

The true upconversion quantum yield was calculated to be $\boldsymbol{\Phi_{UC}} = 0.587\ \% \approx \boldsymbol{0.6\ \%}$**.** So, only about 5 % of the upconverted light was lost to the (secondary) inner filter effect. The determined upconversion quantum yield of 0.6 % is in line with the values previously reported [43]. Even though the value might seem low, it ought to be enough for the potential future applications e.g., in triggered drug release and bioimaging.

5.4. Upconversion of Micelles in Nanocellulose Hydrogel

The upconversion emission spectrum of PdTPTBP loaded CrEL micelles (unmodified) entrapped in hydrogel was measured using different PD_{exc}, and they are presented in the Figure 21.

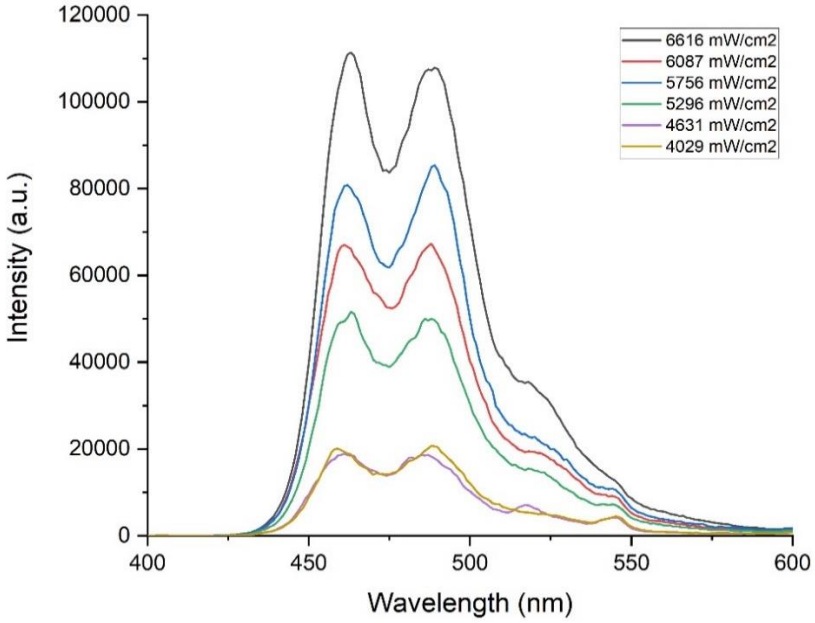

Figure 21. *The emission spectra of micelles entrapped in hydrogel measured at six different* PD_{exc} $[mW/cm^2]$.

Upconversion emission of micelles entrapped in hydrogel was observed, successfully recorded and even visible to the naked eye. However, high excitation power densities had to be used suggesting that the oxygen sensitivity of the studied system might be too high. So, although this specific system might not be suitable for future applications, it still presents the potential to generate upconversion in hydrogel.

6. CONCLUSIONS

In conclusion, five different micellar formulations were studied using different surfactants and sensitizer – annihilator pairs. These micellar systems have been previously presented in Table 2. *Micellar suspensions* in water were characterized by measuring their hydrodynamic sizes (ζ -average sizes), size distributions and surface charges (surface ζ -potential). The release rates of three of these micellar formulations, CrEL:EO:STA, CrEL:EO and T80:EO:DOTAP loaded with PdTPTBP – TTBPer dye pair, from nanofibrillar cellulose hydrogel (1-m%) were tested. Two different types of micelle loadings were studied: *High-loading gel* with 630 µl of *Micelle suspension* per 1 g gel and *Low-loading gel* with 63 µl of *Micelle suspension* per 1 g gel. Upconversion properties of micelles in water suspension were studied by determining the power density threshold for all CrEL based micelles and upconversion quantum yield for PdTPTBP – TTBPer loaded CrEL:EO micelles. Finally, upconversion spectra of PdTPTBP – TTBPer loaded CrEL:EO entrapped in hydrogel was recorded using different excitation power densities.

All micelle suspensions used in this work were monodisperse (PDI < 0.3) and the size of the micelles varied between 10 and 30 nm depending on the formulation and the amount of loaded dyes. The measured surface ζ-potentials of STA- and DOTAP-modified micelles were neutral (close to 0 mV). This was in line with the surface ζ-potentials of Cy5 labeled liposomes used in the unpublished work by Auvinen et. al which worked as an inspiration for this research. Additionally, the initial ζ-potential was -20 mV for CrEL:EO micelles not loaded with dyes and -12.4 mV for dye-loaded T80:EO micelles. Thus it is clear that either or both the addition of the charge modifier and dye loading can make the micelles more cationic. However, this would have to be confirmed by measuring the ζ-potential of the dye-loaded CrEL:EO micelles and T80:EO micelles not loaded with dyes. Overview on the results is presented in the Appendix D.

CrEL:EO micelles entrapped in *High-loading gel* were retained best with just 35 % of micelles released over the course of two weeks making this formulation most suitable in for future applications in this regard. Generally the release rate was faster from *Low-loaded gel* regardless of the type of loaded micelles and high loading of micelles should thus be favoured. Opposed to the initial hypothesis, STA-modification of CrEL micelles caused them to be released faster (60 % released in two weeks). This not only suggests that the small size of the micelles outweighs any Coulombic interactions between micelles and cellulose nanofibrils but also that STA-modification could cause the micelles to become more unstable overall. T80:EO:DOTAP micelles were released completely from the hydrogel in just 6 days and would not be suitable for future applications. Additionally,

the stability of TTBPer fluorescence intensity measured from the micelles released from hydrogel was studied. It was observed that the intensity decreased as a function of time and this decrease was greater in micelles released from *Low-loading gel*. This decrease in intensity seems to be slower in the released T80 micelles but these were followed only for 6 days. In CrEL:EO micelles released from the *High-loading gel* the decrease was only 15 % further suggesting the superiority of this formulation. Overview on the results is presented in the Appendix D.

The quantum yield of PdTPTBP – TTBPer CrEL:EO:STA micelles in water suspension was relatively reasonable, 0.6 % which is in line with previously reported values [43] making the pair potentially sufficient for future applications. The power density threshold of these micelles was relatively low in anoxic conditions (143 mW/cm^2). This value was relatively higher (789 mW/cm^2) for unmodified PdTPTBP – TTBPer CrEL:EO micelles (in anoxia) but this formulation contained much less TTBPer than the STA modified counterpart making the overall TF-UC process harder to induce hence the need for higher excitation power density. However, even this higher power density threshold could be useful depending on the upconversion quantum yield of the micelles which was not determined in this work. Additionally, the power density threshold of PtOEP – TTBPer loaded CrEL:EO micelles was also relatively low in anoxic conditions (240 mW/cm^2) and upconversion was recorded even in oxic conditions with the power density threshold of 2424 mW/cm^2. Overview on the results is presented in the Appendix D.

Finally, upconversion spectra of PdTPTBP – TTBPer CrEL:EO micelles loaded in nanofibrillar cellulose hydrogel was recorded using different excitation power densities. For this, a *Medium-loading gel* was used (167 µl of *Micellar suspension* per 1 g gel). By using the highest excitation power densities provided by the equipment the weak annihilation regime was reached and upconverted light even visible to the naked eye was induced. However, this suggests that the hydrogel is not able work as a secondary barrier for molecular oxygen, and micelles with better initial oxygen scavenging ability should be used. So, in conclusion, CrEL based micelles performed better overall in terms of their retention in hydrogel as opposed to T80 based micelles, and higher loading of micelles was found to improve both their retention and stability of TTBPer intensity in the released micelles. The charge modifications of micelles did improve the surface charge of the micelles from anionic to neutral, but it also caused the micelles to be released faster from hydrogel than the unmodified ones as well as the TTBPer intensity in the released micelles to decrease faster. Thus charge modification as studied in this work is unsuitable method to improve retention of micelles. Out of the sensitizer – annihilator pairs tested the PdTPTBP – TTBPer pair was studied the most and it performed as expected when loaded

in CrEL:EO:STA micelles and its upconversion spectrum in hydrogel while loaded into CrEL:EO micelles was successfully recorded. However, this dye pair might not be the best one in terms of its oxygen sensitivity and PtOEP – TTBPer might be a better suited option instead. To confirm this, the PtOEP – TTBPer pair would have to be tested for its quantum yield in solution, but the power density threshold of about 2400 mW/cm^2 might be enough for it to work in hydrogel as well. Additionally, working with stiffer gel, e.g., 2 m-%, might help with both micelle retention and better prevent oxygen diffusion. Also, cross-linking of hydrogel might be another viable idea to improve retention as opposed to laborious optimization of suitable micelles. Finally, it seems that the determination of power density threshold and even upconversion quantum yield of micelles entrapped in hydrogel is potentially possible once a better oxygen resistant system, micelles, hydrogel or both, is assessed.

REFERENCES

[1] Chen X, Peng D, Ju Q, Wang F. Photon upconversion in core-shell nanoparticles. Chem Soc Rev 2015;44:1330. https://doi.org/10.1039/c4cs00151f.

[2] Monguzzi A, Tubino R, Hoseinkhani S, Campione M, Meinardi F. Low power, non-coherent sensitized photon up-conversion: modelling and perspectives. Physical Chemistry Chemical Physics 2012;14:4322–32. https://doi.org/10.1039/C2CP23900K.

[3] Askes SHC, Bahreman A, Bonnet S. Activation of a Photodissociative Ruthenium Complex by Triplet-Triplet Annihilation Upconversion in Liposomes**. Angewandte Chemie 2014;53:1029–33. https://doi.org/10.1002/anie.201309389.

[4] Bharmoria P, Kasper M-P, Bildirir H, Moth-Poulsen K. Triplet-triplet annihilation based near infrared to visible molecular photon upconversion. Chem Soc Rev 2020;49:6529. https://doi.org/10.1039/d0cs00257g.

[5] Askes SHC, Bonnet S. Solving the oxygen sensitivity of sensitized photon upconversion in life science applications. Nature Reviews Chemistry 2018;2:437–52. https://doi.org/10.1038/s41570-018-0057-z.

[6] Zhu X, Su Q, Feng W, Li F. Anti-Stokes shift luminescent materials for bio-applications. Chem Soc Rev 2017;46:1039. https://doi.org/10.1039/c6cs00415f.

[7] Filatov MA, Baluschev S, Landfester K. Protection of densely populated excited triplet state ensembles against deactivation by molecular oxygen. Chem Soc Rev 2016;45:4668. https://doi.org/10.1039/c6cs00092d.

[8] Cui X, Zhao J, Yang P, Sun J. Zinc(II) tetraphenyltetrabenzoporphyrin complex as triplet photosensitizer for triplet–triplet annihilation upconversion. Chem Commun 2013;49:10221–3. https://doi.org/10.1039/c3cc45843a.

[9] Tao R, Zhao J, Zhong F, Zhang C, Yang W, Xu K. H2O2-activated triplet-triplet annihilation upconversion via modulation of the fluorescence quantum yields of the triplet acceptor and the triplet-triplet-energy-transfer efficiency. Chem Commun 2015;51:12406. https://doi.org/10.1039/c5cc04325e.

[10] Liu Q, Wang W, Zhan C, Yang T, Kohane DS. Enhanced Precision of Nanoparticle Phototargeting in Vivo at a Safe Irradiance. Nano Lett 2016;16:16. https://doi.org/10.1021/acs.nanolett.6b01730.

[11] Bharmoria P, Hisamitsu S, Nagatomi H, Ogawa T, Morikawa M-A, Yanai N, et al. Simple and Versatile Platform for Air-Tolerant Photon Upconverting Hydrogels by Biopolymer−Surfactant−Chromophore Co-assembly. J Am Chem Soc 2018;140:10848–55. https://doi.org/10.1021/jacs.8b05821.

[12] Wardle B. Principles and Applications of Photochemistry: 1 Introductory Concepts. 2010.

[13] Wardle B. Principles and Applications of Photochemistry: 3. The Physical Deactivation of Excited States. John Wiley & Sons, Incorporated; 2009.

[14] Parker CA, Hatchard CG. Delayed fluorescence from solutions of anthracene and phenanthrene. Proceedings of the Royal Society of London Series A Mathematical and Physical Sciences 1962;269:574–84.

[15] Isokuortti J. NEW PORPHYRINS FOR EFFICIENT TTAUC IN VISCOUS SOLUTIONS. 2019.

[16] Kimizuka N, Yanai N, Morikawa M-A. Photon Upconversion and Molecular Solar Energy Storage by Maximizing the Potential of Molecular Self-Assembly. Langmuir 2016;32:12304–22. https://doi.org/10.1021/acs.langmuir.6b03363.

[17] Schulze TF, Schmidt TW. Photochemical upconversion: present status and prospects for its application to solar energy conversion. Energy & Environmental Science 2015;8:103–25. https://doi.org/10.1039/c4ee02481h.

[18] Singh-Rachford TN, Castellano FN. Photon upconversion based on sensitized triplet-triplet annihilation. Coordination Chemistry Reviews 2010;254:2560–73. https://doi.org/10.1016/j.ccr.2010.01.003.

[19] Hoseinkhani S, Tubino R, Meinardi F, Monguzzi A. Achieving the photon up-conversion thermodynamic yield upper limit by sensitized triplet–triplet annihilation. Phys Chem Chem Phys 2015;17:4020–4. https://doi.org/10.1039/c4cp03936j.

[20] Borisov SM, Larndorfer C, Klimant I. Triplet-triplet annihilation-based anti-stokes oxygen sensing materials with a very broad dynamic range. Advanced Functional Materials 2012;22:4360–8. https://doi.org/10.1002/adfm.201200794.

[21] Durandin N, Isokuortti J, Efimov A, Vuorimaa-Laukkanen E, Tkachenko N v., Laaksonen T. Efficient photon upconversion at remarkably low annihilator concentrations in liquid polymer matrix: when less is more. Chem Commun 2018. https://doi.org/10.1039/C8CC07592A.

[22] Durandin NA, Isokuortti J, Efimov A, Vuorimaa-Laukkanen E, Tkachenko N v, Laaksonen T. Critical Sensitizer Quality Attributes for Efficient Triplet−Triplet Annihilation Upconversion with Low Power Density Thresholds. J Phys Chem C 2019;123:22865–72. https://doi.org/10.1021/acs.jpcc.9b08026.

[23] Braslavsky SE. Glossary of terms used in photochemistry 3rd edition: (IUPAC Recommendations 2006). Pure and Applied Chemistry 2007;79:293–465. https://doi.org/10.1351/PAC200779030293/MACHINEREADABLECITATION/RIS.

[24] Zhou Y, Castellano FN, Schmidt TW, Hanson K. On the Quantum Yield of Photon Upconversion via Triplet−Triplet Annihilation. ACS Energy Letters 2020;5:2322–6. https://doi.org/10.1021/acsenergylett.0c01150.

[25] On the Quantum Yield of Photon Upconversion via Triplet−Triplet Annihilation. ACS Energy Lett 2020;5:2322–6. https://doi.org/10.1021/acsenergylett.0c01150.

[26] Monguzzi A, Mezyk J, Scotognella F, Tubino R, Meinardi F. Upconversion-induced fluorescence in multicomponent systems: Steady-state excitation power threshold. Physical Review B 2008;78:195112. https://doi.org/10.1103/PhysRevB.78.195112.

[27] Edhborg F, Olesund A, Albinsson B. Best practice in determining key photophysical parameters in triplet-triplet annihilation photon upconversion. Photochemical & Photobiological Sciences 2022. https://doi.org/10.1007/s43630-022-00219-x.

[28] Wang X, Ye C, Wang B, Hao R, Wang X, Ding P, et al. Oil-in-water microemulsion: an effective medium for triplet-triplet annihilated upconversion with efficient triplet acceptors. J Mater Chem C 2014;2:8507–14. https://doi.org/10.1039/c4tc00791c.

[29] Liu Q, Xu M, Yang T, Tian B, Zhang X, Li F. Highly Photostable Near-IR-Excitation Upconversion Nanocapsules Based on Triplet−Triplet Annihilation for in Vivo Bioimaging Application. ACS Appl Mater Interfaces 2018;10:9883–8. https://doi.org/10.1021/acsami.7b17929.

[30] Liu Q, Yin B, Yang T, Yang Y, Shen Z, Yao P, et al. A General Strategy for Biocompatible, High-Effective Upconversion Nanocapsules Based on Triplet−Triplet Annihilation. J Am Chem Soc 2013;135:5029–37. https://doi.org/10.1021/ja3104268.

[31] Seok Kwon O, Seok Song H, Kim H, Artzi N, Kim J-H. Dual-Color Emissive Upconversion Nanocapsules for Differential Cancer Bioimaging In Vivo. ACS Nano 2016;10:1512–21. https://doi.org/10.1021/acsnano.5b07075.

[32] Turshatov A, Busko D, Baluschev S, Miteva T, Landfester K. Micellar carrier for triplet-triplet annihilation-assisted photon energy upconversion in a water environment. New Journal of Physics 2011;13. https://doi.org/10.1088/1367-2630/13/8/083035.

[33] Moulik SP. Micelles: Self-organized surfactant assemblies. Current Science 1996;71:368–76.

[34] IUPAC, McNaught AD, Wilkinson A. Critical Micelle Concentration. In: Chalk SJ, editor. Compendium of Chemical Terminology (the “Gold Book”) Online version (2019-). 2nd ed., Oxford: Blackwell Scientific Publications; 1997. https://doi.org/10.1351/goldbook.c01395.

[35] IUPAC, McNaught AD, Wilkinson A. Krafft point. In: Chalk SJ, editor. Compendium of Chemical Terminology (the “Gold Book”) Online version (2019-). 2nd ed., Oxford: Blackwell Scientific Publications; 1997. https://doi.org/10.1351/goldbook.k03415.

[36] Rafique AS, Khodaparast S, Poulos AS, Sharratt WN, J Robles ES, Cabral JT. Micellar structure and transformations in sodium alkylbenzenesulfonate (NaLAS) aqueous solutions: effects of concentration, temperature, and salt. Soft Matter 2020;16:7835–44. https://doi.org/10.1039/d0sm00982b.

[37] Bittinger T, Bradburn D. Micelles : Structural Biochemistry, Formation and Functions & Usage. Hauppauge, New York: Nova Science Publishers, Inc; 2013.

[38] Mattiello S, Monguzzi A, Pedrini J, Sassi M, Villa C, Torrente Y, et al. Self-Assembled Dual Dye-Doped Nanosized Micelles for High-Contrast Up-Conversion Bioimaging.

Advanced Functional Materials 2016;26:8447–54. https://doi.org/10.1002/adfm.201603303.
[39] Liu Q, Yang T, Feng W, Li F. Blue-Emissive Upconversion Nanoparticles for Low-Power-Excited Bioimaging in Vivo. J Am Chem Soc 2012;134:5390–7. https://doi.org/10.1021/ja3003638.
[40] Sanders SN, Gangishetty MK, Sfeir MY, Congreve DN. Photon Upconversion in Aqueous Nanodroplets. Journal of American Chemical Society 2019;141:9180–4. https://doi.org/10.1021/jacs.9b03992.
[41] Gelderblom H, Verweij J, Nooter K, Sparreboom A. Cremophor EL: the drawbacks and advantages of vehicle selection for drug formulation. European Journal of Cancer 2001;37:1590–8.
[42] Inactive Ingredient Search for Approved Drug Products. US Food & Drug Administration (FDA) n.d. https://www.accessdata.fda.gov/scripts/cder/iig/index.cfm?event=browseByLetter.page&Letter=P (accessed April 4, 2022).
[43] Isokuortti J, Kiiski I, Sikanen T, Durandin N, Laaksonen T. Microfluidic oxygen tolerability screening of nanocarriers for triplet fusion photon upconversion. J Mater Chem C 2022;10:4871–7. https://doi.org/10.1039/d2tc00156j.
[44] Silva AL, Júnior FA, Mafra Verissimo L, Fassarella Agnez-Lima L, Carmem L, Egito M, et al. Physical Factors Affecting Plasmid DNA Compaction in Stearylamine-Containing Nanoemulsions Intended for Gene Delivery. Pharmaceuticals 2012;5:643–54. https://doi.org/10.3390/ph5060643.
[45] Naqvi AZ, Noori S. Experimental and Theoretical Approach to Mixed Systems of Non-Ionic Cremophor EL and Cationic Gemini Surfactants in Aqueous Solution. Z Phys Chem 2015;229:395–415. https://doi.org/10.1515/zpch-2014-0577.
[46] Falsini S, Ristori S. Lipoplexes from Non-viral Cationic Vectors: DOTAP-DOPE Liposomes and Gemini Micelles. Non-Viral Gene Delivery Vectors Methods in Molecular Biology 2016;1445:33–43. https://doi.org/10.1007/978-1-4939-3718-9_3.
[47] Malvern Instruments Ltd. Zetasizer Nano Series User Manual 2004.
[48] Curvello R, Raghuwanshi VS, Garnier G. Historical perspective: Engineering nanocellulose hydrogels for biomedical applications. Advances in Colloid and Interface Science 2019;267:47–61. https://doi.org/10.1016/j.cis.2019.03.002.
[49] Zhu H, Luo W, Ciesielski PN, Fang Z, Zhu JY, Henriksson G, et al. Wood-Derived Materials for Green Electronics, Biological Devices, and Energy Applications. Chemical Reviews 2016;116:9305–74. https://doi.org/10.1021/acs.chemrev.6b00225.
[50] Rånby BG. Fibrous macromolecular systems. Cellulose and muscle. The colloidal properties of cellulose micelles. Discuss Faraday Soc 1951;11:158–64. https://doi.org/10.1039/DF9511100158.
[51] Klemm D, Kramer F, Moritz S, Lindström T, Ankerfors M, Gray D, et al. Nanocelluloses: A New Family of Nature-Based Materials. Angewandte Chemie - International Edition 2011;50:5483–5466. https://doi.org/10.1002/anie.201001273.
[52] Saito T, Kimura S, Nishiyama Y, Isogai A. Cellulose Nanofibers Prepared by TEMPO-Mediated Oxidation of Native Cellulose 2007. https://doi.org/10.1021/bm0703970.
[53] Meir R, Hirschhorn T, Kim S, Fallon KJ, Churchill EM, Wu D, et al. Photon Upconversion Hydrogels for 3D Optogenetics 2021. https://doi.org/10.1002/adfm.202010907.
[54] Olmsted J. Calorimetric Determinations of Absolute Fluorescence Quantum Yields. Determinations of Fluorescence Quantum Yields The Journal of Physical Chemistry 1979;83:2584.
[55] Kumar Panigrahi S, Kumar Mishra A. Inner filter effect in fluorescence spectroscopy: As a problem and as a solution. Journal of Photochemistry and Photobiology C: Photochemistry Reviews 2019;41. https://doi.org/10.1016/j.jphotochemrev.2019.100318.
[56] Edinburgh Instruments. FLS980 Series Reference Guide: Integrating Sphere for Measurements of Fluorescence Quantum Yields and Spectral Reflectance. 2016.

APPENDIX A: MICELLE CHARACTERIZATION

Table 7. *Characterization of CrEL:EO:STA micelles: ζ-average sizes [Z-Ave], polydispersity indexes [PdI] and ζ-potentials [ZP] of the replicated micelle formulation as well as their average values and standard deviations. (Excel: AVEGARE and STDEV.S formulas)*

Replicate	Z-Ave (d.nm)	PdI	ZP (mV)	ZP error (+/- mV)
1	32,84	0,224	-3,26	3,76
2	25,06	0,259	-0,32	9,49
3	32,27	0,232	3,62	1,61
4	19,83	0,143	1,33	1,52
Average	27,50	0,215	0,34	4,09
Standar deviation	6,22	0,050	-	-

Table 8. *Characterization of T80:EO:DOATP micelles: ζ-average sizes [Z-Ave], polydispersity indexes [PdI] and ζ-potentials [ZP] of the replicated micelle formulation as well as their average values and standard deviations. (Excel: AVEGARE and STDEV.S formulas)*

Replicate	Z-Ave (d.nm)	PdI	ZP (mV)	ZP error (+/- mV)
1	11,54	0,217	-3,70	0,57
2	11,02	0,270	-1,72	1,04
Average	11,28	0,244	-2,71	0,80
Standar deviation	0,37	0,037	-	-

APPENDIX B: RELEASE STUDIES

Emission Spectra for Release Studies

CrEL:EO:STA micelles in *High-loading gel*, three replicates:

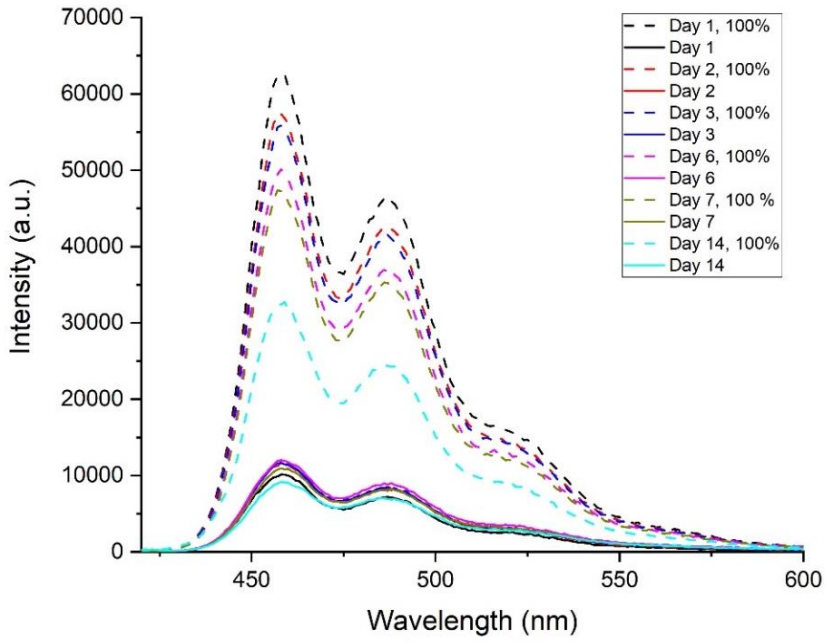

***Figure 22. CrEL:EO:STA** micelles release from **High-loading gel, 1st triplicate**. Dashed lines represent the 100 % release sample measured on the same day as the actual release samples (solid lines).*

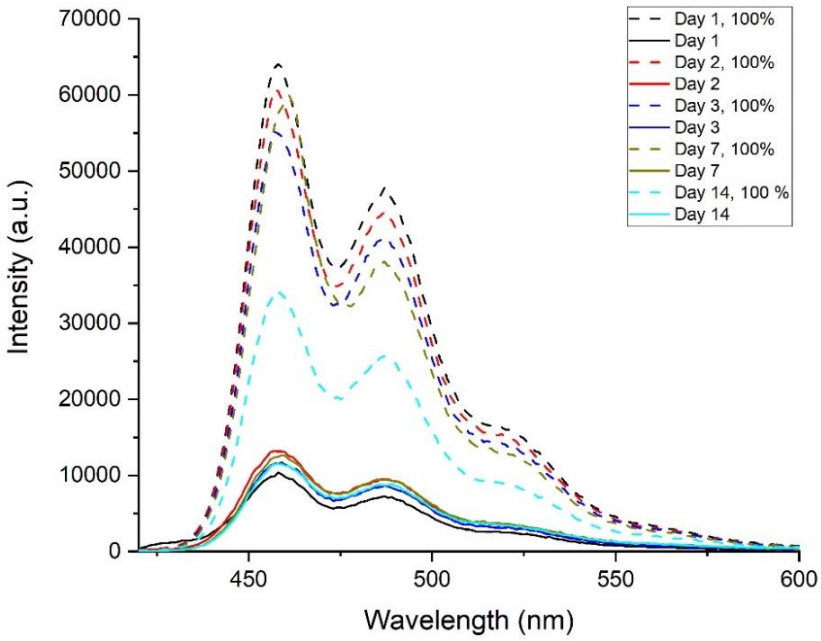

***Figure 23. CrEL:EO:STA** micelles release from **High-loading gel, 2nd triplicate**. Dashed lines represent the 100 % release sample measured on the same day as the actual release samples (solid lines).*

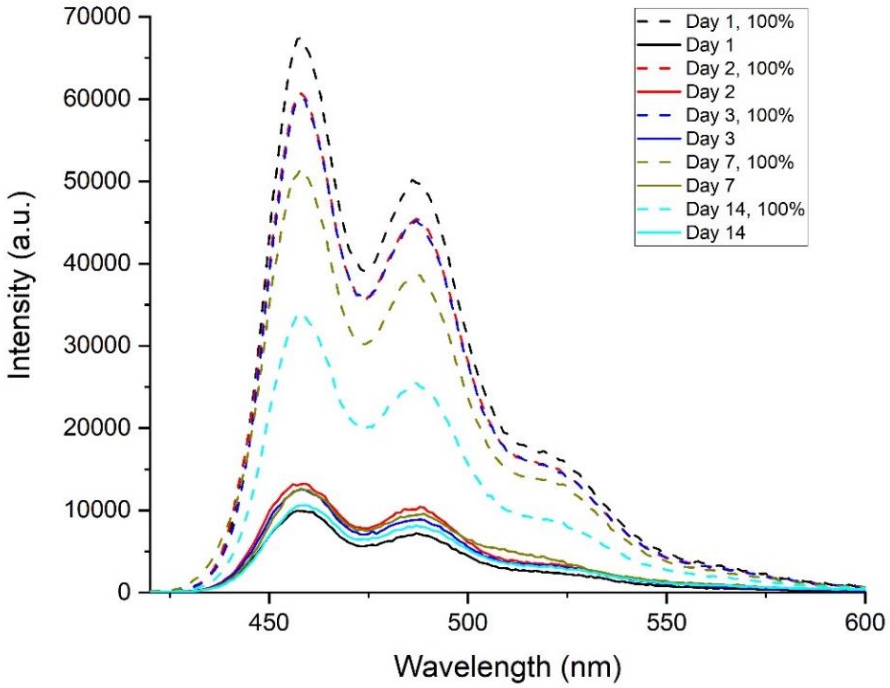

***Figure 24. CrEL:EO:STA** micelles release from **High-loading gel, 3rd triplicate**. Dashed lines represent the 100 % release sample measured on the same day as the actual release samples (solid lines).*

CrEL:EO:STA micelles in *Low-loading gel*, three replicates:

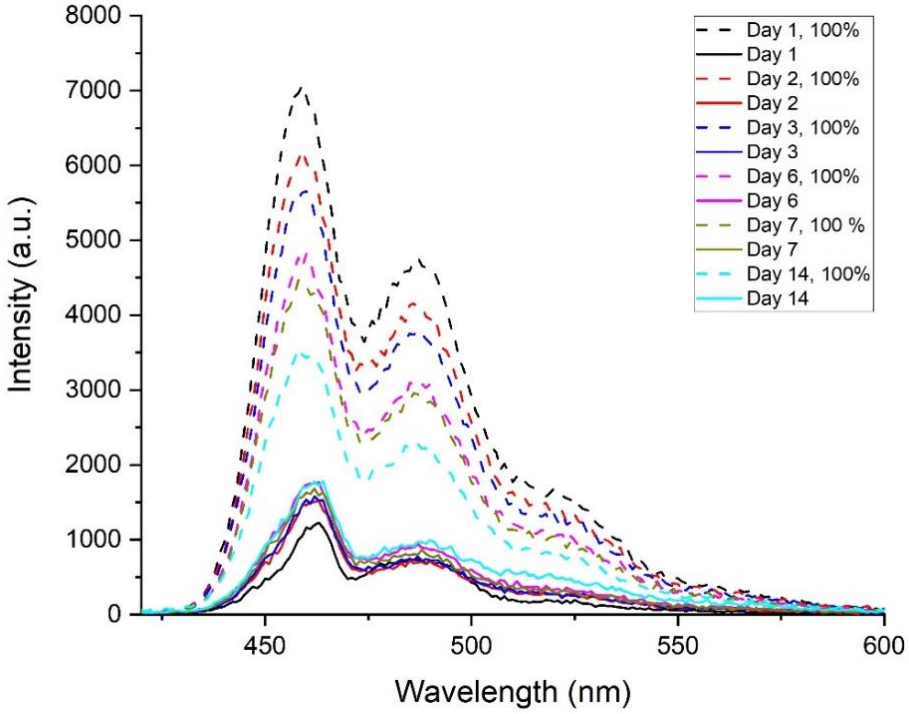

***Figure 25. CrEL:EO:STA** micelles release from **Low-loading gel, 1st triplicate**. Dashed lines represent the 100 % release sample measured on the same day as the actual release samples (solid lines).*

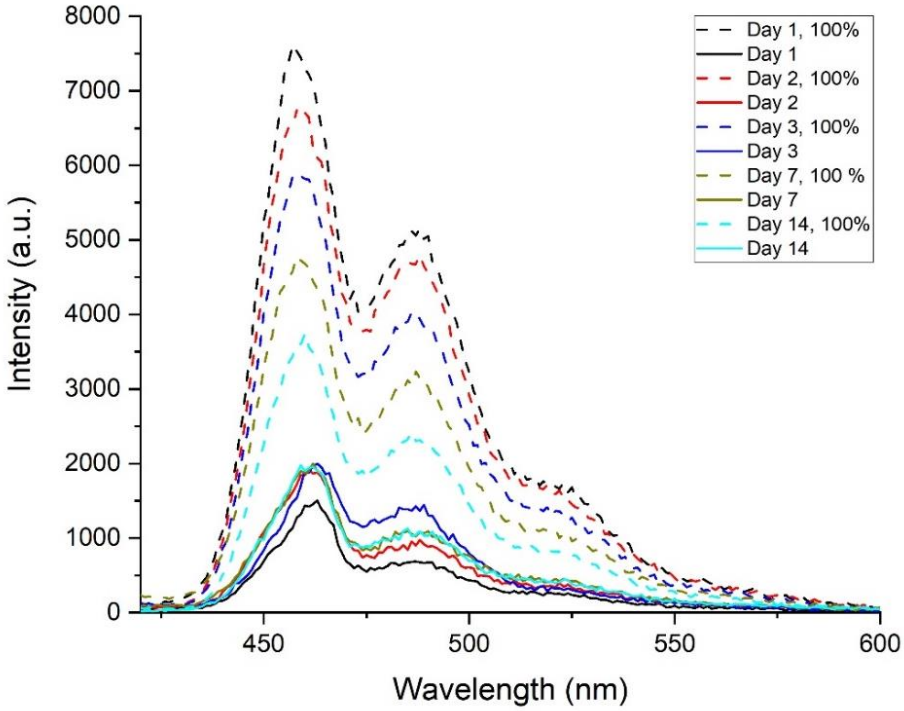

Figure 26. CrEL:EO:STA *micelles release from* ***Low-loading gel, 2nd triplicate****. Dashed lines represent the 100 % release sample measured on the same day as the actual release samples (solid lines).*

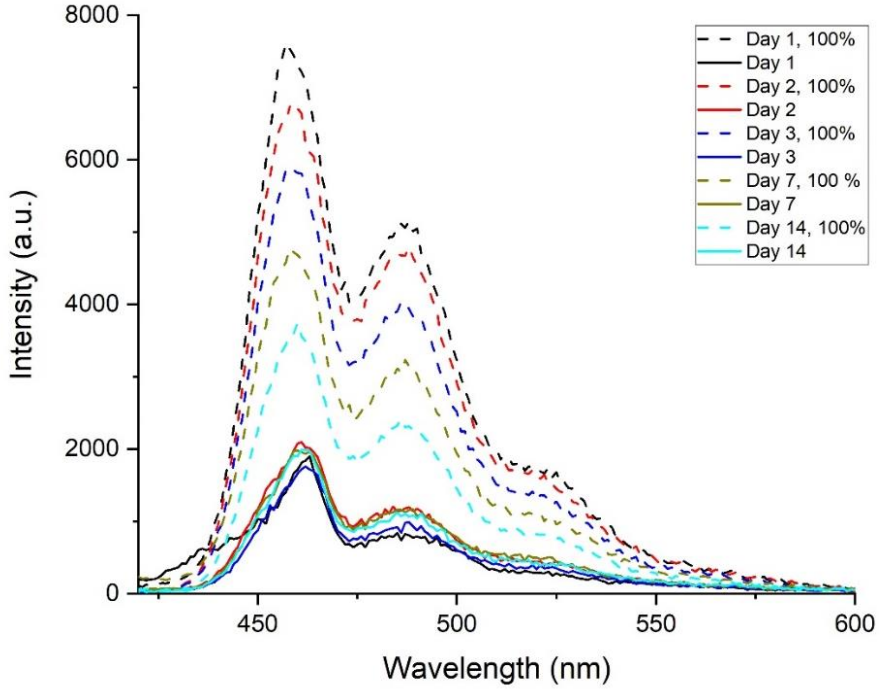

Figure 27. CrEL:EO:STA *micelles release from* ***Low-loading gel, 3rd triplicate****. Dashed lines represent the 100 % release sample measured on the same day as the actual release samples (solid lines).*

CrEL:EO micelles in *High-loading gel*, three replicates:

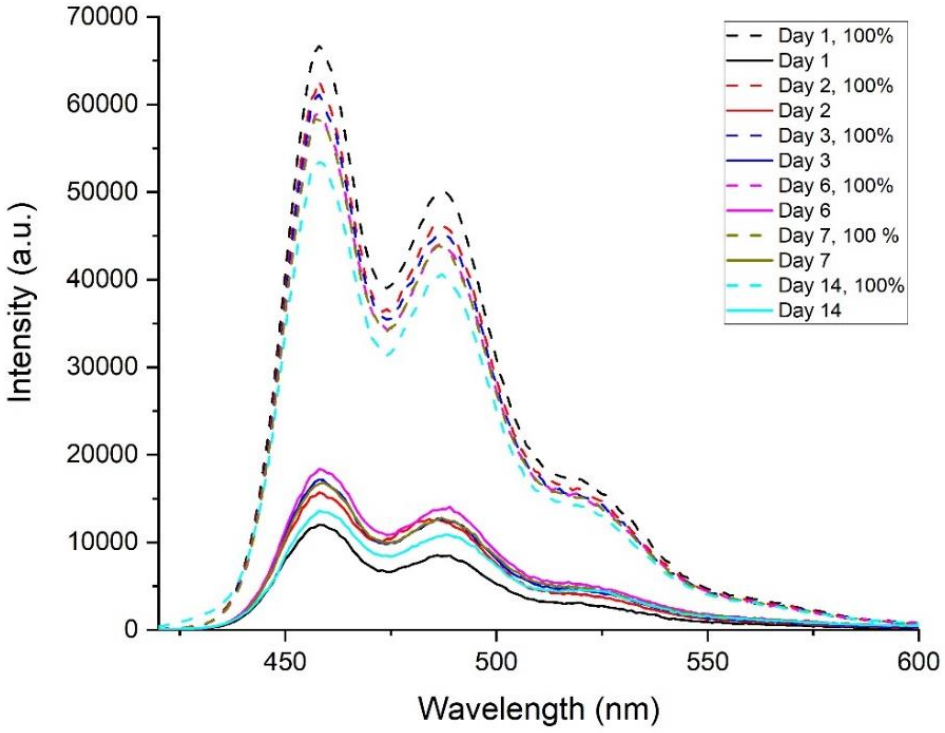

***Figure 28. CrEL:EO** micelles release from **High-loading gel, 1st triplicate**. Dashed lines represent the 100 % release sample measured on the same day as the actual release samples (solid lines).*

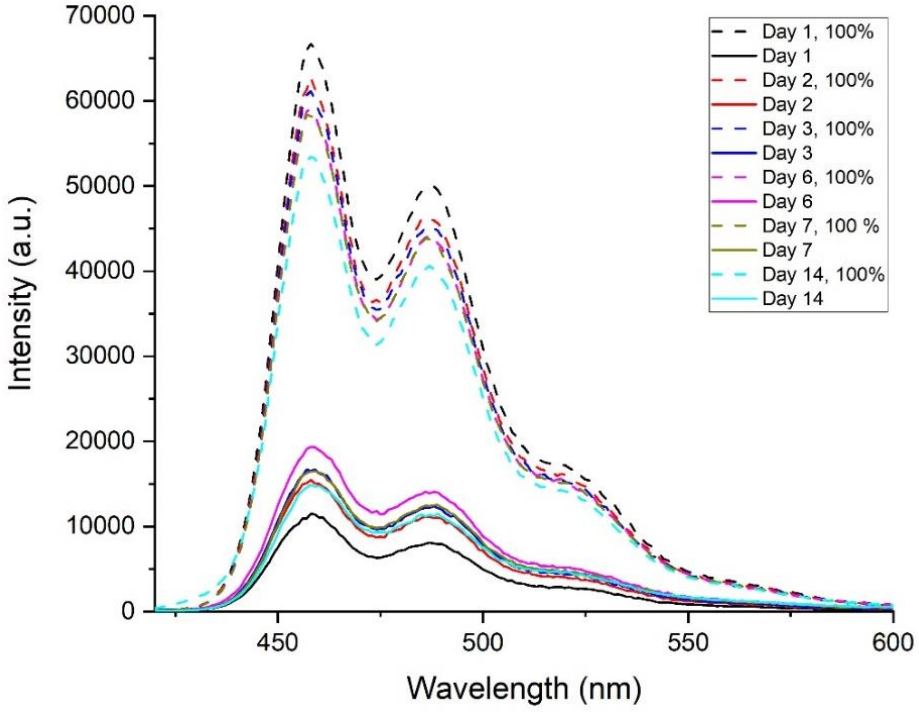

***Figure 29. CrEL:EO** micelles release from **High-loading gel, 2nd triplicate**. Dashed lines represent the 100 % release sample measured on the same day as the actual release samples (solid lines).*

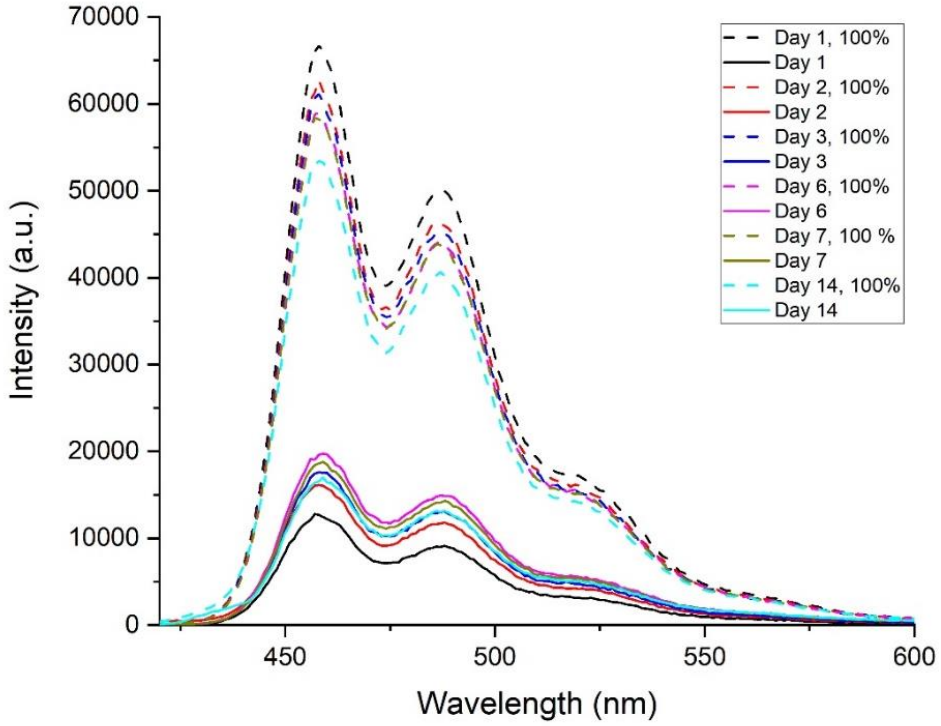

***Figure 30. CrEL:EO** micelles release from **High-loading gel, 3rd triplicate**. Dashed lines represent the 100 % release sample measured on the same day as the actual release samples (solid lines).*

CrEL:EO micelles in *Low-loading gel*, three replicates:

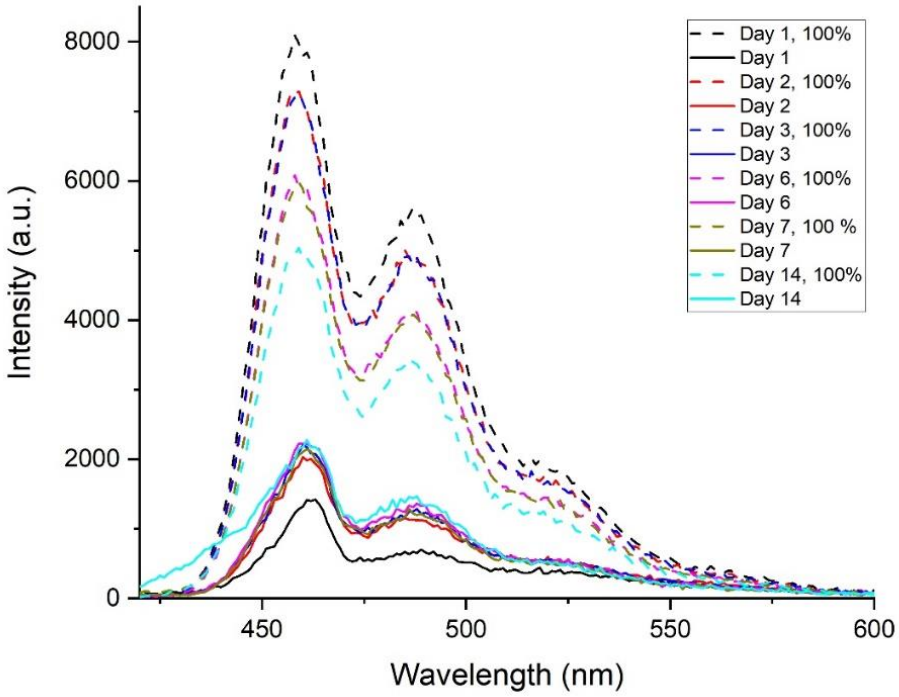

***Figure 31. CrEL:EO** micelles release from **Low-loading gel, 1st triplicate**. Dashed lines represent the 100 % release sample measured on the same day as the actual release samples (solid lines).*

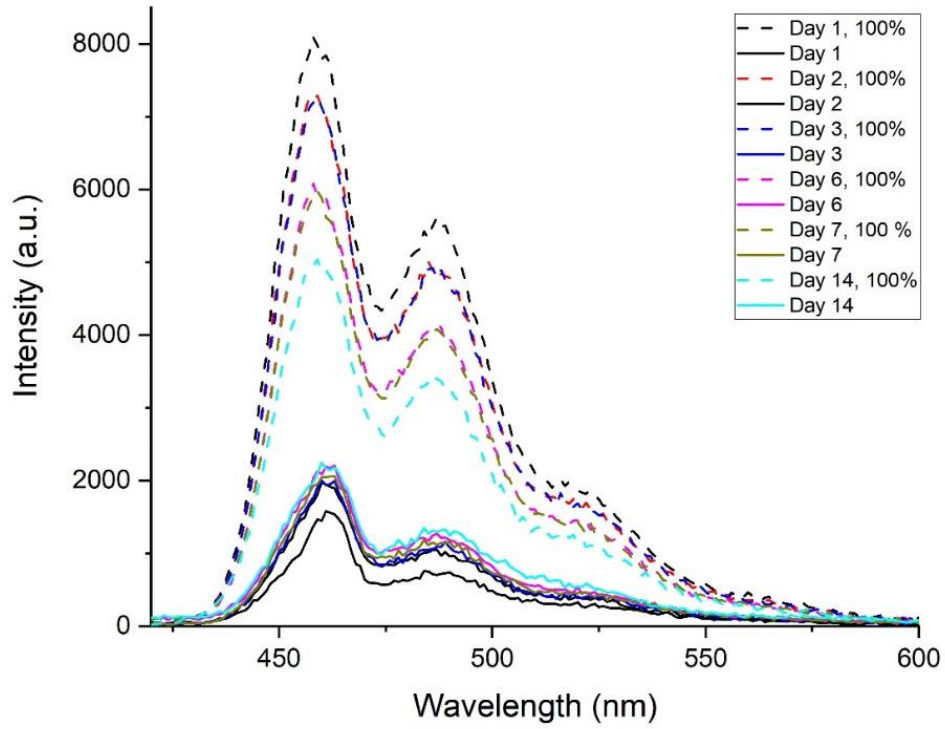

***Figure 32. CrEL:EO** micelles release from **Low-loading gel, 2nd triplicate**. Dashed lines represent the 100 % release sample measured on the same day as the actual release samples (solid lines).*

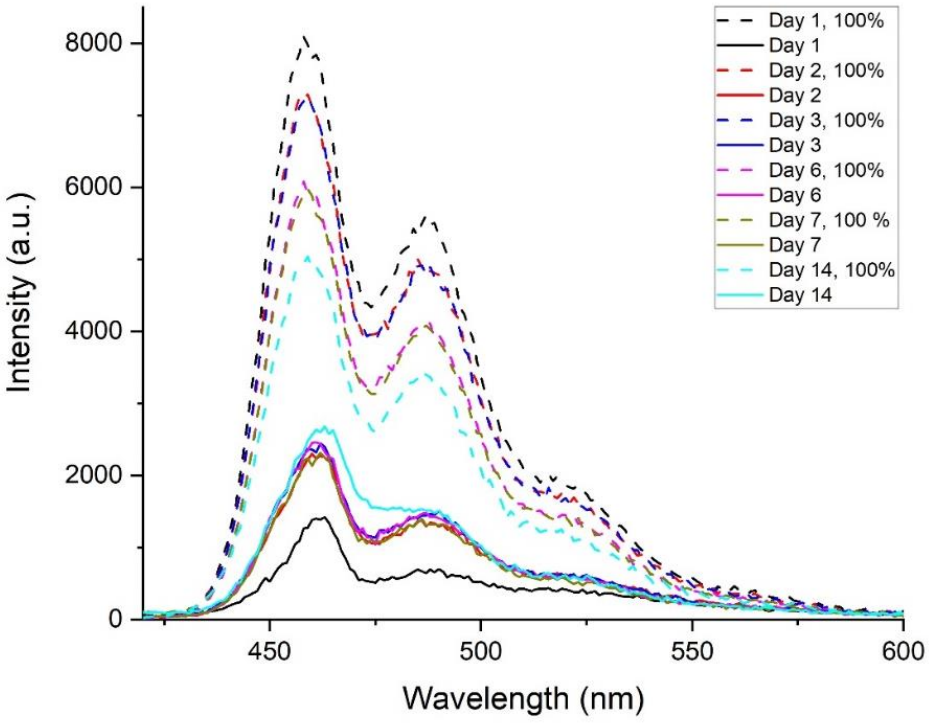

***Figure 33. CrEL:EO** micelles release from **Low-loading gel, 3rd triplicate**. Dashed lines represent the 100 % release sample measured on the same day as the actual release samples (solid lines).*

T80:EO:DOTAP micelles in *High-loading gel*, three replicates:

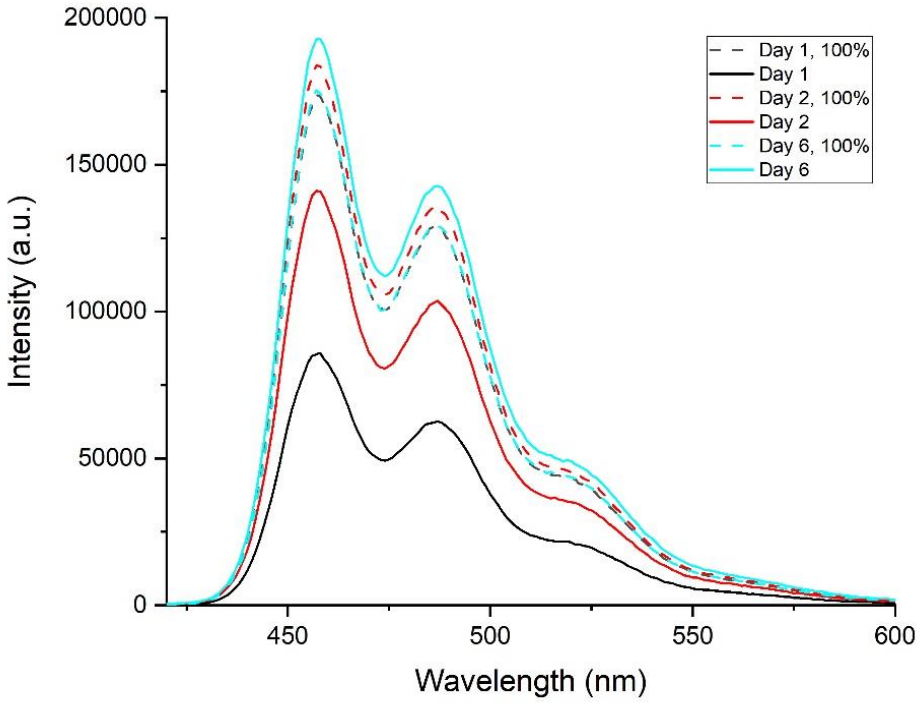

***Figure 34. T80:EO:DOTAP** micelles release from **High-loading gel, 1st triplicate**. Dashed lines represent the 100 % release sample measured on the same day as the actual release samples (solid lines).*

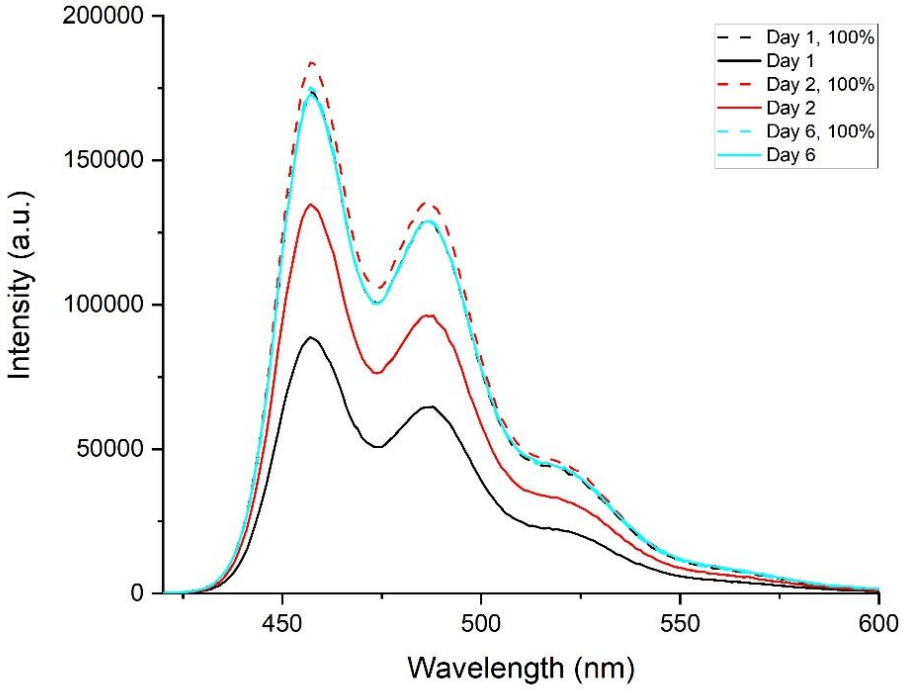

***Figure 35. T80:EO:DOTAP** micelles release from **High-loading gel, 2nd triplicate**. Dashed lines represent the 100 % release sample measured on the same day as the actual release samples (solid lines).*

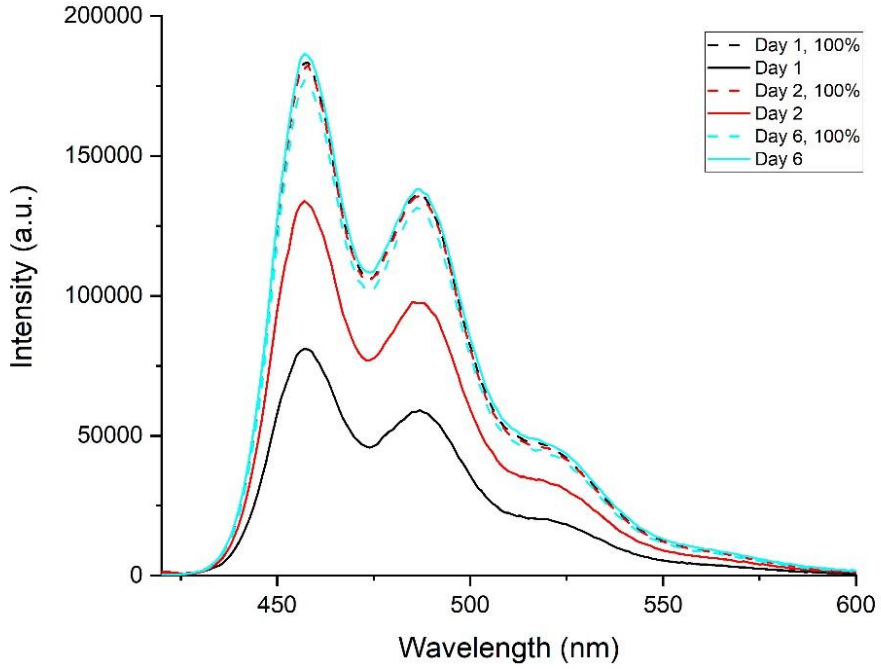

***Figure 36. T80:EO:DOTAP** micelles release from **High-loading gel, 3rd triplicate**. Dashed lines represent the 100 % release sample measured on the same day as the actual release samples (solid lines).*

T80:EO:DOTAP micelles in *Low-loading gel*, three replicates:

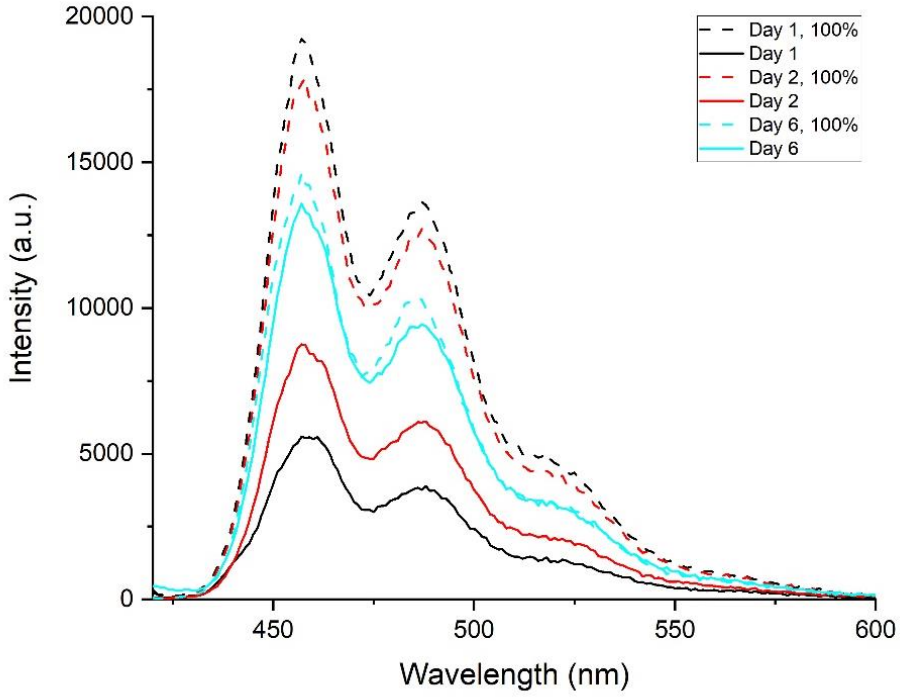

***Figure 37. T80:EO:DOTAP** micelles release from **Low-loading gel, 1st triplicate**. Dashed lines represent the 100 % release sample measured on the same day as the actual release samples (solid lines).*

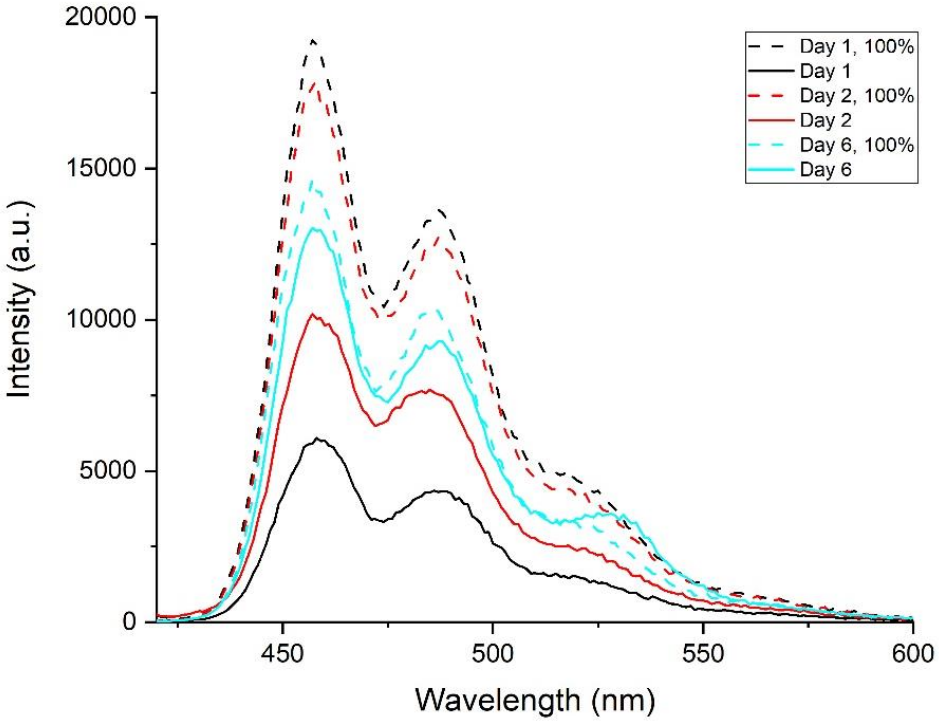

***Figure 38. T80:EO:DOTAP** micelles release from **Low-loading gel, 2nd triplicate**. Dashed lines represent the 100 % release sample measured on the same day as the actual release samples (solid lines).*

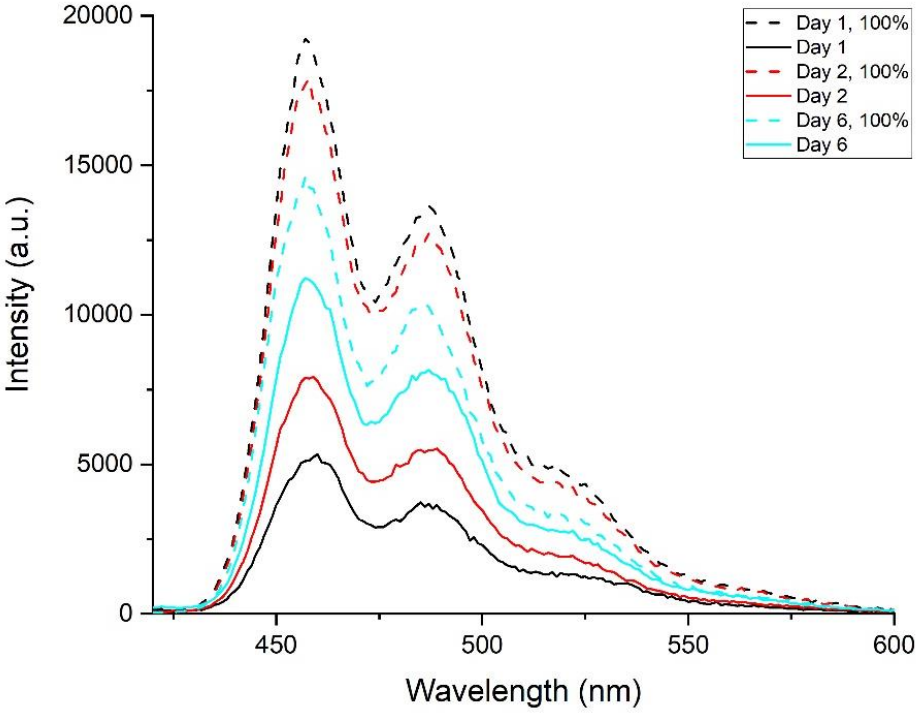

***Figure 39. T80:EO:DOTAP** micelles release from **Low-loading gel, 3rd triplicate**. Dashed lines represent the 100 % release sample measured on the same day as the actual release samples (solid lines).*

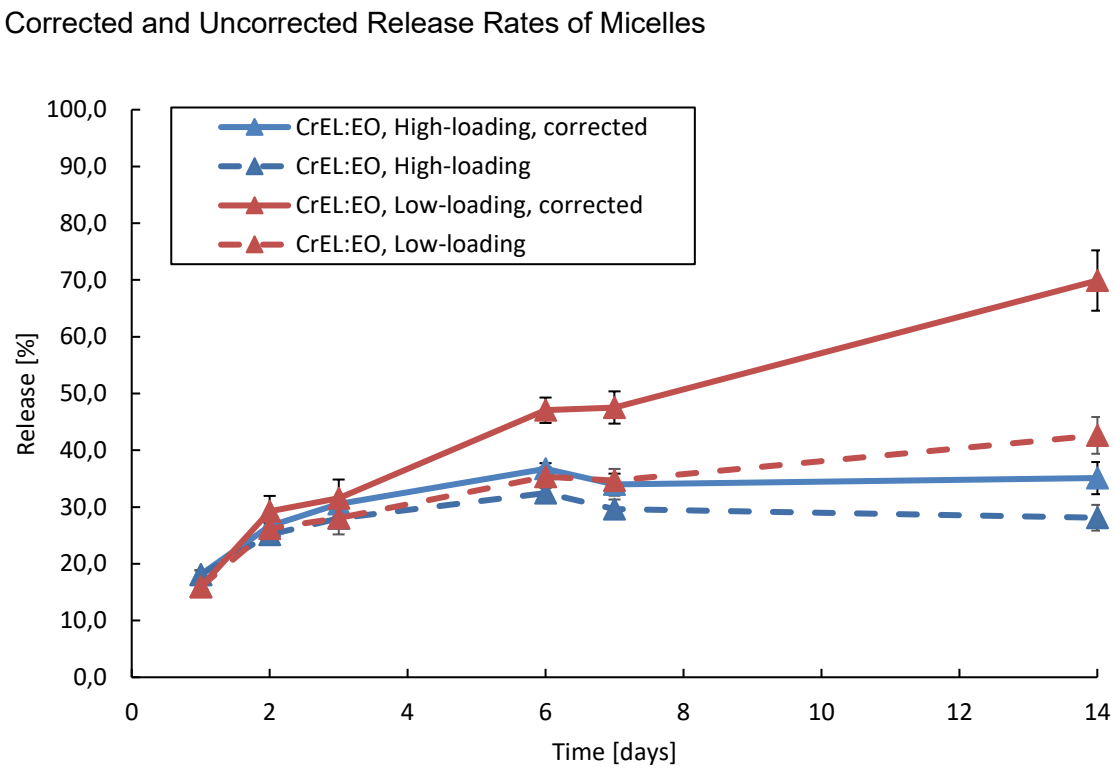

Figure 40. *Corrected and uncorrected release rates of unmodified CrEL:EO (PdTPTBP-TTBPer) micelles from High-loading and Low-loading gel.*

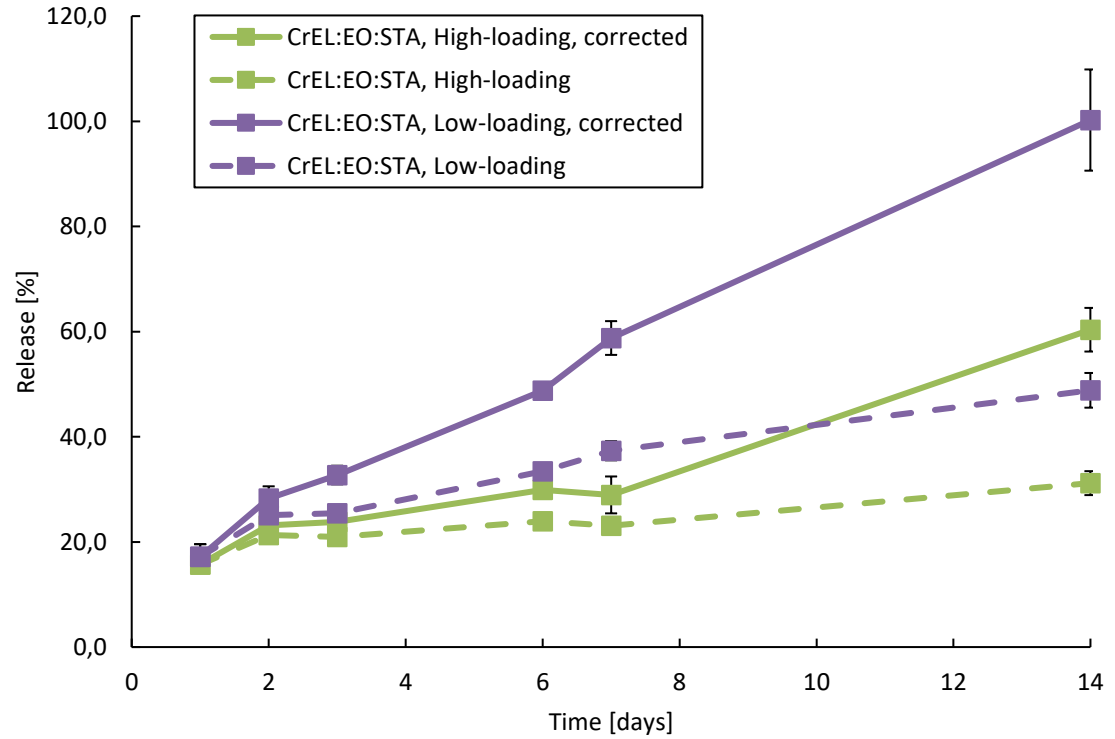

Figure 41. *Corrected and uncorrected release rates of unmodified CrEL:EO:STA (PdTPTBP-TTBPer) micelles from High-loading and Low-loading gel.*

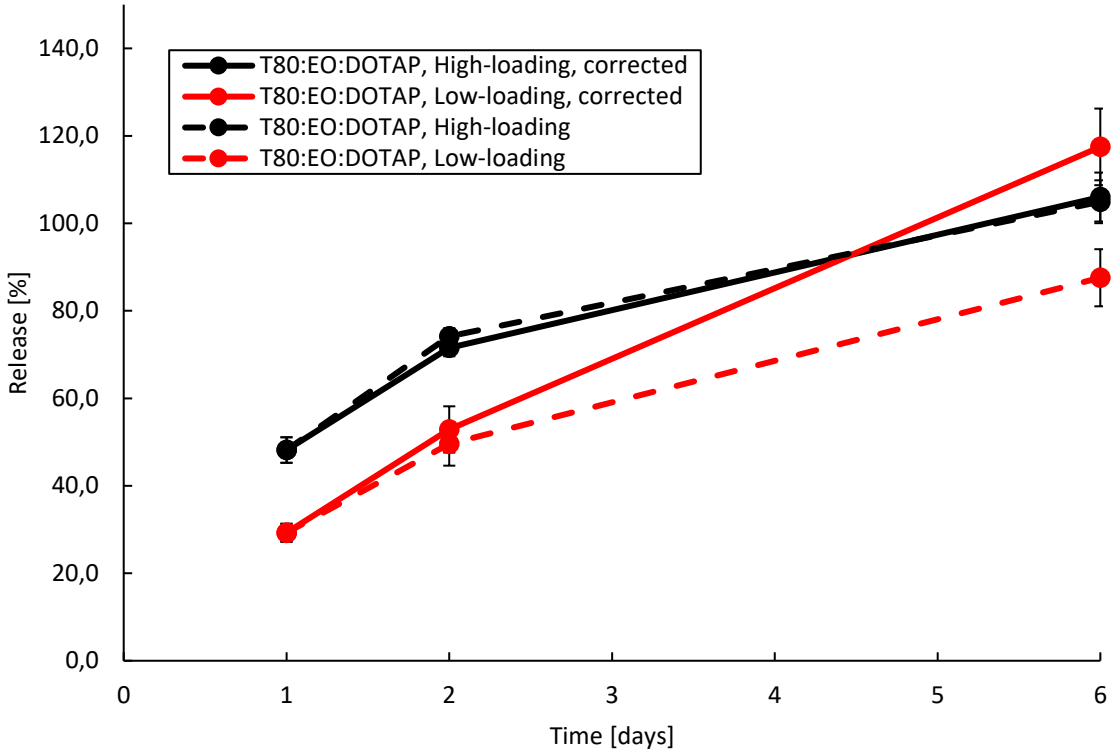

Figure 42. *Corrected and uncorrected release rates of unmodified T80:EO:DOTAP (PdTPTBP-TTBPer) micelles from High-loading and Low-loading gel.*

APPENDIX C: UPCONVERSION STUDIES

Emission Spectra of Micelles for Power Density Threshold

a)

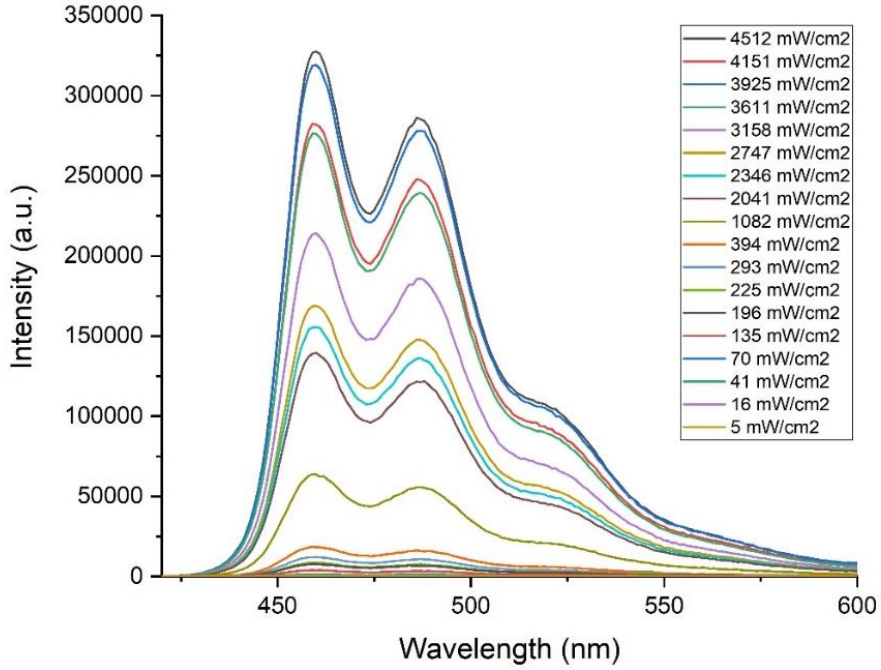

b)

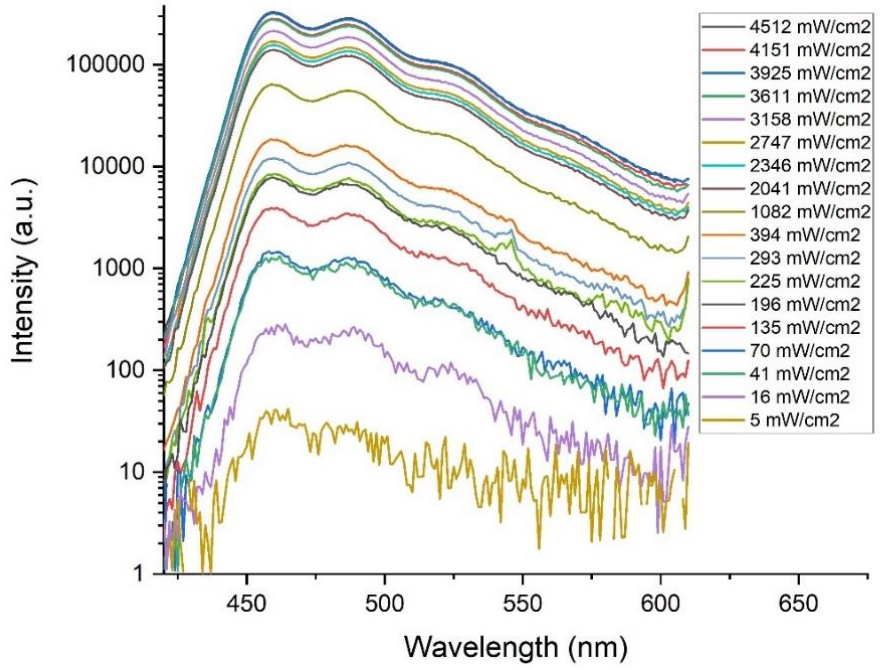

Figure 43. *Emission spectra of CrEL:EO:STA (PdTPTBP-TTBPer) in water suspension measured in anoxia using different excitation power densities,* $PD_{exc}, [mW/cm^2]$. *Spectra are presented in a) linear and b)logarithmic scale in terms of intensity.*

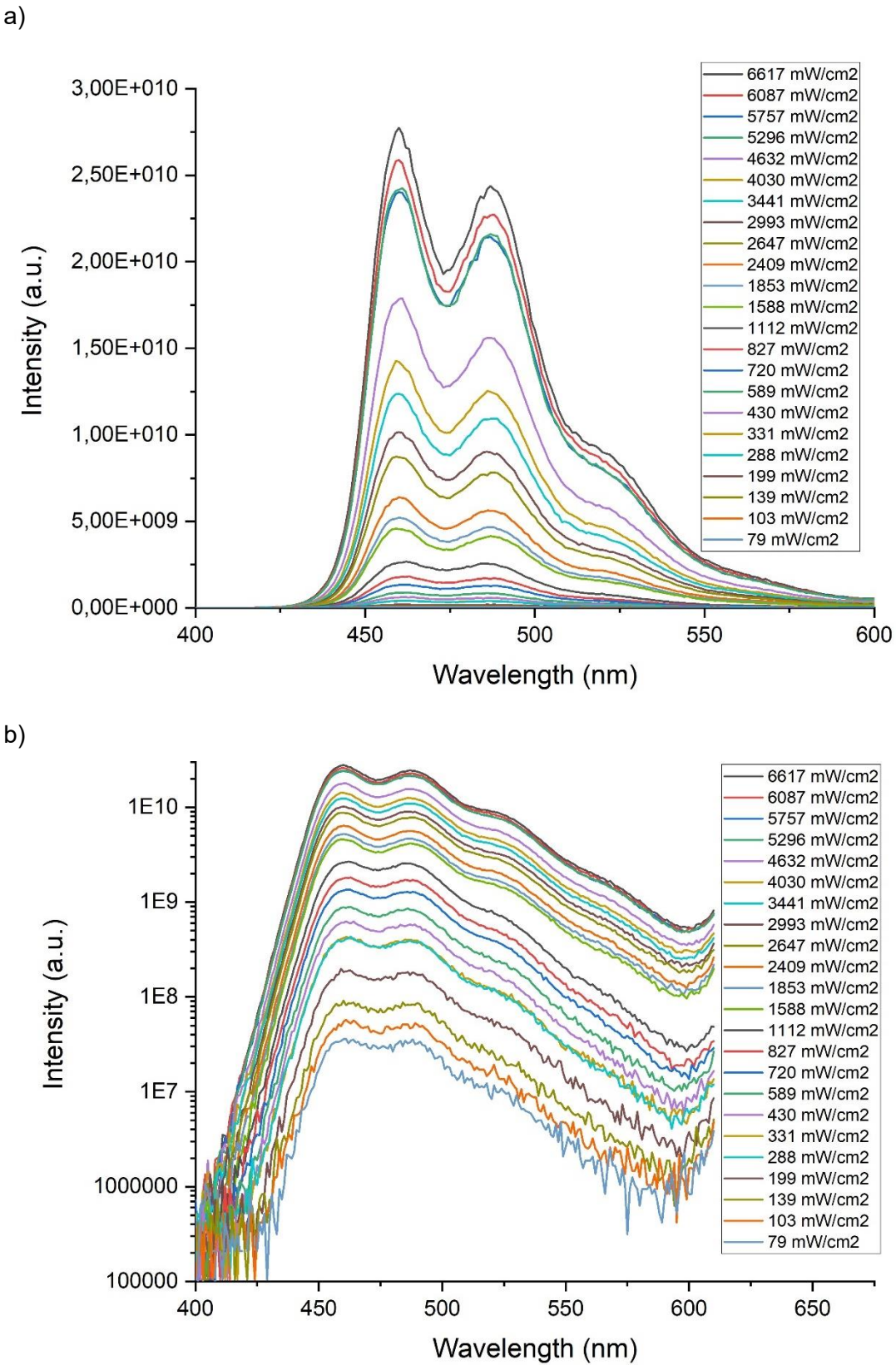

Figure 44. *Emission spectra of CrEL:EO (PdTPTBP-TTBPer) in water suspension measured in anoxia using different excitation power densities,* $PD_{exc}, [mW/cm^2]$*. Spectra are presented in a) linear and b)logarithmic scale in terms of intensity.*

a)

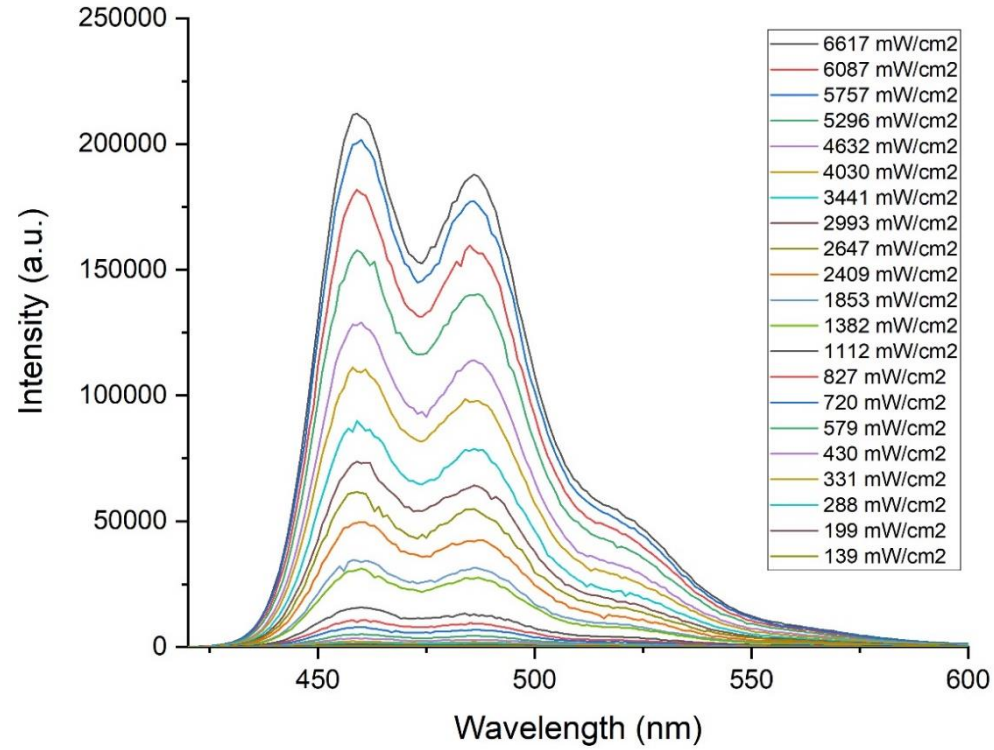

b)

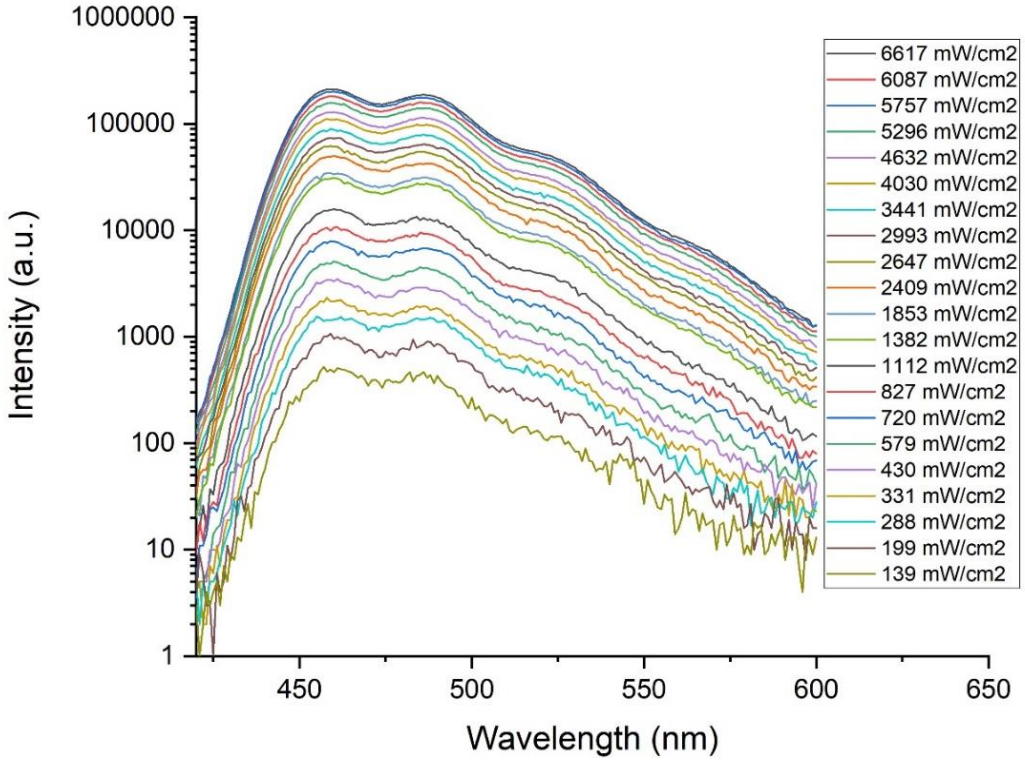

Figure 45. *Emission spectra of CrEL:EO (PtTPTBP-TTBPer) in water suspension measured in anoxia using different excitation power densities, PD_{exc}, $[mW/cm^2]$. Spectra are presented in a) linear and b)logarithmic scale in terms of intensity.*

a)

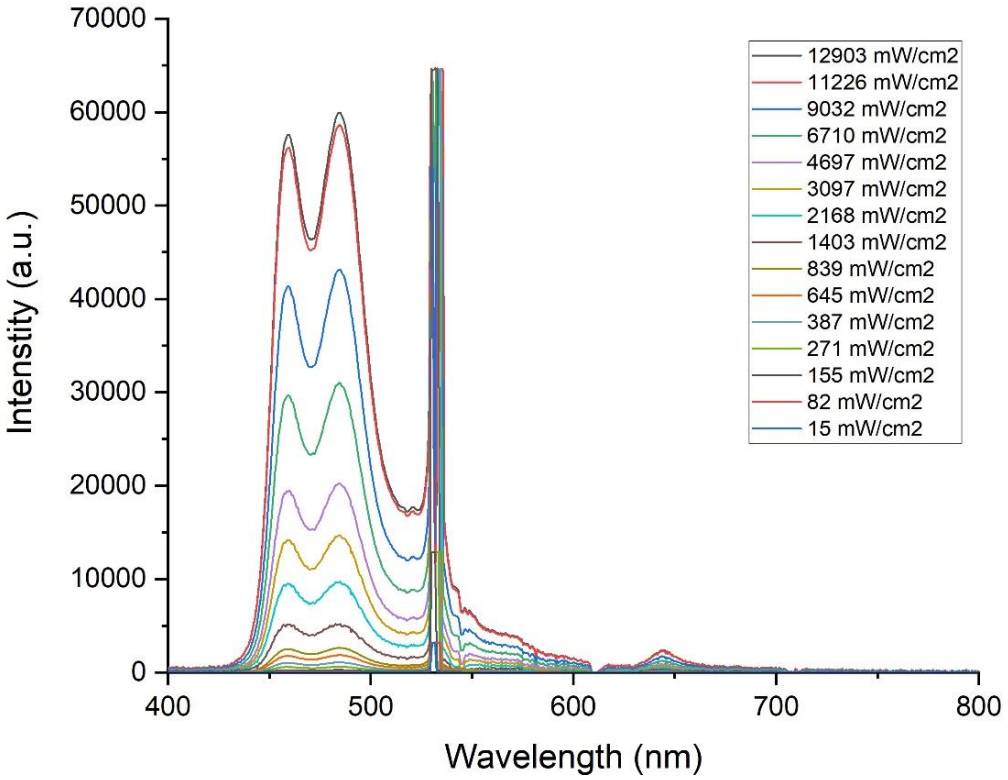

b)

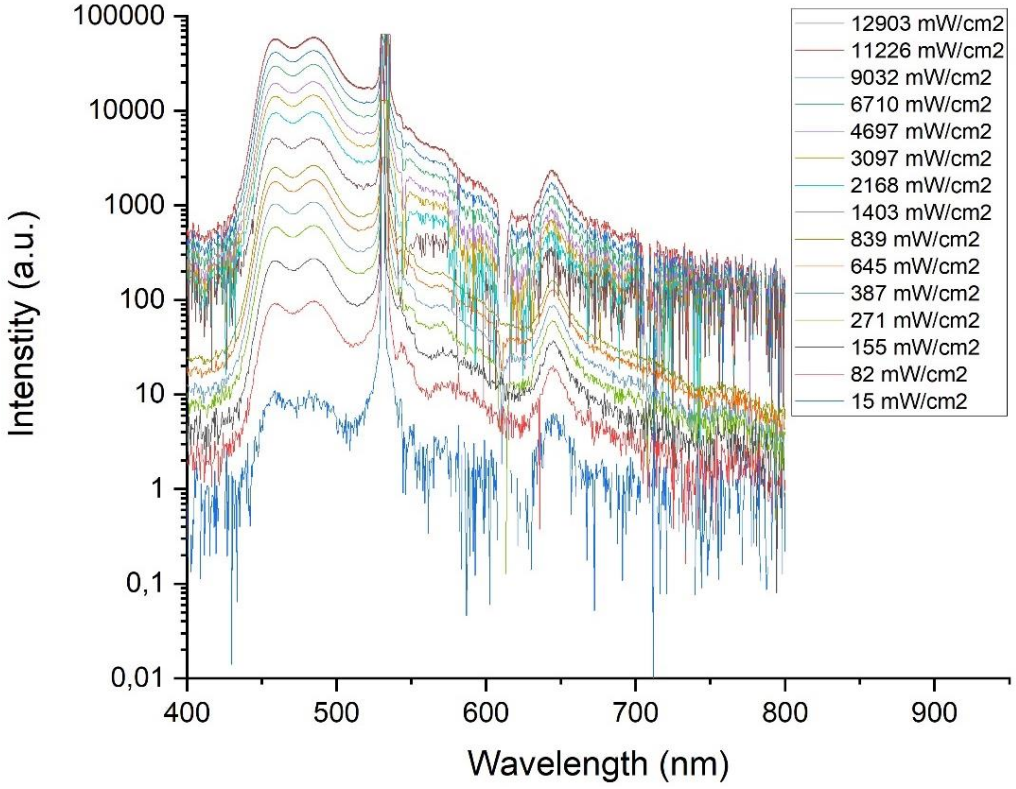

Figure 46. *Emission spectra of CrEL:EO (PtOEP-TTBPer) in water suspension measured in anoxia using different excitation power densities, $PD_{exc}, [mW/cm^2]$. Spectra are presented in a) linear and b)logarithmic scale in terms of intensity.*

a)

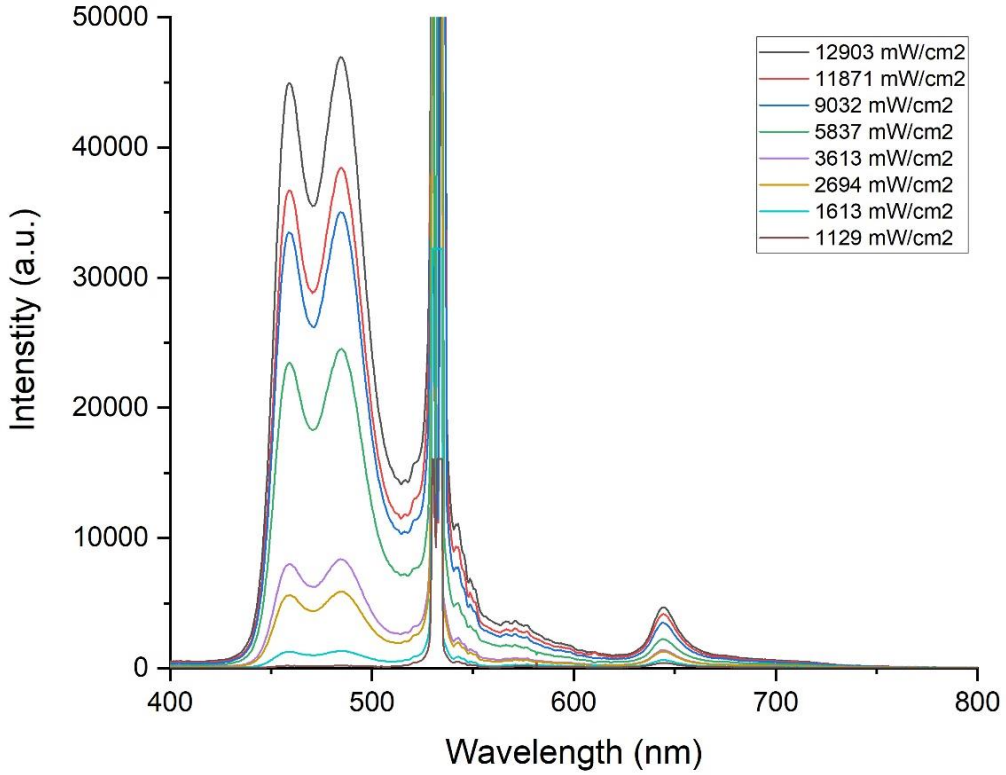

b)

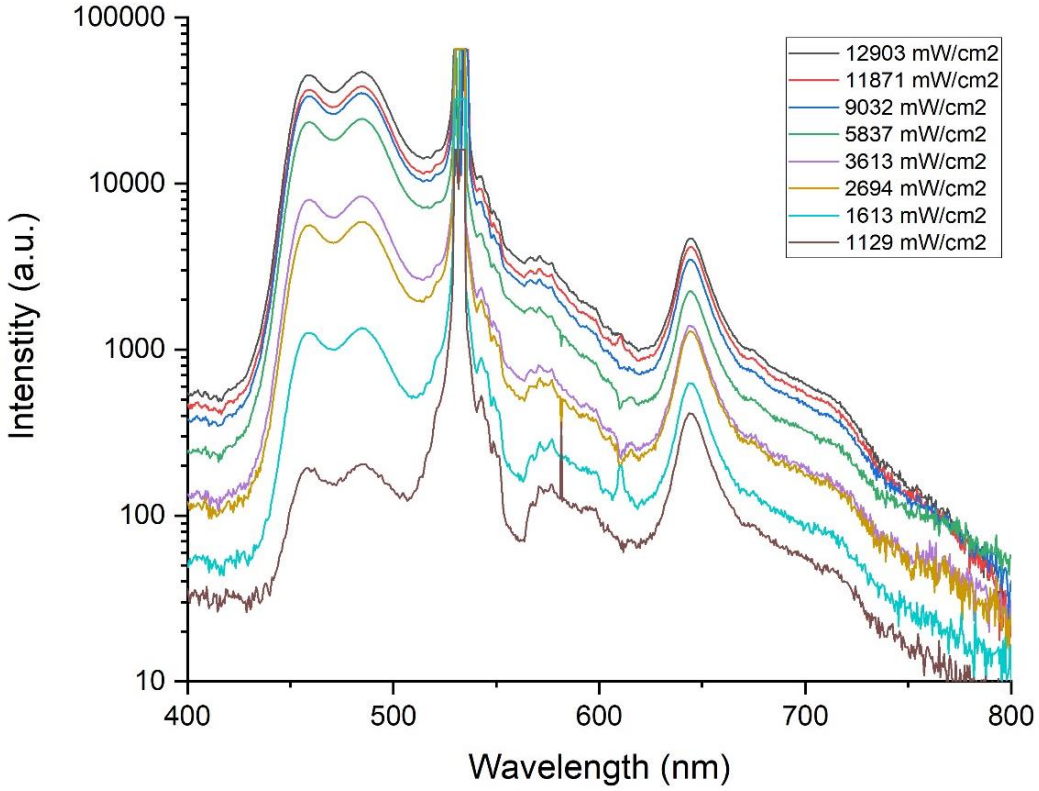

Figure 47. *Emission spectra of CrEL:EO (PtOEP-TTBPer) in water suspension measured in oxia using different excitation power densities, $PD_{exc}, [mW/cm^2]$. Spectra are presented in a) linear and b)logarithmic scale in terms of intensity.*

Emission Spectra of Micelles and Standard for Quantum Yield

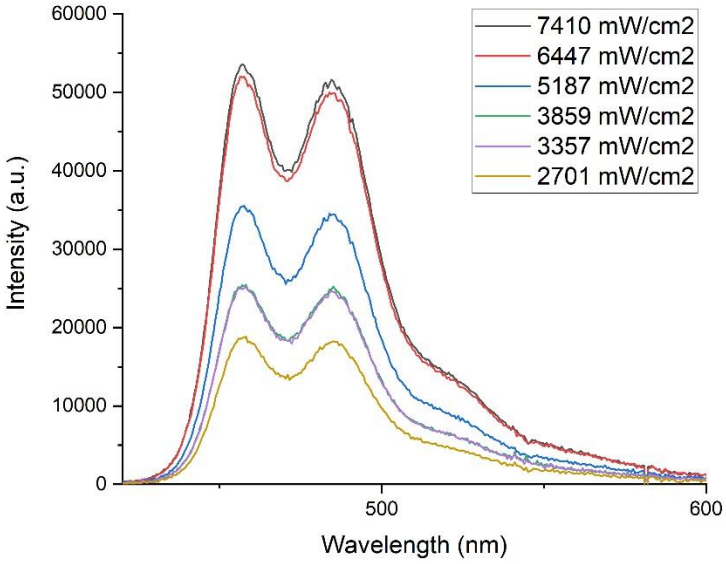

Figure 48. *Emission spectra of PdTPTBP – TTBPer loaded CrEL:EO:STA micelles in water suspension measured using different excitation power densities,* $PD_{exc}, [mW/cm^2]$.

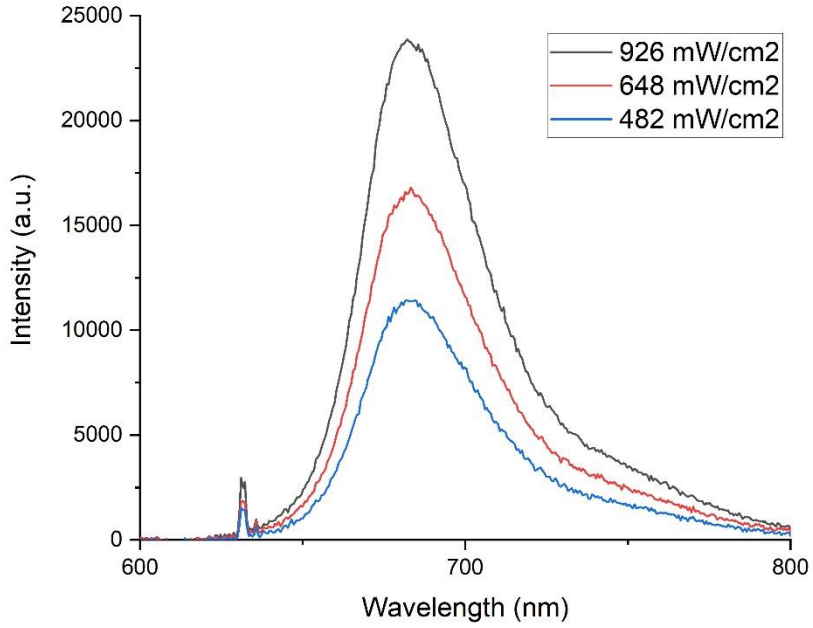

Figure 49. *Emission spectra of Methylene Blue standard in water measured using different excitation power densities,* $PD_{exc}, [mW/cm^2]$.

APPENDIX D: OVERVIEW ON THE CHARACTERIZATION RESULTS

UC pair	**PdTPTBP–TTBPer**			**PtTPTBP–TTBPer**	**PtOEP–TTBPer**
Stokes Shift	633 nm to 460 nm (red to blue)			635 nm to 460 nm (red to blue)	533 nm to 460 nm (green to blue)
Characterization of MICELLES					
Micelle formulation	Modified	Unmodified	Modified	Unmodified	Unmodified
Surfactant	CrEL	CrEL	T80	CrEL	CrEL
Oil	EO	EO	EO	EO	EO
Charge Modifier (co-surfactant)	STA	None	DOTAP	None	None
Micelle Structure					
Size	27.50 ± 6.22	30.49* / 17.52**	11.28 ± 0.37	17.36 nm	17.87 nm
ζ-potential	0.34 ± 4.09	-	-2.71 ± 0.80	-	-
UC properties of Micelles					
Power Density Threshold, Anoxia	143 mW/cm2	789 mW/cm2**	-	1221 mW/cm2	240 mW/cm2
Power Density Threshold, Oxia	-	-	-	-	2424 mW/cm2
Quantum Yield	0,6 %	-	-	-	-
Characterization of Micelles in GEL					
Release-% of Micelles from Gel					
High-loading gel	60 % (2 weeks)	35 % (2 weeks)*	100 % (6 days)	-	-
Low-loading gel	100 % (2 weeks)	70 % (2 weeks)*	100 % (6 days)	-	-
TTBPer fluorescence intensity decrease of Micelles released from Gel					
High-loading gel	50 % (2 weeks)	20 % (2 weeks)*	2 % (6 days)	-	-
Low-loading gel	48 % (2 weeks)	40 % (2 weeks)*	25 % (6 days)	-	-
UC properties of Micelles in Gel					
UC spectrum recorded	No	Yes	No	-	-
Resistance to oxygen	-	No	-	-	-

* Amount of TTBPer in *Micelle suspension*: 2.55 mM (same as in modified CrEL:EO:STA micelles)

** Amount of TTBPer in *Micelle suspension*: 1.5 mM (less than in modified CrEL:EO:STA micelles)